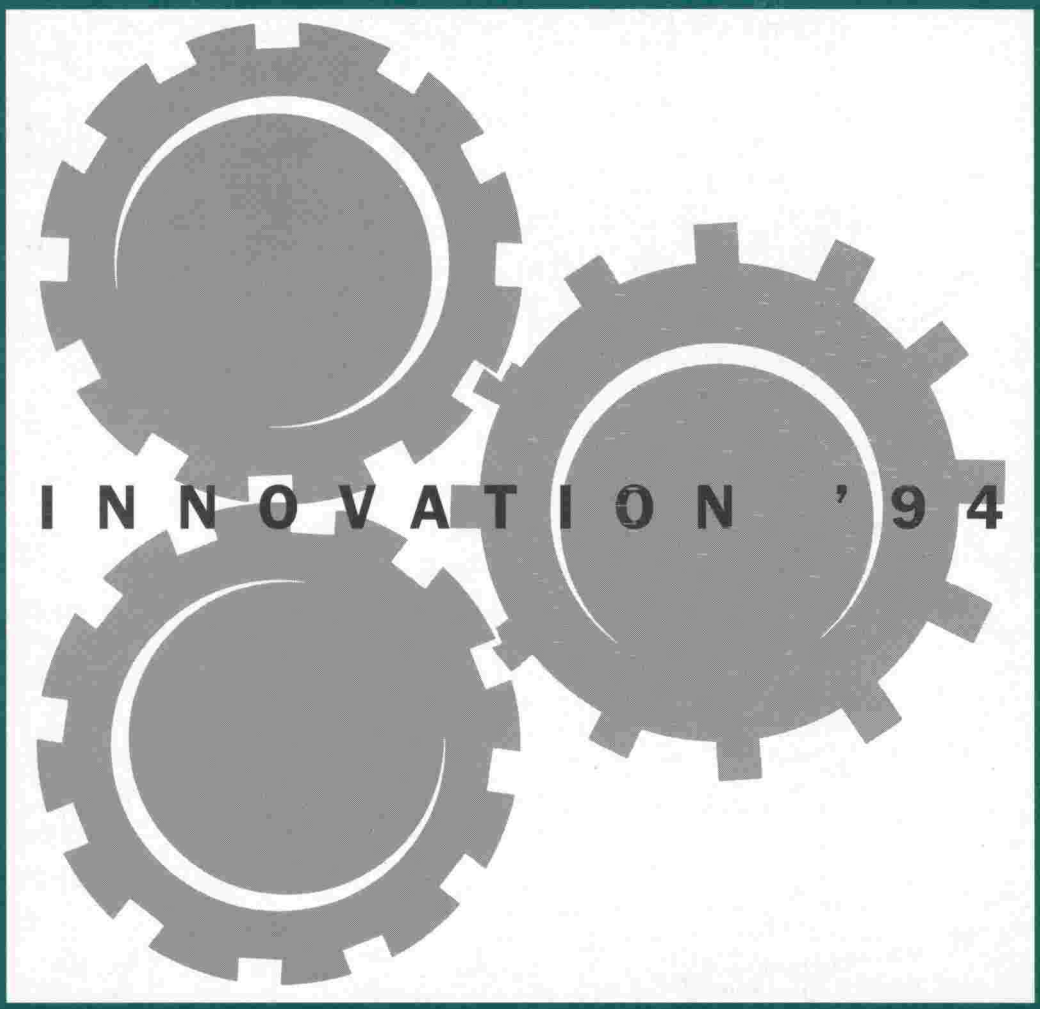

First Meeting of the Society of Magnetic Resonance

Works in Progress Supplement

JMRI Journal of Magnetic Resonance Imaging

Table of Contents

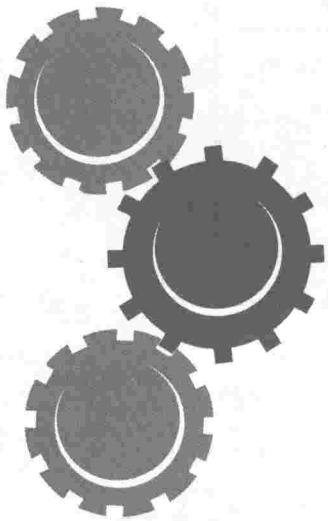

Letter from the 1993 SMRI President

Dear Colleague:

The Society of Magnetic Resonance invites you to its First Meeting! This meeting, to be held in Dallas March 5-9, 1994, was organized through the program committees of the Society for Magnetic Resonance Imaging prior to its merger with the Society of Magnetic Resonance in Medicine on January 1, 1994. In my capacity as 1993 SMRI President and 1994 SMR President, I invite you to join us in Dallas.

This First SMR Meeting will contain several major programs, beginning with the Educational Program on Saturday and Sunday, March 5 and 6. The Economics Symposium, a component of the Educational Program, will be on Monday, March 7.

The Scientific Program, consisting of plenary and proffered paper sessions, will run Sunday through Wednesday. The centerpiece of the Scientific Program will be the Topical Conference on Sunday, March 6 concerning "MRI in a Quality and Cost-Conscious Environment".

Additionally, the Morning Tutorial Program this year will be expanded to three sessions per day, and will be held Monday, Tuesday, and Wednesday mornings from 6:45 AM - 7:45 AM . Also, the Scientific Poster Exhibition, a showcase of recent scientific developments, is available throughout the meeting.

Another essential part of the 1994 SMR Dallas program is the Works-in-Progress program. These works comprise late breaking developments in the techniques and applications of magnetic resonance. Due to the timely nature of the work contained in these abstracts, the Program Committee felt it important for this material to be presented at the meeting. I encourage you to read the abstracts contained in this Program Supplement and to attend the presentations for those abstracts which you find interesting.

This First SMR Meeting will also provide ample opportunity to meet and confer with your colleagues on an informal basis. Special events include the Technical Exhibits Reception (Saturday, 5:00 PM - 7:00 PM), the Poster Reception (Sunday, 5:30 PM - 7:30 PM) and the Gala Reception (Monday, 7:30 PM - 10:30 PM). Please plan to attend these special social events.

The SMR has two official journals, the Journal of Magnetic Resonance Imaging (JMRI) and Magnetic Resonance in Medicine (MRM). Both are proven resources for current developments in the field of magnetic resonance as applied to medicine and biology. You are strongly encouraged to submit manuscripts based on your work to either of these journals.

The SMR is excited about its First Meeting as a merged Society and cordially invites you to participate. We look forward to seeing you in Dallas!

Sincerely,

Stephen J. Riederer

Stephen J. Riederer, PhD
SMRI President, 1993
SMR President, 1994

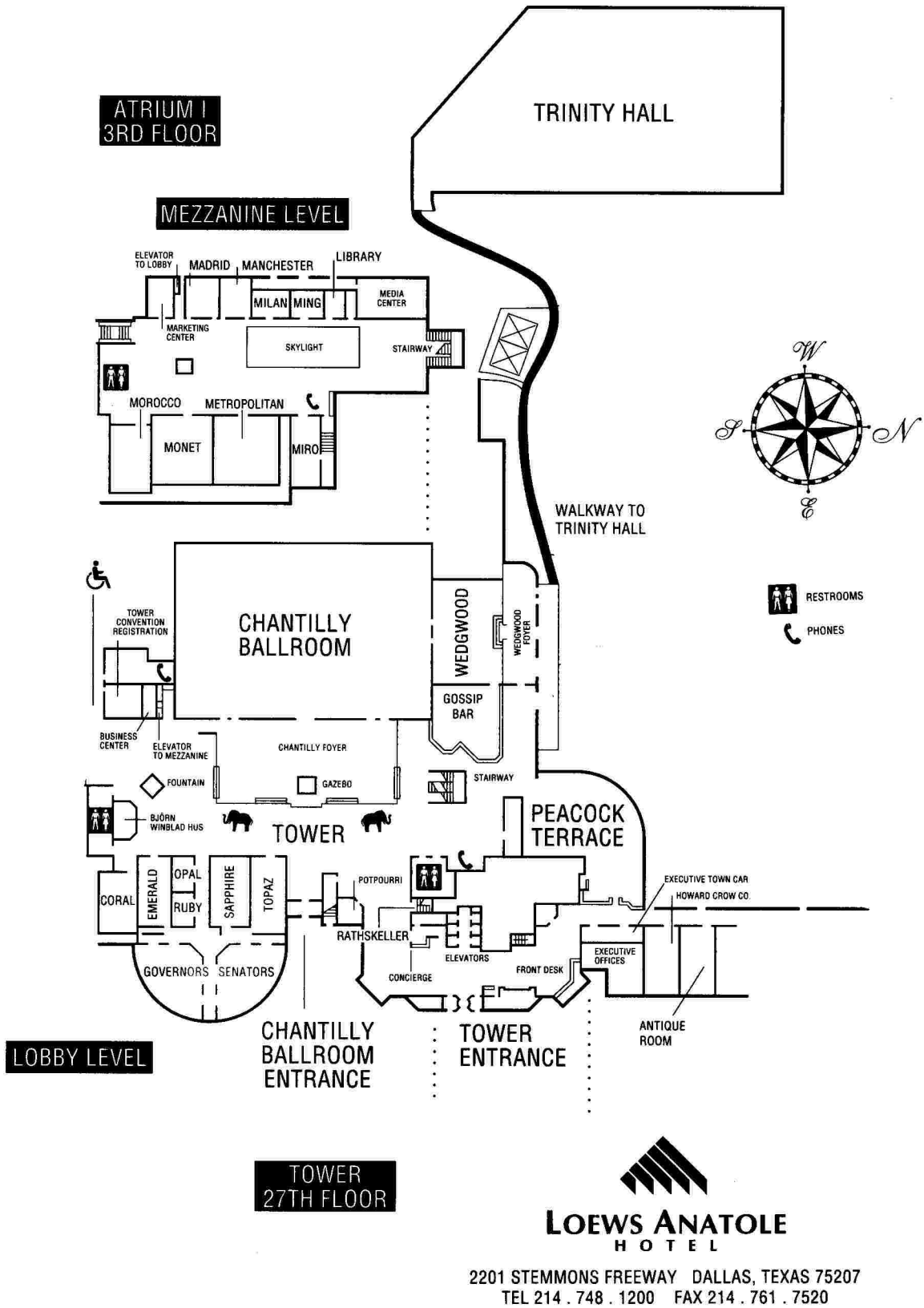

LOEWS ANATOLE
HOTEL

2201 STEMMONS FREEWAY DALLAS, TEXAS 75207
TEL 214 . 748 . 1200 FAX 214 . 761 . 7520

Proffered Papers

The 1994 Works in Progress Program will present 94 presentations, Sunday, March 6 – Wednesday, March 9 during the Scientific Program parallel sessions. To plan your itinerary, refer to the following pages for a complete listing of the sessions. Abstracts may be found following the schedules.

Please note: Works in Progress presentations may be presented at the end of a scientific session. Otherwise, an entire session has been devoted to Works in Progress presentations. These presentations have been highlighted on the following pages.

Seating for the scientific sessions is on a space-available basis. You are invited and encouraged to move from one meeting room to another during a time block to hear different presentations. Please, however, be sensitive to the presenter and the other attendees while implementing your Works in Progress itinerary.

1994 SMR Proffered Papers

SUN PM
3/6

Monet Room Papers 001-010 ***RAPID IMAGING*** Moderators: ***S Patz, MD*** ***J Pauly, PhD***	**Metropolitan Room** Papers 011-019 ***INTERVENTIONAL MR*** Moderators: ***R Kikinis, MD*** ***R B Lufkin, MD***	**Miro Room** Papers 021-029 ***BRAIN I (GENERAL)*** Moderators: ***R B Dietrich, MD*** ***J S Ross, MD***	**Morrocco Room** Papers 031-039 ***UPPER ABDOMEN I (HEPATIC, FAST)*** Moderators: ***J P Mugler III, PhD*** ***P T Weatherall, MD***	**Sapphire Room** Papers 041-049 ***FLOW QUANTITATION*** Moderators: ***R B Buxton, PhD*** ***D Saloner, PhD***	**Topaz Room** Papers 051-060 ***CONTRAST AGENTS/ OTHER NUCLEI*** Moderators: ***T Ceckler, MD*** ***P A Rinck, PhD***
001 **3:45 PM**	011 **3:45 PM**	021 **3:45 PM**	031 **3:45 PM**	041 **3:45 PM**	051 **3:45 PM**
002 **3:57 PM**	012 **3:57 PM**	022 **3:57 PM**	032 **3:57 PM**	042 **3:57 PM**	052 **3:55 PM**
003 **4:09 PM**	013 **4:09 PM**	023 **4:09 PM**	033 **4:09 PM**	043 **4:09 PM**	053 **4:05 PM**
004 **4:21 PM**	014 **4:21 PM**	024 **4:21 PM**	034 **4:21 PM**	044 **4:21 PM**	054 **4:15 PM**
005 **4:33 PM**	015 **4:33 PM**	025 **4:33 PM**	035 **4:33 PM**	045 **4:33 PM**	055 **4:25 PM**
006 **4:45 PM**	016 **4:45 PM**	026 **4:45 PM**	036 **4:45 PM**	046 **4:45 PM**	056 **4:35 PM**
007 **4:57 PM**	017 **4:57 PM**	027 **4:57 PM**	037 **4:57 PM**	047 **4:57 PM**	057 **4:45 PM**
008 **5:09 PM**	018 **5:09 PM**	028 **5:09 PM**	038 **5:09 PM**	048 **5:09 PM**	058 **4:55 PM**
009 **5:21 PM**	019 **5:19 PM**	029 **5:19 PM**	039 **5:19 PM**	049 **5:19 PM**	059 **5:05 PM**
010 **5:31 PM**					060 **5:15 PM**

1994 SMR Proffered Papers

MON PM
3/7

Monet Room Papers 101-109 ***CONTRAST AGENTS I*** Moderators: ***R L Nunnally, PhD*** ***D D Stark, MD***	**Metropolitan Room** Papers 111-119 ***BRAIN II (RAPID IMAGING)*** Moderators: ***R L De La Paz,MD*** ***F J Laine, MD***	**Miro Room** Papers 121-128 ***PELVIS (FEMALE)*** Moderators: ***J J Brown, MD*** ***R C Smith, MD***	**Morrocco Room** Papers 131-139 ***CARDIAC*** Moderators: ***B Chen, MD*** ***E R McVeigh, MD***	**Sapphire Room** Papers 141-149 ***SPECTROSCOPY I (TECHNIQUES)*** Moderators: ***H C Charles, MD*** ***P A Narayana, PhD***	**Topaz Room** Papers 151-159 ***IMAGING TECHNIQUES I*** Moderators: ***C R Crawford, PhD*** ***J Listerud, MD, PhD***
101 **3:45 PM**	111 **3:45 PM**	121 **3:45 PM**	131 **3:45 PM**	141 **3:45 PM**	
102 **3:57 PM**	112 **3:57 PM**	122 **3:57 PM**	132 **3:57 PM**	142 **3:57 PM**	151 **3:45 PM**
103 **4:09 PM**	113 **4:09 PM**	123 **4:09 PM**	133 **4:09 PM**	143 **4:09 PM**	152 **3:57 PM**
104 **4:21 PM**	114 **4:21 PM**	124 **4:21 PM**	134 **4:21 PM**	144 **4:21 PM**	153 **4:09 PM**
105 **4:33 PM**	115 **4:33 PM**	125 **4:33 PM**	135 **4:33 PM**	145 **4:33 PM**	154 **4:21 PM**
106 **4:45 PM**	116 **4:45 PM**	126 **4:45 PM**	136 **4:45 PM**	146 **4:45 PM**	155 **4:33 PM**
107 **4:57 PM**	117 **4:57 PM**	127 **4:57 PM**	137 **4:57 PM**	147 **4:57 PM**	156 **4:45 PM**
108 **5:09 PM**	118 **5:07 PM**	128 **5:07 PM**	138 **5:09 PM**	148 **5:09 PM**	157 **4:57 PM**
109 **5:19 PM**	119 **5:17 PM**		139 **5:19 PM**	149 **5:19 PM**	158 **5:07 PM**
					159 **5:17 PM**

1994 SMR Proffered Papers

TUE AM
3/8

Monet Room Papers 201-208 ***MAMMOGRAPHY (SILICONE)*** Moderators: ***P J Fritzsche, MD*** ***T A Spraggins, PhD***		**Metropolitan Room** Papers 211-218 ***FUNCTIONAL IMAGING*** Moderators: ***J A Helpern, PhD*** ***B R Rosen, MD***		**Miro Room** Papers 221-230 ***IMAGE QUALITY (MOTION & ARTIFACTS)*** Moderators: ***J A Sorenson, PhD*** ***M L Wood, PhD***		**Morrocco Room** Papers 231-239 ***SPECTROSCOPY II (BRAIN)*** Moderators: ***F Arias-Mendoza, MD, PhD*** ***I R Young, PhD***		**Sapphire Room** Papers 241-249 ***UPPER ABDOMEN II (HEPATIC, CONTRAST)*** Moderators: ***P L Choyke, MD*** ***R J Herfkens, MD***		**Topaz Room** Papers 251-260 ***VASCULAR IMAGING*** Moderators: ***M Bernstein, PhD*** ***D N Firmin, PhD***	
201	**10:30 AM**	211	**10:30 AM**	221	**10:30 AM**	231	**10:30 AM**	241	**10:30 AM**	251	**10:30 AM**
202	**10:42 AM**	212	**10:42 AM**	222	**10:42 AM**	232	**10:42 AM**	242	**10:42 AM**	252	**10:42 AM**
203	**10:54 AM**	213	**10:54 AM**	223	**10:54 AM**	233	**10:54 AM**	243	**10:54 AM**	253	**10:54 AM**
204	**11:06 AM**	214	**11:06 AM**	224	**11:06 AM**	234	**11:06 AM**	244	**11:06 AM**	254	**11:06 AM**
205	**11:18 AM**	215	**11:18 AM**	225	**11:18 AM**	235	**11:18 AM**	245	**11:18 AM**	255	**11:18 AM**
206	**11:30 AM**	216	**11:30 AM**	226	**11:30 AM**	236	**11:30 AM**	246	**11:30 AM**	256	**11:30 AM**
207	**11:42 AM**	217	**11:42 AM**	227	**11:42 AM**	237	**11:42 AM**	247	**11:42 AM**	257	**11:42 AM**
208	**11:54 AM**	218	**11:52 AM**	228	**11:54 AM**	238	**11:54 AM**	248	**11:54 AM**	258	**11:54 AM**
				229	**12:06 PM**	239	**12:04 PM**	249	**12:04 PM**	259	**12:06 PM**
				230	**12:16 PM**					260	**12:16 PM**

TUE PM
3/8

Monet Room Papers 301-309 ***PERFUSION AND FUNCTIONAL IMAGING*** Moderators: ***T J Brady, MD*** ***W T Dixon, MD***		**Metropolitan Room** Papers 311-318 ***CONTRAST AGENTS II*** Moderators: ***G D Fullerton, PhD*** ***S W Young, MD***		**Miro Room** Papers 321-330 ***MUSCULOSKELETAL I (JOINTS)*** Moderators: ***J V Crues III, MD*** ***E C Unger, MD***		**Morrocco Room** Papers 331-338 ***ABDOMEN AND MALE PELVIS*** Moderators: ***D G Mitchell, MD*** ***A Yang, MD***		**Sapphire Room** Papers 341-349 ***HEAD AND NECK*** Moderators: ***A N Hasso, MD*** ***K L Nelson, MD***		**Topaz Room** Papers 351-359 ***SPINE*** Moderators: ***M Rothmann, MD*** ***B D Flannigan-Sprague, MD***		**Chantilly West** Papers 361-369 ***VASCULAR IMAGING/PULSE SEQUENCES*** Moderators: ***G H Glover, PhD*** ***M S Silver, PhD***	
301	**3:45 PM**	311	**3:45 PM**	321	**3:45 PM**	331	**3:45 PM**	341	**3:45 PM**	351	**3:45 PM**	361	**3:45 PM**
302	**3:57 PM**	312	**3:57 PM**	322	**3:57 PM**	332	**3:57 PM**	342	**3:57 PM**	352	**3:57 PM**	362	**3:55 PM**
303	**4:09 PM**	313	**4:09 PM**	323	**4:09 PM**	333	**4:09 PM**	343	**4:09 PM**	353	**4:09 PM**	363	**4:05 PM**
304	**4:21 PM**	314	**4:21 PM**	324	**4:21 PM**	334	**4:21 PM**	344	**4:21 PM**	354	**4:21 PM**	364	**4:15 PM**
305	**4:33 PM**	315	**4:33 PM**	325	**4:33 PM**	335	**4:33 PM**	345	**4:33 PM**	355	**4:33 PM**	365	**4:25 PM**
306	**4:45 PM**	316	**4:45 PM**	326	**4:45 PM**	336	**4:45 PM**	346	**4:45 PM**	356	**4:45 PM**	366	**4:35 PM**
307	**4:57 PM**	317	**4:57 PM**	327	**4:57 PM**	337	**4:57 PM**	347	**4:57 PM**	357	**4:57 PM**	367	**4:45 PM**
308	**5:07 PM**	318	**5:09 PM**	328	**5:09 PM**	338	**5:09 PM**	348	**5:09 PM**	358	**5:09 PM**	368	**4:55 PM**
309	**5:17 PM**			329	**5:19 PM**			349	**5:19 PM**	359	**5:21 PM**	369	**5:05 PM**
				330	**5:29 PM**								

1994 SMR Proffered Papers

WED AM
3/9

Monet Room Papers 401-409 ***CARDIAC II (CORONARY IMAGING)*** Moderators: ***D Li, MS*** ***J D Pearlman, MD, PhD***	**Metropolitan Room** Papers 411-419 ***MR ANGIOGRAPHY I (NEURO)*** Moderators: ***C Dumoulin, PhD*** ***K R Maravilla, MD***	**Miro Room** Papers 421-429 ***MUSCULOSKELETAL II*** Moderators: ***J B Kneeland, MD*** ***S Marjumdar, PhD***	**Morrocco Room** Papers 431-439 ***IMAGING TECHNIQUES II*** Moderators: ***K Butts, PhD*** ***E M Haacke, PhD***	**Sapphire Room** Papers 441-448 ***IMAGE PROCESSING*** Moderators: ***J R MacFall, MD*** ***S Napel, PhD***	**Topaz Room** Papers 451-460 ***FLOW QUANTITATION*** Moderators: ***M H Buonocore, MD*** ***J Huston, MD***
401 **10:30 AM**	411 **10:30 AM**	421 **10:30 AM**	431 **10:30 AM**	441 **10:30 AM**	451 **10:30 AM**
402 **10:42 AM**	412 **10:42 AM**	422 **10:42 AM**	432 **10:42 AM**	442 **10:42 AM**	452 **10:40 AM**
403 **10:54 AM**	413 **10:54 AM**	423 **10:54 AM**	433 **10:54 AM**	443 **10:54 AM**	453 **10:50 AM**
404 **11:06 AM**	414 **11:06 AM**	424 **11:06 AM**	434 **11:06 AM**	444 **11:06 AM**	454 **11:00 AM**
405 **11:18 AM**	415 **11:18 AM**	425 **11:18 AM**	435 **11:18 AM**	445 **11:18 AM**	455 **11:10 AM**
406 **11:30 AM**	416 **11:30 AM**	426 **11:30 AM**	436 **11:30 AM**	446 **11:30 AM**	456 **11:20 AM**
407 **11:42 AM**	417 **11:42 AM**	427 **11:42 AM**	437 **11:42 AM**	447 **11:42 AM**	457 **11:30 AM**
408 **11:54 AM**	418 **11:54 AM**	428 **11:54 AM**	438 **11:54 AM**	448 **11:54 AM**	458 **11:40 AM**
409 **12:04 PM**	419 **12:04 PM**	429 **12:04 PM**	439 **12:04 PM**		459 **11:50 AM**
					460 **12:00 PM**

WED PM
3/9

Monet Room Papers 501-508 ***MAMMOGRAPHY II (CONTRAST)*** Moderators: ***S E Harms, MD*** ***C L Partain, MD, PhD***	**Metropolitan Room** Papers 511-519 ***BRAIN III (CSF FLOW, OTHER)*** Moderators: ***W G Bradley, Jr., MD, PhD*** ***V M Runge, MD***	**Miro Room** Papers 521-529 ***MR ANGIOGRAPHY II*** Moderators: ***J E Siebert, MD*** ***S Wann, MD***	**Morrocco Room** Papers 531-539 ***SPECTROSCOPY III*** Moderators: ***D N Levin, MD*** ***M D Osbakken, PhD***	**Sapphire Room** Papers 541-550 ***DIFFUSION*** Moderators: ***J A Helpern, PhD*** ***R R Price, PhD***	**Topaz Room** Papers 551-559 ***OTHER (INSTRUMENTATION, SAFETY, RELAXOMETRY)*** Moderators: ***E Kanal, MD*** ***S R Thomas, PhD***
501 **2:45 PM**	511 **2:45 PM**	521 **2:45 PM**	531 **2:45 PM**	541 **2:45 PM**	551 **2:45 PM**
502 **2:57 PM**	512 **2:57 PM**	522 **2:57 PM**	532 **2:57 PM**	542 **2:57 PM**	552 **2:57 PM**
503 **3:09 PM**	513 **3:09 PM**	523 **3:09 PM**	533 **3:09 PM**	543 **3:09 PM**	553 **3:09 PM**
504 **3:21 PM**	514 **3:21 PM**	524 **3:21 PM**	534 **3:21 PM**	544 **3:21 PM**	554 **3:21 PM**
505 **3:33 PM**	515 **3:33 PM**	525 **3:33 PM**	535 **3:33 PM**	545 **3:33 PM**	555 **3:33 PM**
506 **3:45 PM**	516 **3:45 PM**	526 **3:45 PM**	536 **3:45 PM**	546 **3:45 PM**	556 **3:45 PM**
507 **3:57 PM**	517 **3:57 PM**	527 **3:57 PM**	537 **3:57 PM**	547 **3:57 PM**	557 **3:57 PM**
508 **4:09 PM**	518 **4:07 PM**	528 **4:09 PM**	538 **4:09 PM**	548 **4:09 PM**	558 **4:09 PM**
	519 **4:17 PM**	529 **4:19 PM**	539 **4:19 PM**	549 **4:19 PM**	559 **4:21 PM**
				550 **4:29 PM**	

SMR '94 Works in Progress
Proffered Paper Abstracts

Sunday Afternoon • Monet Room
Papers 009–010

RAPID IMAGING
MODERATORS: S Patz, MD
J Pauly, PhD

009 • 5:21 PM
Optimized Dynamic Scanning Protocol for Tracking Instant Center of Rotation Motions in the Shoulder
DT Hung, CP Ho, R Bell, MS Kreidler, EA Ryan
Resonex, Inc, Fremont, CA

Purpose: With static MRI scans, subtle shoulder instabilities are difficult to detect. We have built a set of tools for detecting shoulder instabilities with dynamic MR scanning. Translations of the instant center of rotation of the humeral head are measured and presented graphically and in cine loops. This is useful for looking at instability and abnormal motion associated with muscle dysfunction and possible passive instability associated with derangement or laxity of capsule, labrum, and ligaments.
Methods: We scan with a fast gradient-echo pulse sequence optimized for contrast, SNR, and scan speed (9-ms echo, 0.018-sec TR, 45° flip angle, 10 sequential and continuously acquired slices). During dynamic scanning, the patient's shoulder is in constant motion. To minimize motion artifact, a positioning device is required. The angular rotation of the shoulder joint is allowed to be no more than 3° per 64 phase-encode lines. We acquire only the middle 50% of phase-encode lines in a 128 × 256 matrix to reduce motion artifact. For analysis, we calculate the instant center of rotation from the curvature of the humeral head and refer translations to the glenoid.
Results: We acquired cine loops showing abduction/adduction and internal/external rotation. Graphs of the instant center of rotation translations aided in evaluation of the glenohumeral joint, especially when the joint moved as a whole across the images in the cine loop.
Conclusion: A combination of fast acquisition methods, patient positioning devices, and analysis software form a new tool for detecting shoulder instabilities.
D.T. Hung is an employee of Resonex, Inc.

010 • 5:31 PM
Multiphase Multislice Myocardial Tagging in a Single Breath Hold with Echo-Planar Imaging
C Tang, E Atalar, E McVeigh, E Zerhouni
Johns Hopkins School of Medicine, Baltimore, MD

Purpose: EPI tagging is used to obtain tagged images from the entire LV in a single breath hold.
Methods: Tagging pulses were added to a multiphase multislice EPI sequence (eight slices, eight phases, voxel size = 1.2 × 4.7 × 8 mm, four interleaves, TR = R-R interval, TE = 13 ms, 0.5 NEX, 50-ms temporal resolution, one breathhold, 32 heart beats per breath hold). All slices and phases were obtained in a single breath hold to minimize respiratory motion artifact and misregistration. Axial images were acquired with a prototype GE single-axis SR-230 echo planar system, which switches the x gradient from 0 to 2.3 G/cm in 100 μs. The tag lines are perpendicular to the readout direction. Tag/myocardial contrast-to-noise ratio (CNR) was compared with that of the segmented k-space gradient-echo technique (eight slices, 12 phases, voxel size 1.2 × 4.7 × 8 mm, TR = 6.5 ms, TE = 2.3 ms, 1 NEX, 33-ms temporal resolution, eight breath-hold periods, 19 heartbeats per breath hold).
Results: In the same heart, EPI improved the contrast between tagged and nontagged regions by a factor of 1.7 and 3.2 at 30- and 360-ms delay after trigger, respectively. The tag lines were also found to persist further into the cardiac cycle with EPI.
Conclusion: The EPI tagging technique offers improved tag CNR while covering the entire heart within one breath hold.

Sunday Afternoon • Metropolitan Room
Papers 018–019

INTERVENTIONAL MR
MODERATORS: R Kikinis, MD
RB Lufkin, MD

018 • 5:09 PM
MRI-monitored Noninvasive Ultrasound Surgery of Highly Perfused Tissues
K Hynynen, CA Damianou, F Jolesz, A Alexander, E Unger, HH Cline
Department of Radiology, Brigham and Women's Hospital, Boston, MA

Purpose: The purpose was to optimize the sonication parameters and demonstrate the feasibility of MRI-guided and monitored noninvasive ultrasound surgery to necrose highly perfused tissues through the body wall.
Methods: A theoretical simulation study was first performed to evaluate the optimal sonication parameters for the surgery. Then a hydraulic MR-compatible positioning device was used to manipulate a focused ultrasound transducer (frequency = 1.656 MHz, F-number = 0.8) in an MRI scanner. The system was used to sonicate rabbit kidneys (three rabbits) at various power levels and sonication times. The temperature elevation during the sonication was followed with a gradient-echo (SPGR) imaging sequence.
Results: The theoretical simulation study demonstrated that sharply focused transducers with relatively short sonication times (30 s or shorter) have to be used in order to avoid necrosis of the skin and muscle layer in the body wall. This is because these tissues have a much lower blood perfusion rate than the kidney. This results in higher temperatures in the overlying tissues if the exposures are long. The experiments showed that the gradient-echo imaging sequence was sensitive enough to detect the temperature elevation during sonication, thus indicating the actual location of the focus. The histologic evaluations post mortem showed that the transducer was able to induce kidney necrosis consistently without damaging the overlying skin and muscle.
Conclusion: This study shows that highly perfused tissues can be necrosed through the body wall noninvasively by using focused ultrasound and that MRI can be used to guide and monitor this surgery.
H.H. Cline is an employee of GE Medical Systems.

019 • 5:19 PM

MR Peritoneography: MRI Evaluation of the Saline-distended Peritoneal Cavity prior to and during Treatment of Peritoneal Carcinomatosis

GR Magre, P Colletti, M Terk, W Boswell
Imaging Department, University of Southern California School of Medicine, Los Angeles, CA

Purpose: In selected cases of peritoneal carcinomatosis, treatment with intraperitoneal instillation of various chemotherapeutic agents is appropriate. Pretreatment evaluation to determine the extent of disease, as well as the likelihood of adequate distribution of treatment agents instilled intraperitoneally, is important in initial therapy planning. Posttreatment evaluation of response will determine continuation or modification of treatment regimens. We present the first patient series describing the use of MRI in conjunction with intraperitoneal saline in the evaluation of peritoneal surfaces (MRIP).
Methods: Six patients, aged 41–74 years, were evaluated on seven different occasions. All examinations were performed on a 1.5-T Signa MR system (GE Medical Systems, Milwaukee, Wis). Patients were studied with conventional spin-echo as well as fast spin-echo techniques. Typical fast spin-echo imaging parameters were 90 Ef/4,000–7,000/48 cm/10 mm/3–4/256 × 192 (TE/TR/FOV/thickness/NEX/matrix). Version 5.3 software was used. MRI was performed after the intraperitoneal instillation of 1,500 mL of sterile isotonic saline via permanently placed chemotherapy infusion catheters. All catheters were placed at the time of a "first look" staging and debulking operation.
Results: Two patients demonstrated normal intraperitoneal distribution of saline and no evidence of residual disease. One patient demonstrated saline extravasation due to a malfunctioning catheter, and one demonstrated residual intraperitoneal hematoma related to recent surgery. One patient showed subtle findings of recurrent disease. One patient demonstrated widespread intraperitoneal metastases, and in this case intraperitoneal distribution of saline was abnormal.
Conclusion: Our initial study indicates that MRI, with a fast spin-echo technique used in conjunction with intraperitoneal saline instillation, permits excellent visualization of the peritoneum. Detection of peritoneal implants is thereby greatly facilitated. Additionally, MRI peritoneography can show normal and abnormal patterns of saline distribution, which may be useful in predicting response to intraperitoneal chemotherapy.

Sunday Afternoon • Miro Room
Papers 028–029

BRAIN I: General

MODERATORS: RB Dietrich, MD
JS Ross, MD

028 • 5:09 PM

EPISTAR Perfusion Echo-Planar Imaging of Human Brain Tumors

J Gaa, S Warach, P Wen, V Thangaraj, PA Wielopolski, RR Edelman
Department of MRI, Beth Israel Hospital, Boston, MA

Purpose: To study the vascularity of human brain tumors, comparing echo planar dynamic contrast-enhanced blood volume imaging with EPISTAR, a noninvasive method of imaging relative cerebral perfusion with echo-planar imaging (EPI).
Methods: The study sample consisted of 12 patients (aged 27–64 years) with diagnoses of astrocytoma (n = 9), oligodendroglioma (n = 1), lymphoma (n = 1), and meningioma (n = 1). Multislice T2*-weighted EPI scans (FID sequence TE = 60 msec, eight 7-mm contigous slices every 2 seconds) was utilized during bolus injection of Gd-DTPA. The EPISTAR technique is a subtraction angiographic technique that visualizes the distribution of blood flow by tagging a volume of blood proximal to the imaging slice with a 180° inversion prepulse followed by an echo planar readout of the imaging slice; untagged images are subtracted from tagged images to produce relative cerebral blood flow maps.
Results: Areas of hypoperfusion and hyperperfusion were demonstrated in both tumors and surrounding areas of edema on either EPISTAR or T2* contrast-enhanced images. Although there was good agreement between the T2* and EPISTAR techniques, mismatches were found that may be due to differences in cerebral blood volume versus cerebral blood flow, respectively.
Conclusion: Abnormal tumor perfusion data identified with EPISTAR were complementary to perfusion data obtained from dynamic blood volume imaging, presumably reflecting the closer relationship to cerebral blood flow of the former technique. EPISTAR therefore may provide unique information about brain tumor pathophysiology.

029 • 5:19 PM

Imaging Gray Matter with a Double-Inversion-Recovery Pulse Sequence to Suppress CSF and White Matter Signals

TW Redpath, FW Smith
MRI Centre, Aberdeen Royal Infirmary, University of Aberdeen, Aberdeen, Scotland

Purpose: Partial volume effects can invalidate relaxation time measurements and estimates of tissue volume in MR imaging. Brain structures are complex and comprise CSF and white and gray matter, each with significantly different T1 values. The use of a double-inversion-recovery (DIR) sequence to suppress white matter and CSF signals and thus image gray matter directly was investigated.
Methods: A DIR sequence consists of two 180° inverting pulses separated by a time TI_1, followed by a conventional spin-echo imaging sequence TI_2 seconds after the second inversion pulse. Imaging was carried out on a 1-T Siemens Impact MR system. Computer simulations of the Bloch equations were based on T1 values of 3 s for CSF and 500 ms for white matter.
Results: Analysis of the Bloch equations showed that TI_1 and TI_2 values could be found to null CSF and white matter signals over a wide range of TR values. Calculations showed that TR values of less than about 6 s will have low SNR and a low T1 range of useful contrast. Images of normal volunteers obtained with TR = 8 s, TI_1 = 2,200 ms, TI_2 = 340 ms, and TE = 20 ms gave good CSF and white matter suppression, as predicted by theory. Comparison with T2-weighted images at matching levels showed that the DIR images can better delineate cortex structure, by reduction of partial volume effects.
Conclusion: DIR sequences can simultaneously null CSF and white matter signals to image gray matter alone. The technique has potential where measurements of brain cortex function, T2 relaxation time, volume, etc, must to be made without partial volume contamination.

Sunday Afternoon • Morocco Room
Papers 038–039

UPPER ABDOMEN I: Hepatic, Fast

MODERATORS: JP Mugler, III, PhD
PT Weatherall, MD

038 • 5:09 PM

Three-dimensional MR Cholangiopancreatography in the Diagnosis of Bile Duct Obstruction

L Guibaud, PM Bret, C Reinhold, M Atri, A Barkun
Department of Diagnostic Radiology, McGill University, Montreal, Quebec, Canada

Purpose: The objective of this study was to assess the accuracy of MR cholangiopancreatography using T2-weighted fast spin echo (FSE) sequences in evaluating patients with bile duct obstruction.
Methods: Forty-five consecutive patients with suspected bile duct obstruction were examined with MRI within a 2-month period. T2-weighted FSE sequences were used

(8,000/144/16 [TR/eff TE/ETL]). Axial, coronal, and oblique acquisitions were obtained, and the images were processed with a maximum-intensity projection algorithm and reformatting software. MRI results were compared with those of endoscopic retrograde cholangiopancreatography (ERCP) (26 cases) or direct cholangiography (six cases) or correlated with findings of other imaging modalities and follow-up (13 cases).
Results: In one patient with claustrophobia, MRI was not performed. ERCP was unsuccessful in six patients. There was no bile duct obstruction in 22 cases, and no false-positive findings were encountered with MRI. Bile duct obstruction was present in 23 of 45 patients and was diagnosed with MRI in 22 cases (96%). The level of obstruction was accurately diagnosed in 21 of 22 patients (95%). The nature of obstruction was unclear after ERCP and follow-up in 4 cases. In the remaining 18 patients, MRI accurately demonstrated the cause of obstruction in 13 cases: 8/9 bile duct stones, 3/3 pancreatic carcinomas, 1/1 pancreatitis, 1/1 inflammatory stenosis.
Conclusion: If these preliminary results are confirmed by a large prospective clinical trial, 3D MR cholangiopancreatography may become an important diagnostic tool in patients with suspected bile duct obstruction and equivocal US results.

039 • 5:19 PM
Monitoring of liver Graft viability with H-1 MR Imaging, Relaxometry, and Spectroscopy
E Winklmayr, F Laengle, R Steininger, E Moser
Department of Medical Physics, University of Vienna, Vienna, Austria

Purpose: H-1 MR relaxometry in vitro and ex vivo, combined with imaging techniques, was used to evaluate liver graft viability in a model of orthotopic liver transplantation in pigs.
Methods: Orthotropic liver transplantation was performed in 25 pairs of pigs via venovenous bypass. Livers were perfused in situ with UW solution and two modified Bretschneider HTK solutions and subsequently stored for 20 hours. T1 and T2 were determined from biopsy specimens with SR and CPMG pulse sequences, as well as ex vivo with a combined SE-IR sequence. Relaxation time images of liver grafts stored on ice were monitored overnight to follow alterations during storage. All relaxation time estimations were performed at 20 MHz. A T2-weighted TSE sequence was used to reconstruct a "venogram" with storage solution as natural contrast agent. Localized proton spectroscopy (STEAM-20) was performed to estimate the fat content of the organ.
Results: In vitro data confirm our previous results from rat liver investigations, which indicated that H-1 MR relaxometry is useful in liver graft viability testing, reflecting tissue alterations due to specific properties of storage solutions (1). We found that even relaxation time images yield reproducible results for viability testing if a strict protocol is maintained. A good correlation between in vitro and ex vivo results was obtained. Contrast of TSE images allowed 3D reconstruction of (larger) vessels.
Conclusion: A combination of imaging, relaxometry, and spectroscopy is useful for viability testing of liver grafts, which may be performed noninvasively within two hours on a clinical imager.
1. E. Moser et al. Transplantation 53 (1992) 536–540

Sunday Afternoon • Sapphire Room
Papers 048–049

FLOW QUANTITATION
MODERATORS: RB Buxton, PhD
D Saloner, PhD

048 • 5:09 PM
Comparative Study of Quantitative MR Flow Measurement, Color-coded Doppler US, and Digital Subtraction Angiography
TE Bomhard, HJ Oellinger, HB Schedel Jr, CH Hirth Jr, RN Felix Sr
Strahlenklinik und Poliklinik, Freie Universitat Berlin, Berlin, Germany

Purpose: The comparison of these methods was executed in order to evaluate the clinical application and their overall performance in patients with stenoses primarily in the internal carotid arteries (ICAs).
Methods: Thirteen patients with 17 ICA stenoses, nine female (mean, 58.9 yrs) and 4 male (mean, 62.9 yrs), were examined by means of MRI, color-coded Doppler US (CCDU), and digital subtraction angiography (DSA). The calculated degrees of stenosis were compared with the results of DSA. A 1.5-Tesla Magnetom imager (SP 63) was used with a neck coil (Siemens, Erlangen, Germany). A rephased technique was used for MR flow measurement (MRFM) and a FLASH 3D (time of flight) sequence for MRA. For CCDU, a Toshiba imager was used. Blood velocities and flow rates were measured 20 mm proximally, within the stenosis, and 15 mm distally.
Results: The average examination time was 70 minutes for MRFM, including MR angiography, and 30 minutes for CCDU. Compared with DSA, the degree of stenosis correlated well for MRI in 70% and for CCDU in 85%. In two patients a steal phenomenon could be detected in the vertebral artery with MRFM only.
Conclusion: Despite the fact that MRFM provides the most complete picture in comparison with the other two methods, for the time being CCDU may be the first choice for routine clinical use, followed by DSA.

049 • 5:19 PM
Phase-Contrast Phased-Array Reconstruction
MA Bernstein, M Grgic, TJ Brosnan, NJ Pelc
GE Medical Systems, Milwaukee, WI

Purpose: Phase-contrast (PC) angiography can depict flow direction and volume rate and can also provide angiograms with excellent stationary tissue suppression. We present a phase-contrast reconstruction that is compatible with a phased-array multicoil and that, unlike with a previous method, retains directional flow and quantitative information.
Methods: Central to phase-contrast reconstructions is the restoration of the phase difference $\Delta\Phi$. Consider the phase difference measured by coil k, $\phi_k = \arg(Z_{1k}/Z_{2k})$. The variance in ϕ_k is inversely proportional to M_k^2, so the linear combination of $\{\phi_k\}$ that minimizes the variance of the combined result uses magnitude-squared weighting. Thus, one estimate of the true phase difference is $\Delta\Phi = \Sigma M_k^2\phi_k/\Sigma M_k^2$. This combination is subject to errors when the $\{\phi_k\}$ straddle the velocity aliasing boundary. This defect can be avoided by accumulating *complex exponentials* rather than angles. Since the variance of $\exp(i\phi_k)$ is also inversely proportional to M_k^2, complex exponentials call for magnitude-squared weighting as well. We can exploit the intrinsic magnitude-squared scaling in the terms $Z_{1k}Z_{2k}^* = M_{1k}M_{2k}\exp((i\phi_k)$ Thus, the estimate for the phase difference becomes $\Delta\Phi = \arg\{\Sigma Z_{1k}Z_{2k}^*/\sigma_k^2\}$, where σ_k is the spatially independent noise estimate for the kth coil-preamplifier-receiver chain, measured during prescan calibration.
Results: We have reconstructed phase-contrast, phased-array scans of normal volunteers with both the phase difference and complex difference methods. In one case, S/N improved from 6.7 to 10.1 compared with body coil images. The four-

coil reconstruction times were only twice as long as single-coil times due to common processing.
Conclusion: Feasibility of a new phase-contrast phased-array multicoil reconstruction has been demonstrated.
M.A. Bernstein and M. Grgic are employees of GE Medical Systems.

Sunday Afternoon • Topaz Room
Papers 051–060

CONTRAST AGENTS/OTHER NUCLEI

MODERATORS: T Ceckler, MD
PA Rinck, PhD

051 • 3:45 PM

Gadolinium Zeolite as an Orally Administered Gastrointestinal MR Contrast Agent

SW Young, K Balkus, D Rubin, F Qing, JK Lang, JD Mutch, WC Dow, RA Miller
Pharmacyclics, Inc, Mountain View, CA

Purpose: To evaluate Gadolite Oral Suspension (GOS), an oral MRI contrast agent.
Methods: GOS is a suspension of gadolinium sodium aluminosilicate (gadolinium zeolite). Rat single-dose studies included intraperitoneal toxicity, oral toxicity, and ulcerogenicity. Subchronic 14-day toxicity and absorption studies were performed in rats and dogs. The concentrations used were 120 μg to 15 mg Gd(III)/mL; the volumes, 10–40 mL/kg. MRI signal intensities (SI) of GOS standards in 1.2–300 μg Gd(III)/mL suspension were evaluated with T1- and T2-weighted spin-echo, and T1-weighted gradient-echo pulse sequences. MRI was performed in dogs (T1, fast spin echo [FSE], and GRE). The oral dose was 15 mL/kg of a 150- (n = 2), 75- (n = 2), or 9.6- (n = 8) μg Gd(III)/mL suspension. The contrast-to-noise ratio (C/N) and the percentage of contrast enhancement (%E) were calculated for bowel and stomach 1.5 hours after administration.
Results: No evidence of toxicity or systemic absorption was detected in any of the toxicity studies. Maximum phantom SI at 75 μg: (300/15), 2,241.3; GRE (133/7/60°), 1,991.9; zeolite suspension (no gadolinium), 308. MRI in dogs demonstrated excellent enhancement of the stomach and small bowel. The SI, C/N, and %E were significantly different from those of surrounding muscle for all concentrations and pulse sequences ($P < .05$). The bowel loops were all well filled, with no segmentation or flocculation observed. The SI for T1 and FSE were as follows: 150 μg/mL, 485.3/67.3; 75 μg/mL, 411.8/358.8; 9.6 μg/mL, 289.8/402.4.
Conclusion: GOS appears to be an excellent oral MRI contrast agent, providing positive (white) signal intensities with all pulse sequences commonly used today. There appears to be no toxicity or systemic absorption.
S.W. Young is a cofounder of Pharmacyclics, Inc.

052 • 3:55 PM

Derivatives of Gd-DTPA-bis(Phenylalanine) as Hepatobiliary Contrast Agents

DL White, VS Vexler, L Milco, D Marinkovic, G Shevlin, T Best
Department of Radiology, Contrast Media Laboratory, University of California, San Francisco, CA

Purpose: The Gd(III) chelates of DTPA-bis(phenylalanine) exhibit both renal and hepatobiliary excretion in rats and are potentially useful MRI contrast agents for the kidneys, liver, biliary tree, and small intestine. The purpose of this study was to examine the influence of aromatic ring substituents on biliary excretion and the dynamics of MRI enhancement in rats.
Methods: Ligands were prepared from DTPA cyclic anhydride and substituted phenylalanine derivatives. The relative amounts of biliary excretion over 1 hour of a 0.1-mmol/kg dose of Gd-153–labeled chelate was determined by cannulating the rat common bile duct. T1-weighted coronal MR images (2.0 T; SE 300/6) of rat abdomen were acquired before and up to 90 minutes after injection of 0.1 mmol Gd/kg of contrast agent.
Results: The cumulative amounts (% injected dose) of Gd-153 recovered in bile for the parent L-phenylalanine derivative, its ethoxy-L, and its t-butyl-DL-analog were 6.4% ± 1.8, 23.6% ± 2.2, and 42.8% ± 8.5, and the corresponding values for Gd-153 found in the exsanguinated liver at 1 hour were 2.0% ± 0.7, 4.98% ± 0.7, and 4.4% ± 1.5, respectively. MRI contrast enhancement values in rat liver at 5 minutes were 43% ± 9, 93% ± 11, and 106% ± 17, and the corresponding values at 60 minutes were 35% ± 5, 62% ± 10, and 72% ± 16, respectively. The relaxivities in water (2.0 T; 25°C) were 4.4, 5.5, and 5.6 $mmol^{-1}Lsec^{-1}$, respectively.
Conclusion: Liver gadolinium concentrations closely correlate with MRI liver enhancement values but do not correlate with biliary gadolinium excretion levels. Relatively minor structural modifications of chelates can have significant effects upon their biliary excretion without large changes in their in vitro relaxivity and MRI efficacy. Biliary elimination results alone are not necessarily good indicators of MRI efficacy for hepatobiliary contrast agents.
L. Milco, D. Marinkovic, G. Shevlin, and T. Best are employees of Molecular Biosystems, Inc. D.L. White and V.S. Vexler have a research contract with Molecular Biosystems, Inc.

053 • 4:05 PM

Mechanisms of Myocardial T1 Enhancement after Bolus Administration of Contrast Agent

RM Judd, MK Atalay, EA Zerhouni
The Johns Hopkins University, Baltimore, MD

Purpose: To determine the effects of myocardial water exchange rates, if any, on the relationship between contrast concentration and myocardial T1 for bolus administration of contrast.
Methods: Contrast agents were administered under controlled hemodynamic conditions in six isolated, perfused, nonbeating canine interventricular septa. Myocardial T1 was estimated three times per second, based on the attenuation of T1-weighted FIDs. Polylysine Gd-DTPA (Schering) and gadoteridol (Squibb) were administered at several concentrations and two coronary flows. The concentrations were carefully chosen to represent expected in vivo concentrations.
Results: For polylysine Gd-DTPA, the change in myocardial 1/T1 (ΔR1) during bolus transit did not scale linearly with contrast concentration, consistent with a limitation of myocardial water exchange across the capillary wall. For gadoteridol, ΔR1 scaled roughly linearly with contrast concentration, but the magnitude of ΔR1 was much smaller than that predicted on the basis of fast myocardial water exchange.
Conclusion: The results can be explained on the basis of a limited vascular-interstitial water exchange, resulting in a dramatic increase in T1 enhancement on a per-molecule basis when the contrast agent enters the myocardial interstitium. We conclude that myocardial first-pass T1 enhancement, with use of clinically approved contrast agents, primarily represents extravasation of contrast.

054 • 4:15 PM

Optimization of a Negative Oral Contrast Agent for MR Imaging: First Clinical Results

MD Davis, TH Pels Rijcken, SA Fine
Department of Radiology, University of Massachusetts Medical Center, Worcester, MA

Purpose: Previous in vivo animal studies, aimed at developing a negative oral MRI contrast agent, showed favorable results on T1- and T2-weighted images with barium sulfate and bentonite mixed together (1). This material is safe, relatively inexpensive, and FDA approved for GI radiography. We investigated the effect of the barium sulfate and bentonite (Ba-Ben) suspension on T1- and T2-weighted image quality and tolerance in patients.
Methods: Six patients undergoing abdominal MRI studies were scanned at 1.5 T, with SE and FSE sequences, on a GE Signa MR unit. Suspensions of Ba (25%–40% w/w) containing Ben (2.5–4.0% w/w) were used. Patients were NPO-for-

solids 6 hours before imaging. Oral administration of 450–800 mL of the Ba-Ben mixture was performed 60 and 30 minutes before the MRI study.

Results: The Ba-Ben mixtures gave excellent contrast on T2- and generally good contrast on T1-weighted images. All sequences exhibited good bowel filling and depiction with less artifact than noncontrast controls. Patient tolerance was good, although most commented on the "chalky" taste of the mixture. All patients, except one, drank the prescribed dose (the one patient drank 450 of 600 mL).

Conclusion: The Ba-Ben mixtures and perflubron are currently the only negative MRI oral contrast agents available for clinical use. Our initial clinical use of the Ba-Ben agent showed good results with respect to bowel filling, delineation from adjacent structures, and reduction of motion artifacts. SNR, CNR, and SIR values for tissue signal intensities and background noise will be presented. Patient tolerance was good but can be improved by adding flavoring to the mixture.

1. Michael A. Davis MD, ScD, Hong Mei MSc, Ger H. Ritsema MD, PhD. Optimization of Barium-Based Formulations as Negative Oral Contrast Agents for MRI. Presented at the 41st annual meeting of the Association of University Radiologists, May 1993, Cincinnati, OH.

M.D. Davis is a consultant for E-Z-Em, Inc.

055 • 4:25 PM

Novel Technique for Quantification of Tissue Blood Volume with Ultrashort-TI Inversion-Recovery Echo-Planar MR Imaging

DM Shames, TP Roberts, CF Van Dijke, A Mühler, JS Mann, RC Brasch

Department of Radiology, University of California, San Francisco, Berkeley, CA

Purpose: Quantification of fractional tissue blood volume (TBV_f) with use of spin-lattice relaxation rates (R_1) determined before and after administration of macromolecular Gd-labeled contrast media has been impeded by the inability to account for the effects of water proton exchange across the capillary endothelium. We propose a novel technique of determining the R_1 of tissue by measuring R_1 before proton exchange has had time to produce significant effects on longitudinal relaxation.

Methods: Axial images of the liver were acquired in four rats with ultrashort TI inversion recovery (ULSTIR) echo-planar imaging (EPI) before and 3 minutes after injection of albumin $(Gd\text{-}DTPA)_{35}$. Images were obtained with TIs of 5–100 ms. For comparison with the standard technique of measuring tissue R_1, additional longer TIs were employed (up to 3.4 sec). The ratio of ΔR_1s (postcontrast R_1 minus precontrast R_1) of liver to blood corresponding to the TBV_f of liver was compared with in vitro measurement of the TBV_f of liver determined by measurement of Gd with inductively coupled plasma atomic emission spectroscopy.

Results: Estimates of the TBV_f of liver with ULSTIR (.264 ± .054) were closer to those measured in vitro (.301 ± .061) than were estimates made using standard R_1 measurements (.209 ± .089). Furthermore, as predicted by theory, the conventional estimates of TBV_f were less than those obtained by using ULSTIR in three of four rats.

Conclusion: A novel technique developed for estimation of TBV_f, ultrashort TI inversion recovery imaging, is more accurate than conventional R_1 imaging because it corrects for the effects of water proton exchange across membrane barriers on longitudinal relaxation rate.

056 • 4:35 PM

Evaluating the Influence of Draining Afferent Lymphatic Vessels on the Accumulation of USPIO in Lymph Nodes

X Zhang, A Mühler, HJ Weinmann

MRI Contrast Media Research, Schering AG, Berlin, Germany

Purpose: Previous reports have demonstrated two pathways contributing to the delivery of ultrasmall superparamagnetic iron oxide (USPIO) to the lymph nodes following intravenous administration. The present study quantitatively assessed the influence of the draining lymphatic vessel obstruction on the clustering of USPIO in lymph nodes.

Methods: Afferent lymphatic ligation (n = 5) and sham ligation (n = 3) of the right popliteal lymph nodes were performed in rats with hyperplastic nodes induced by subcutaneous injection of egg yolk emulsion into the foodpads. The contralateral limb and normal rats (n = 5) served as controls. A dose of 200 μmol/kg of USPIO was intravenously administrated 24 hours following surgery. Three rats without injection of USPIO served as baseline controls. The rats given USPIO were sacrificed 24 hours after USPIO administration, and their bilateral popliteal lymph nodes were removed. Iron concentrations were measured by means of ICP-AES at a wavelength of 342.247 nm and calculated as μmol/g of lymphoid tissue.

Results: The complete afferent lymphatic obstructions were demonstrated by a strong Evans blue staining of popliteal nodes in the sham ligated group and no visible staining in the ligated group. The relevant results of iron concentration measured by means of ICP-AES were summarized as follows: ligated group, right, 1.97 μmol/g lymphoid tissue ± 0.45, left, 1.95 μmol/g ± 0.44; sham-operated group; right, 1.89 μmol/g ± 0.48, left, 1.95 μmol/g ± 0.28; normal controls, 2.04 μmol/g ± 0.42; and baseline controls, 1.25 μmol/g ± 0.21. Thus, the accumulated amounts of iron in the rats with afferent lymphatic obstruction were virtually identical to those in sham-operated and normal control rats.

Conclusion: The results of the current study confirm that the permeable membranes of intranodal blood capillaries are the major delivery pathway following intravenous injection of USPIO in rats. Even in the situation of lymphatic edema, these results may imply effective use of MR lymphography with USPIO.

057 • 4:45 PM

New Selective MR Contrast Agent, Ferrioxamine–Dermatan Sulfate: Improved Enhancement of AT-1 Rat Prostate Carcinomas

EJ Dadey, RP Mason, DF Ranney, J Fareed, D Hoppenstradt, A Constantinescu, H Chen, JM Zadei, PP Antich

Access Pharmaceuticals, Inc; University of Texas Southwestern Medical Center, Dallas, TX; and Loyola University Medical Center, Maywood, IL, Dallas, TX

Purpose: A novel water-soluble selective T1 MRI contrast agent was prepared by binding ferrioxamine (F), a stable paramagnetic iron(III) chelate, to dermatan sulfate (DS), an acidic glycosaminoglycan carrier with polyvalent affinity for neovascular endothelial cells. Our goal was to assess the selectivity, potency, subregion delineation, and site-retention time of F-DS.

Methods: T1-weighted, 3D spin-echo (TR/TE = 250/8) images of transplanted 1–2.5-cm AT-1 prostate carcinomas of Copenhagen rats were acquired at 4.7 T, before and 7, 20, 40, and 60 minutes after injection (MPI) of F-DS (0.155 mmol/kg). Histologic staining was performed at 60 MPI to correlate metal-ion positivity.

Results: With F-DS (n = 10), the rapidly and highly perfused vascular tumor pedicle and outer rim exhibited pronounced immediate ($\leq$7 MPI) and sustained ($\geq$60 MPI) MRI enhancement; the less rapidly perfused central tumor subregions exhibited much lower immediate enhancement but achieved significant delayed enhancement (40–60 MPI). Good subregion delineation was possible at times up to 40 MPI. Histologic stains were highly positive in the outer tumor rim and moderately positive in the central tumor; both subregions stained positively at endothelial, subendothelial, and tumor intracellular sites. Free F (no carrier; 0.155 mmol/kg; n = 6) gave no significant MRI enhancement. Gadolinium-DTPA (0.100 mmol/kg; n = 6) gave much lower rim and overall tumor enhancement, with rapid washout (20–40 MPI) and delayed sequestration in isolated central sites.

Conclusion: F-DS (*a*) selectively adheres to tumor-induced endothelium, (*b*) loads tumor extracellular and intracellular sites, (*c*) gives rapid and sustained tumor enhancement, and (*d*) improves imaging selectivity, potency, temporal flexibility,

and delineation of tumor boundaries and functional subregions.

E.J. Dadey is MRI project manager at Access Pharmaceuticals, Inc.

058 • 4:55 PM

Na-23 T2 Imaging of the Rat Kidney

N Bansal, V Seshan, MJ Germann
Department of Radiology, University of Texas Southwestern Medical Center at Dallas, Dallas, TX

Purpose: The analysis of sodium relaxation time may furnish direct information on the environment surrounding the examined nuclei and on its functional aspects. This study was planned to investigate the regional T2 relaxation characteristics of Na+ in rat kidney by means of 3D Na-23 imaging.

Methods: The left kidney of anesthetized rats was exposed via a flank incision and placed in a volume coil. 3D Na-23 images were collected on a 4.7-T Omega system using a spin-echo sequence with exorcycle phase cycling at echo times of 2.5, 5, 10, 20, 30, and 40 ms. The signal intensities at each pixel were fit to a monoexponential function to obtain 3D sodium T2 maps.

Results: The 3D T2 images demonstrated a significant heterogeneity of sodium relaxation times in different regions of the kidney. The measured T2 relaxation times ranged from 5 to 50 ms with a median at 17 ms. The average T2 times were longer in the medullary region of the kidney than in the cortex, because the renal medulla has more extracellular sodium.

Conclusion: These results demonstrate that Na-23 MR imaging can be used to determine the regional characteristics of sodium in the kidney in vivo. This technique should prove useful in understanding the mechanism by which the whole kidney handles sodium under different physiologic conditions.

059 • 5:05 PM

Tumor Architecture: A Chronologic Perspective with F-19 3D MR Imaging

RP Mason, P Peschke, EW Hahn, A Constantinescu, PP Antich
Department of Radiology, University of Texas Southwestern Medical Center, Dallas, TX

Purpose: MRI provides a noninvasive means for long-term monitoring of tumor growth or regression. We have developed a novel approach for investigating tumor architecture using combined F-19 and H-1 MRI following infusion of perfluorocarbon emulsion.

Methods: We examined the Dunning prostate tumor AT1 grown in a skin pedicle and a Novikoff hepatoma in the thigh. When the tumors reached ~1 cm, Oxypherol (4 × 4-mL emulsion of perfluorotributylamine) was infused over 2 days in tumor-bearing rats, which were then examined with 3D H-1 and F-19 MRI for several weeks at 4.7 T.

Results: H-1 MRI disclosed no structural heterogeneities in either tumor. F-19 MRI revealed the distribution of perfluorocarbon in the tumors. After 2 days vascular clearance was complete and F-19 MRI revealed the enhanced peripheral distribution of sequestered PFC in the AT1. Over the next 16 days the tumor doubled in diameter. Comparison of sequential images indicated that the PFC largely retained its original distribution and did not redistribute, indicating preferential growth from the periphery outward. For the Novikoff hepatoma F-19 MRI indicated a multinodular tumor structure with peripheral PFC. Over a period of weeks the tumor regressed spontaneously and the outline of the PFC was observed to shrink but essentially maintain a constant pattern.

Conclusion: Sequestered PFC provides architectural landmarks by which growth and regression are readily perceived. The long-term retention of PFCs makes them particularly appropriate for the assessment of relatively slow tissue remodeling processes.

060 • 5:15 PM

Novel F-19 MR Imaging Agents: Imaging Potential with Polylysines

VD Mehta, RP Mason, PV Kulkarni, PP Antich
Advanced Radiological Sciences, University of Texas Southwestern Medical Center, Dallas, TX

Purpose: Fluorine-labeled probes with prolonged retention in the vascular compartment should facilitate F-19 MR investigations of tumors, lesions, and regions of inflammation. As part of our continuing efforts, we report the imaging potential of a novel F-19–labeled macromolecular probe, TFA-polylysine (TFA-PLL).

Methods: The amino groups in polylysine (98k, Sigma) were selectively trifluoroacetylated with S-ethyltrifluorothioacetate to produce TFA-PLL. The product was isolated in good yield (85%) and characterized by means of F-19 MR spectroscopy and imaging. A phantom containing 40 mg of TFA-PLL in 1 mL of methanol was used for imaging experiments.

Results: TFA-PLL exhibits a single sharp F-19 MR resonance with a line width of ~40 Hz and chemical shift essentially coincident with CF_3CO_2Na. F-19 relaxation times were found to be ~700 ms for T1 and ~100 ms for T2 at 4.7 T. F-19 images of the phantom were obtained in 1 minute with a driven-equilibrium enhanced spin-echo sequence with a signal-to-noise ratio (SNR) of ~7 and in-plane resolution of ~700 μm. This represents significant enhancement in F-19 detection sensitivity compared with TFA-albumin (SNR of ~4 in 20 minutes for the same concentration).

Conclusion: Polylysines have been successfully derivatized, providing fluorine-labeled molecular probes with useful MR characteristics. The degree of labeling is sufficient to facilitate imaging with exceptional time resolution. Further investigations for faster imaging and to assess in vivo applications are in progress.

Monday Afternoon • Monet Room
Papers 108–109

CONTRAST AGENTS I

MODERATORS: RL Nunnally, PhD
DD Stark, MD

108 • 5:09 PM

Gadobutriol: A New Contrast Agent Used in Female Breast MR Imaging

HJ Oellinger, BR Balzer, RT Petzhold, TE Bomhard, HB Schedel, RN Felix
Universitatsklinikum Rudolf Virchow, Freie Universität, Berlin, Germany

Purpose: For gadobutriol (Schering, Berlin, Germany), a new MR contrast agent, the optimal dose for female breast MR imaging (FBMRI) is being evaluated in a G II phase study.

Methods: Fifteen patients with signs suspicious for malignancy at mammography or sonography (mean age, 44.3 yrs) were investigated with FBMRI. They were subdivided into three groups, with each group receiving a different bolus of gadobutriol (0.1, 0.2, or 0.3 mmol/kg). A 1.5-T, Magnetom SP 63 imager was used, with a double breast coil (Siemens, Erlangen, Germany). A FLASH 3D sequence was used, with a semidynamic, thin-layer method.

Results: Thirteen carcinomas were diagnosed and histologically verified. At 0.1 mmol/kg the enhancing characteristics of gadobutriol seem to be equivalent to those of gadolinium. Two patients had a proliferative mastopathia of higher order only, and two showed multifocality not seen before with mammography. The bolus of 0.2 mmol/kg seems appropriate for the FBMRI method used.

Conclusion: For the semidynamic thin-layer FBMRI method, 0.2 mmol/kg seems to be the correct dose, but this finding is only preliminary.

109 • 5:19 PM

Lesion Detection as a Function of Contrast Dose in Gd-enhanced MR Imaging of Brain Metastases

P Van Dijk, M Oudkerk, MA Vereijcken, TJA Kuijpers, PE Sijens
Department of Radiology, Dr Daniel den Hoed Cancer Center, Rotterdam, The Netherlands

Purpose: An MR imaging study with three doses of Gd-DTPA was performed in patients suspected of brain metastases to define an optimal dose for screening metastases.
Methods: The MR protocol consisted of axial T1W scans (TR = 610 ms, TE = 14 ms) at cumulative doses of 0, 0.1, 0.2, and 0.3 mmol/kg, spaced at 8-minute intervals, and a blank T2W scan (TR = 2,000 ms, TE = 80 ms). A quantitative evaluation of the contrast between metastases and normal brain parenchyma was performed, with a constant ROI used through the four series. The size and homogeneity of the lesion were recorded as well. The images on film were independently analysed by three radiologists. Per dose, the number of metastases larger than 3 mm was recorded. The patient population consisted of 107 persons, in 39 of whom brain metastases were diagnosed.
Results: The quantitative results for contrast in 300 metastases showed a steady increase with dose. This was reflected in the increasing total number of metastases found on the images for different doses: 96, 278, 310, and 365, respectively, ie, changes after contrast agent administration of 190%, 12%, and 18%, respectively. In one case, metastases were found first at 0.2 mmol/kg and in one case at 0.3 mmol/kg. Furthermore a good correlation of contrast uptake with lesion size was found for homogeneously enhancing metastases.
Conclusion: The detection of more brain metastases at a higher dose of contrast medium was established. Differentiation of results according to lesion size, underlying tumor, and treatment will be the subjects of further study.

Monday Afternoon • Metropolitan Room
Papers 118–119

BRAIN II: Rapid Imaging

MODERATORS: RL De La Paz, MD
FJ Laine, MD

118 • 5:09 PM

Value of Echo-Planar Imaging in the Detection of Brain Lesions

B Siewert, S Warach, MR Patel, MF Mueller, CM Poser, PA Wielopolski, RR Edelman
Department of Radiology, Beth Israel Hospital, Boston, MA

Purpose: To assess the utility of echo-planar imaging (EPI) for the detection of brain lesions.
Methods: EPI and conventional T2-weighted spin-echo imaging (SE) were compared in 15 patients with multiple sclerosis. A 1.5-T whole-body imager with EPI capability was used. A double-echo T2-weighted SE sequence was performed, with TR/TE of 2,400 ms/30–80 ms and an acquisition time of 7 min 44 sec. EPI sequences (128 × 128 matrix) included proton density (EPI-FID) and T2-weighted (EPI SE T2) as well as high-resolution (256 × 256 matrix) EPI images. An entire 20-slice brain screen can be completed in as little as 1 sec. The sequences were compared regarding signal-difference-to-noise (SD/N) measurements and sensitivity.
Results: With the conventional SE T2-weighted sequence used as the gold standard, 285 lesions were depicted. High-resolution EPI (sensitivity, 90%) was superior to EPI-FID (83%) and EPI SE T2 (80%) for lesion detection. Lesions missed with EPI were either small (81% were smaller than 5 mm), obscured by susceptibility artifacts at the skull base or frontal sinuses (13%), and/or located close to the cerebrospinal fluid, from which they were indistinguishable (16%). Comparison of SD/N between sequences showed a significant effect attributable to the higher mean SD/N for conventional SE T2 ($P < .01$) relative to other sequences.
Conclusion: EPI is of diagnostic value for lesion detection, especially in uncooperative and unstable patients and for lesions larger than 10 mm.

119 • 5:19 PM

Fast Three-dimensional Volume Imaging with Optimized Burst Excitation Pulses

SL Talagala, L Zha, IJ Lowe
Department of Radiology, University of Pittsburgh, Pittsburgh, PA

Purpose: An optimized version of the burst imaging method with improved SNR has been demonstrated recently with a clinical scanner. Since the SNR of this technique is inherently low, we have explored 3D acquisitions, using optimized burst excitations as a means of improving SNR.
Methods: In the optimized burst method, a train of echoes is collected by refocusing the magnetization produced by a train of low-flip-angle RF pulses of phases 0°/180°. In the 3D version, multiple echo trains were collected. Each echo train (64 echoes) was phase encoded along two dimensions by the use of a constant, low-level encoding gradient and a variable-amplitude pulsed gradient. Slab selection was accomplished during the refocusing pulse. A second 180° pulse was applied after the echo train to drive the longitudinal magnetization (undisturbed by the excitation RF train) inverted by the refocusing pulse toward the equilibrium condition.
Results: 3D data of the brain, encompassing a 32 × 16 × 16-cm volume, were collected with a matrix size of 128 × 64 × 32 (freq/phase/slab) and a 2-s TR. The effective TE was 40 ms, and the scan time was 64 s. The SNR of images obtained at 1.5 T was 63:1. Images exhibited contrast similar to T2 weighting, and blood vessels appeared dark.
Conclusion: Fast 3D imaging with reasonable SNR and resolution can be performed by using optimized burst RF excitation. The advantage of this approach is that contrast similar to T2 weighting can be realized with short scan times and low RF power deposition.

Monday Afternoon • Miro Room
Papers 127–128

PELVIS: Female

MODERATORS: JJ Brown, MD
RC Smith, MD

127 • 4:57 PM

Subtraction Technique: A Helpful Method for Cervix Carcinoma Staging in MR Imaging

HJ Oellinger Jr, TH Bomhard Jr, AT Mackela Jr, NE Hosten Jr, WL Lichtenegger, RN Felix
Universitätsklinikum Rudolf Virchow, Freie Universität, Berlin, Germany

Purpose: The infiltration of the parametrial tissue in cervix carcinoma staging is still difficult to assess. This problem was approached by using the subtraction technique.
Methods: Forty-three patients between 30 and 76 years of age (median, 50.1 years) with clinical signs of cervix cancer were investigated preoperatively with MRI. A 1.5-T Magnetom SP unit was used (Siemens, Erlangen, Germany). A body coil was used in 11 patients, a Helmholtz coil in 32. T2- (sagittal plane) and T1-weighted (three planes) SE sequences were used, with Gd-DTPA enhancement (0.1 mmol/kg; Schering, Berlin, Germany). Data postprocessing included calculation of subtraction images. All MRI findings were histologically verified.
Results: MRI gave the right diagnosis with respect to FIGO in 86%. The subtraction images contributed to the right diagnosis in 16% (7 patients). The most important planes were the sagittal for T2- and coronal for T1-weighted images. Lymph nodes were difficult to detect. A positive correlation was found between carcinoma volume and lymph node status.

Conclusion: Compared with other imaging modalities, MRI appears to be the most reliable method. If tumor volume is a reliable indicator for lymph node staging, MRI can probably help avoid an unnecessary laparatomy.

128 • 5:07 PM

MR Imaging of Male Infertility with an Endorectal Surface Coil

MJ Kim, JT Lee, MS Lee, PS Choi, JS Suh, HS Yoo
Department of Diagnostic Radiology, Yonsei University College of Medicine, Seoul, Korea

Purpose: To assess the ability and usefulness of endorectal surface coil MR imaging for evaluation of the uroseminal tract in male infertility.
Methods: We studied a select group of 16 men (aged 27–38 years) who were referred for the evaluation of suspective obstructive azoospermia. MR images were obtained with a 1.5-T (GE) system and an endorectal coil (Medrad). Axial, sagittal, and coronal images were obtained with a fast spin-echo long TR/TE technique, and axial spin-echo short TR/TE images were also obtained. A 10–12-cm of field of view and 3–5-mm scan thickness was used.
Results: Two mullerian duct cysts were detected. In one, the seminal vesicles (SV) and ejaculatory duct (EJD) were mildly dilated. In the other, aplasia of the SV and vas deferens (VD) was associated. Two other cases of aplasia of the SV and VD were associated with eccentric elongated cystic structure from rudimentary EJD. In one patient with a previous long-standing Foley catheter, a degenerative prostatic cyst with hemiatrophy of the prostate and SV was demonstrated. Mild dilatation of the EJD, VD, and SV was seen in one patient, in whom vasography showed no obstruction and implied functional uroseminal obstruction. In two patients with previous history of pulmonary or genitourinary tuberculosis, diffuse thickening and a beaded appearance of the VD and SV were demonstrated. Two remaining patients had only atrophy of prostate and/or SV.
Conclusion: High-resolution MR imaging with an endorectal surface coil can depict in fine detail the anatomic structure of the prostate and ejaculatory apparatus and may have great potential in the evaluation of male infertility.

Monday Afternoon • Morocco Room
Papers 138–139

CARDIAC

MODERATORS: B Chen, MD
ER McVeigh, MD

138 • 5:09 PM

Comparison of Gd-EOB-DTPA–enhanced MR Imaging with Precontrast Fast and Conventional Methods for Experimentally Induced Hepatic Tumors in Rats

MJ Kim, JS Suh, YN Park, HS Yoo
Department of Diagnostic Radiology, Yonsei University College of Medicine, Seoul, Korea

Purpose: To evaluate the efficacy of Gd-EOB-DTPA as a hepatic contrast agent in MR imaging of experimentally induced hepatic tumors, in comparison with fast scanning sequences and conventional spin-echo techniques.
Methods: Hepatic tumors were induced in 12 male Sprague-Dawley rats by feeding of 3-methyl-dimethylaminobenzene for 12 weeks. MR images were obtained with a 1.5-T (GE) system. A dual TMJ coil was used. T2-weighted fast spin-echo (FSE), T1- and T2-weighted conventional spin-echo (CSE), and fast multiplanar spoiled gradient recalled (FMPSPGR) images were obtained. After intravenous injection of 0.1 mmol/kg of Gd-EOB-DTPA, spin-echo T1WI were obtained. The number and contrast-to-noise ratio of the tumors were compared for each sequence.
Results: Overall, 125 tumors were developed. 62% of the tumors were detected on Gd-EOB-DTPA–enhanced T1WI, 36% on conventional T2WI, 39% on T1WI, 59% on FMPSPGR, and 63% on FSE. For tumors more than 5 mm in diameter, the sensitivity was 95% on Gd-EOB-DTPA–enhanced T1WI, 63% on CSE T2WI, 85% on CSE T1WI, 88% on FMPSPGR, and 88% on FSE, respectively. The relative contrast-to-noise ratios compared with FSE were 1.02 for Gd-EOB-DTPA–enhanced T1WI, 0.38 for T2WI, 0.47 for T1WI, and 0.64 for FMPSPGR.
Conclusion: Gd-EOB-DTPA was very useful for increasing the sensitivity and lesion conspicuity for detection of experimentally induced hepatic tumors. Among the precontrast techniques, FSE T2WI appears the most sensitive method, and tumor-to-liver contrast is also highest on FSE images. FMPSPGR imaging compares favorably with CSE T1WI on precontrast scans.

139 • 5:19 PM

Interleaved Echo-Planar Imaging of the Heart

DR Wetter, JF Debatin, GC McKinnon, JA Börner, M Unterweger, GK von Schulthess
Department of Radiology, MRI Center, University Hospital, Zurich, Switzerland

Purpose: The cardiac imaging ability of multiple-shot interleaved echo-planar imaging sequences (EPI) was evaluated as a function of (*a*) the number of interleaves and (*b*) sequential versus nonsequential interleaved acquisition.
Methods: Axial EPI images of the heart were obtained, breath held, in 10 subjects, with the following parameters: 0.5 NEX, 1.6 × 1.6-mm spatial resolution, 10-mm slice thickness, and 45° flip angle. The TR/TEs were 128/14.7 ms, 64/9.9 ms, and 32/7.9 ms, for single shot, two shots, and four shots, respectively. For each sequence the visibility of the coronary arteries and the internal mammary arteries, as well as the ability to distinguish myocardium from intraventricular signal, was graded on a scale of 1–4. In addition, signal-to-noise ratio, contrast-to-noise ratio, and signal homogeneity were determined for the ventricular lumen and myocardium.
Results: Multishot sequences significantly improved the visibility of the evaluated small structures. Intraventricular signal with these sequences was more homogeneous ($P < .1$), facilitating easier myocardial identification. Because of more temporal averaging, sequentially acquired images were characterized by more blurring ($P < .1$). The contrast-to-noise ratio of myocardium to intraventricular signal was worst for single-shot EPI and best for nonsequential interleaved EPI.
Conclusion: Interleaved EPI consistently rendered higher-quality images than single-shot EPI. The nonsequential technique appears superior to sequential acquisitions.

Monday Afternoon • Sapphire Room
Papers 148–149

SPECTROSCOPY I: Techniques

MODERATORS: HC Charles, MD
PA Narayana, PhD

148 • 5:09 PM

Selection of K-Space Samples in Spectroscopic Imaging

SJ Reeves
Department of Electrical Engineering, Auburn University, Auburn, AL

Purpose: Reconstructed images from MR spectroscopic imaging (SI) can be improved significantly by incorporating a priori information such as region of support or smoothness constraints into the reconstruction process. However, in the presence of a priori information, certain irregularly spaced sets of k-space samples will provide significantly more information about the original image than a regularly spaced set. The purpose of this work is to exploit a priori information about the object being imaged to choose the set of k-space samples that minimizes the error in the reconstructed image.
Methods: We derive a simple criterion for selecting k-space samples given region of support information. Assuming a

least-squares reconstruction, this criterion represents the mean-square error in the reconstructed image as a function of a set of k-space samples. This criterion is particularly attractive for optimization. We show that the criterion can be updated efficiently for use in a suboptimal but powerful sequential search strategy. Furthermore, the criterion increases monotonically as the number of selected samples is decreased, making the optimal branch-and-bound search strategy applicable.
Results: For a simple 28-point signal with a 15-point region of support, the suboptimal optimization strategy yielded a mean-square error only 7% above the optimal value at a small fraction of the computational expense. Furthermore, the resolution can be improved significantly over the results obtained with equally spaced k-space samples.
Conclusion: The resulting technique provides much more informative data for SI. Thus, image quality can be improved and/or imaging time can be reduced.

149 • 5:19 PM
Correction of Chemical Shift Displacement by Polarity-cycled Gradient-aligned Slice Selection
JW Hugg, Q Jiang, RA Knight, RJ Ordidge
Neurology Department, Henry Ford Health Sciences Center, Detroit, MI

Purpose: Slice selection is plagued by chemical shift displacement: ie, slices are misaligned because nuclei have differing chemical shifts. This effect can be important in both imaging and volume-localized spectroscopy. Since displacement follows gradient direction, cycling the gradient polarity can ameliorate the chemical shift artifact.
Methods: We modeled the gradient-aligned slice-selection (GASS) scheme on a Macintosh Centris 650 and tested it (MRI, H-1 STEAM, and P-31 ISIS) using our 3-T Magnex clinical system with SMIS console. When the polarity of slice-selection gradients (and RF frequency offsets), are cycled, the chemically shifted slices become concentric, greatly increasing their overlap. By adding outer-volume suppression with opposing-polarity selection gradients, the aligned slices can be collimated to greatly reduce signal contamination from outside the nominal slice. Two averages are required for each selection axis (two for slice, four for column, eight for rhomboid volume).
Results: For example, at 1.5 T with 0.3 G/cm selection gradients, the ISIS slices for PME and β-ATP are shifted ±5.7 mm along each axis, resulting in an overlap of only 24% for misaligned $(3\ cm)^3$ volumes. With GASS, PME/β-ATP overlap becomes 100%, and the mean overlap for all P-31 peaks increases from 63% to 84%. GASS also reduces the outer-volume contamination mean from 8% to less than 1%.
Conclusion: Any imaging or spectroscopy sequence with slice selection can be GASSed to greatly reduce chemical shift misalignment artifact. Outer-volume suppression can reduce contamination.

Monday Afternoon • Topaz Room
Papers 157–159

IMAGING TECHNIQUES I
MODERATORS: CR Crawford, PhD
J Listerud, MD, PhD

157 • 4:57 PM
Phase Encoding with Abbreviated Flow Compensation
G Cao, DS Sherrill, DL Parker, Y Du
Radiology Department, University of Utah Medical Center, Salt Lake City, UT

Purpose: To achieve correct spacial location of vessels, first-order gradient moment nulling must be applied to the phase-encoding axes. However, gradient moment nulling prolongs TE, which may degrade the flow image in regions of complex flow. Phase encoding with abbreviated flow compensation (PEAFC) applies partial flow compensation to the phase-encoding (PE) axis to prevent spatial misregistration of vessels without extending TE.
Methods: A 3D time-of-flight pulse sequence was modified to implement PEAFC. Below a cutoff spatial frequency value, the PE steps are fully compensated, and above the cutoff value the compensation is incomplete. The spatial difference is zero at the cutoff and increases with increasing PE value. Thus the high spatial frequencies of a flowing structure will be mismapped, which can blur vessels. The blurring is governed by the cutoff value and the flow speed. The cutoff value depends on the imaging prescription (slice thickness, FOV, matrix size, etc). We evaluated our pulse sequence in both a phantom and a healthy volunteer.
Results: In agreement with theoretical predictions, phantom images demonstrate that PEAFC correctly placed flow entirely within the tube. In the in vivo study, some intracranial vessel locations without PEAFC differed significantly from their locations with PEAFC. PEAFC images demonstrate correctly imaged flow without significant blurring.
Conclusion: PEAFC prevents spatial misregistration of flow without the longer TE and avoids the image degradation associated with complete flow compensation.

158 • 5:07 PM
Correction of Geometric Distortion with Bipolar Gradients and Polynomial Basis Functions
CR Crawford, AM Linz
GE Medical Systems, Milwaukee, WI

Purpose: To correct geometric distortion caused by patient-induced magnetic susceptibility for MRI applications such as interventional procedures. Extant methods are limited because of the need to unwrap phase (1) or to solve differential equations (2).
Methods: Two images are generated at the same location with use of bipolar polarity readout gradients. Susceptibility will generate geometric distortions, denoted warpings, along the frequency-encode axis on the two images. The direction of warping is reversed in the two images because of the bipolar gradient. Using the two images, a parametric model of the warp can be generated. The model is then used to generate an image without geometric distortion. To model the warp, a basis series expansion consisting of a finite number of orthogonal polynomials is used. The coefficients of the expansion are found by maximizing the integral of the product of the two images after unwarping each image with the model. The first two terms of a Taylor series approximation generates a set of linear equations.
Results: Computer simulations and phantom scans demonstrate that the method corrects low-frequency geometric distortions. Multiple iterations are required to overcome the use of the Taylor series.
Conclusion: A polynomial basis series expansion corrects patient-induced geometric distortion. Additional work is required to remove limitations of the Taylor series approximation and to explore its clinical application.
1. Sunanaweera TS, et al. *IEEE TMI* 1993; 12:251.
2. Chang H, Fizpatrick JM, *IEEE TMI* 1992; 11:319.

159 • 5:17 PM
Short-TR 3D Partial-Flip-Angle Spin-Echo MR Microscopy of Trabecular Microstructure
H Chung, FW Wehrli, H Jara, SL Wehrli
Department of Radiology, University of Pennsylvania Medical Center, Philadelphia, PA

Purpose: To design and implement a rapid 3D spin-echo pulse sequence for microscopic imaging of magnetically inhomogeneous biomaterials and demonstrate its utility for the characterization of trabecular microstructure.
Methods: Intravoxel phase dispersion at the bone marrow interface precludes gradient-echo techniques at high field. 3D spin-echo imaging is hampered by its excessive scan times. For this purpose, a 3D version of RASEE (rapid spin-echo excitation) (1,2) was implemented on a 9.4-T Bruker AM-400 spectrometer/microimaging system. Following marrow removal trabecular bone specimens were suspended in 1 mM

Gd-DTPA aqueous solution to shorten T1 to about 300 ms (comparable to that of fatty marrow).
Results: At TR = 60 msec, isotropic 128^3 data sets from 1-cm^3 specimens were obtained in 20 minutes, providing SNR > 10. Under these conditions the images can easily be segmented for quantitative micromorphometric analysis (3). Images reformatted in the three orthogonal planes demonstrate orientation of trabeculae and permit quantification of structural anisotropy.
Conclusion: It has been shown that 3D partial-flip-angle spin-echo MR microscopy is possible in heterogeneous systems, saving a factor of 5–10 in scan time relative to conventional spin-echo techniques. In contrast to fast spin echo, RASEE does not suffer from point spread function blurring at short T2. Finally, the method has potential for nondestructive bone histomorphometry.
1. AR Bogdan, PM Joseph, *Magn Res Imaging*, 8, 13–19 (1990). 2. H Jara, FW Wehrli, H Chung, *Magn Res Medicine*, 29, 528–539 (1993). 3. Z Wu, H Chung, FW Wehrli, *Magn Res Medicine*, in press (1994).

Tuesday Morning • Monet Room Paper 208

MAMMOGRAPHY: Silicone

MODERATORS: PJ Fritzsche, MD
TA Spraggins, PhD

208 • 11:54 AM

Initial Experience with Gadoteridol as a Contrast Agent for Breast MR Imaging

CW Piccoli, T Matteucci, DG Mitchell
Thomas Jefferson University Hospital, Philadelphia, PA

Purpose: To evaluate the efficacy of gadoteridol as a breast MRI contrast agent.
Methods: Thirty-one patients scheduled for biopsy of either a clinically palpable or a mammographically or sonographically suspicious breast abnormality underwent breast MRI at 1.5 T. Dynamic multiplanar spoiled gradient echo or 3D inversion-recovery prepared GRASS imaging was performed before and after the intravenous administration of 0.1, 0.2, or 0.3 mmol/kg of gadoteridol (Squibb Diagnostics, Princeton).
Results: Twenty-eight patients were biopsied. Twenty patients had only benign findings. Eight had "aggressive" lesions: seven malignancies, one phylloides tumor. Six "aggressive" lesions were detected prospectively with MRI. Retrospectively, one 6-mm intraductal carcinoma was identified as a mildly enhancing linear focus. A 5-mm intraductal carcinoma was obscured by mild diffuse enhancement in an area of prior surgery. Both lesions were detected as microcalcifications at mammography. Occasionally, strong diffuse parenchymal enhancement occurred on the delayed images in premenopausal patients receiving the higher doses, in one case completely obscuring a 2-cm carcinoma. For this preselected population, the categories of (*a*) combined clinical, mammographic, and sonographic examination; (*b*) mammography and/or sonography; and (*c*) MRI, respectively, sensitivity was 100%, 88%, and 75%; PPV was 29%, 26%, and 75%; and specificity was 5%, 40%, and 76%.
Conclusion: Gadoteridol as a contrast agent for breast MRI can depict significant breast disease at the doses tested, but higher doses may result in lesion obscuration at delayed scanning. MRI can improve the PPV of lesions detected with traditional screening methods, but is limited for detection of small intraductal carcinomas.
Research funded by Squibb Diagnostics, Inc.

Tuesday Morning • Metropolitan Room Papers 217–218

FUNCTIONAL IMAGING

MODERATORS: JA Helpern, PhD
BR Rosen, MD

217 • 11:54 AM

Imaging of Functional Increases in Local Cerebral Blood Flow with EPISTAR

S Warach, B Siewert, DG Darby, V Thangaraj, RR Edelman
Department of Neurology, Harvard Medical School, Boston, MA

Purpose: To evaluate a new technique, EPISTAR, for localizing functional brain activity.
Methods: EPISTAR is an MRI method of noninvasive cerebral blood flow mapping. The method combines a spin-tagging radio-frequency pulse of proximal arterial blood, echo-planar readout, and image subtraction. The resulting images provide a qualitative map of CBF at various delays in the transit of blood from proximal arterial branches to capillaries. Using EPISTAR at 1.5 T, we studied 25 subjects doing simple sensorimotor tasks. Imaging slices were 2–10 mm thick and oriented in transverse, coronal, or oblique planes through the target area of cortex. Averages of multiple acquisitions (typically 48) gave rise to relative CBF maps, with a resolution as high as 2 × 2 × 2 mm. For a 90-mm-thick inversion slab centered 60 mm proximal to the imaging slab, a TI of 950 msec tended to be optimal. Rest and activation measurements were made, and the resulting relative CBF maps were subtracted to reveal a CBF difference map, which was superimposed on anatomic images.
Results: CBF difference maps reliably showed marked localized increases in cortical signal intensity ranging from 13% to 193% (mean increase, 58%). The increases mapped precisely to the expected cortical gray matter ribbon, not in subjacent white matter or venous structures.
Conclusion: EPISTAR is a novel MRI method for mapping local brain activity, showing signal increases an order of magnitude greater than BOLD and without contamination from venous signal.

218 • 12:04 PM

Comparison of Magnetoencephalography with Functional MR Imaging in the Same Subjects

R Beisteiner, G Gomiscek, M Erdler, C Teichtmeister, E Moser
Neurological University Clinic, Vienna, Austria

Purpose: We present the first large-scale comparison of magnetoencephalography (MEG) and functional MR imaging (FMRI) to investigate the correlation of neuronal and vascular activity of the brain during motor activation.
Methods: Ten subjects did right index finger tapping (3–4 sec) followed by 3–4-sec rest. MEG (BT1607) was recorded over the left frontocentroparietal cortex, with 28 different channel locations. 150–200 epochs of 1.5-sec baseline (rest) and 1.5-sec finger tapping were recorded and averaged. For FMRI recordings (Magnetom 1.5 T, 256 × 256 resolution, 3-mm slice thickness, gradient-echo sequence, TE = 60 ms, TR = 91 ms, $\alpha = 40°$), 2 min of complete rest was alternated with 2 min of motor activity (=3-sec rest alternating with 3-sec tapping), in total producing three periods of rest and two activation periods. During each period five FMRI images were obtained. Three transverse slices tilted laterally were investigated over the left central hemisphere.
Results and Conclusion: The locations of the best-fitting precentral and postcentral MEG dipoles were compared with FMRI pixels chosen according to the following criteria: a good signal course correlation with the stimulation course, an amplitude change of at least 5%, and no correlation with large vessels on an MR angiogram of the same slice. The coordinates of those pixels were then compared with the coordinates of the MEG dipoles: 77% of the comparisons showed differences below 1.5 cm in all three directions of space, and

12% of the comparisons were even below 1 cm, indicating a good correlation between neuronal and vascular centers of maximum stimulus-correlated change.

Tuesday Morning • Miro Room
Papers 229–230

IMAGE QUALITY: Motion and Artifacts

MODERATORS: JA Sorenson, PhD
ML Wood, PhD

229 • 12:06 PM

Detection and Measurement of Multiaxis Object Displacement and Rotation during Imaging, with a Single "Orbital" Navigator Echo

Z Fu, RC Grimm, PJ Rossman, JP Felmlee, SJ Riederer, RL Ehman
Mayo Clinic, Rochester, MN

Purpose: Adaptive motion correction techniques (retrospective/real-time) require measurement of object motion during image acquisition. This can be achieved with use of navigator echoes, but measurement of multidirectional motion usually requires multiple navigator echoes. The objective of this work was to develop and test a method for measuring rotational and two-axis translational motions simultaneously, using a single navigator echo.
Methods: A spin-echo sequence was modified to incorporate a novel type of navigator echo, in which x- and y-axis gradients are modulated to sweep the sampling point through a circular trajectory in k space. Whereas a conventional projection navigator echo has a linear k-space trajectory along the k_x axis, this new type of navigator echo orbits the origin of k space at a predetermined radius. Theoretical analysis shows that object rotation can be assessed by measuring a shift in the modulus of the untransformed orbital navigator data relative to a reference echo. Displacements along the x and y axes are obtained from measurements of cosine- and sine-modulated phase shifts of the untransformed orbital navigator data, respectively.
Results: Motion phantom studies demonstrated that orbital navigator echoes can measure x and y displacements with a precision of 0.5 image pixels and rotation with angular accuracy of better than 1°. In vivo studies of head motion demonstrated that the single orbital navigator echo can be used to measure and correct the effects of x and y displacement, as well as in-plane rotation.
Conclusion: The orbital navigator echo is an efficient means for detecting/measuring rotation and displacement during imaging.

230 • 12:16 PM

Linear Correction of Respiratory Motion in the Abdomen

ME Brummer, WT Dixon, JM Hawkins
Radiology Department, Emory University, Atlanta, GA

Purpose: Spatial resolution in abdominal images is limited by respiration. Measuring respiration during acquisition may allow compensation during reconstruction, improving spatial resolution. Unlike breath holding, compensation imposes no time limits.
Methods: At each acquisition, chest position was measured with a pneumatic bellows on a belt around the chest. A linear relation was assumed between bellows pressure and craniocaudal position of the viscera, which were modeled as a rigid structure. Sagittal and coronal fat-suppressed SE images were made with a craniocaudal read-gradient direction. Before Fourier transformation, a linear phase adjustment, proportional to an assumed visceral displacement, was made individually to each line of k-space. Displacements were obtained by scaling the bellows pressure. Two methods were used to derive a suitable scaling factor. One method was operator examination of a series of images reconstructed with different scaling factors. The other method allows automatic assignment of a scaling factor. The scaling factor is the quotient of the offset maximizing the cross-correlation of the transforms of two independent measurements of the centerline in k-space, divided by the difference between the corresponding bellows pressures.
Results: In seven scans of two volunteers, compensating reconstruction enhanced features in the liver and corticomedullary borders in the kidney. Scaling factor values obtained automatically were close to the values producing the sharpest images. Motional artifacts from moving viscera decreased, but artifacts from static tissue appeared. Fat suppression reduced this undesired effect.
Conclusion: This linear method improves abdominal images. Any respiratory measurement, including navigator echoes and standard hardware, should be suitable.

Tuesday Morning • Morocco Room
Papers 238–239

SPECTROSCOPY II: Brain

MODERATORS: F Arias-Mendoza, MD, PhD
IR Young, PhD

238 • 11:54 AM

Proton MRS Is Useful for Distinguishing Delayed Radiation Necrosis from Recurrent Brain Tumor

JS Taylor, MH Pui, JW Langston, WE Reddick, R Heideman, PB Kingsley, RJ Ogg, JJ Jenkins, LE Kun
Diagnostic Imaging, St Jude Children's Research Hospital, Memphis, TN

Purpose: Doses of radiation used to treat primary brain tumors can produce necrosis of the irradiated brain, resulting in neurologic deterioration that may be severe. Differentiating radiation necrosis from recurrent tumor is a difficult problem in the management of these patients. Twelve children (aged 3–16 years) with pathologically confirmed primary brain tumors were studied with proton MRS to determine its value in distinguishing recurrent tumor from radiation necrosis.
Methods: All patients underwent serial clinical combined MRS/MR imaging at 1.5 T. Six patients underwent FDG-PET and five TI SPECT studies. Water-suppressed proton MR spectra were obtained from nominal 8-cm^3 volumes localized to the ROI by STEAM (TR/TE = 3,000/20 or 270/30 msec). Spectra were acquired with 2,048 data points, 2-KHz spectral width, 128 acquisitions per volume, and peak areas determined by an automated algorithm. Semiquantitative estimations of MRS-visible metabolites were made by correcting peak areas for receiver gain and normalizing to a standard volume.
Results: Five of 12 patients had histologic diagnoses of radiation necrosis, and seven of active recurrent or residual tumor. Five of seven tumor patients had choline elevated 1.2–4 times above the highest choline levels for the necrosis group and also had creatine levels elevated relative to the necrosis group. Four patients had such low metabolite levels that they were prospectively identified with MRS as having necrosis (three correctly, one false-negative for tumor with necrosis).
Conclusion: Semiquantitative determination of choline and creatine peak areas from MRS can aid in distinguishing necrosis from active tumor. Increased separation of the two groups is visualized best by plotting creatine versus choline values.

239 • 12:04 PM

H-1 MR Spectroscopy Characterization of Brain Metastases of Mammary Carcinoma

PE Sijens, P van Dijk, M Oudkerk
Department of Radiology, Dr Daniel den Hoed Cancer Center, Rotterdam, The Netherlands

Purpose: H-1 MR spectroscopy characterization of brain metastases of mammary carcinoma in relation to Gd-DTPA–enhanced MRI.

Methods: Single voxel H-1 MRS was used to examine brain metastases of mammary carcinoma, 15 lesions measuring at least one-third of the MRS voxel volume (typically 3.4 or 8 cm^3) at T1-weighted MRI with Gd-DTPA contrast.
Results: Metastases showing no lactate (Lact) signal ($n = 11$) had relative choline (Cho) and creatine (Cr) levels of 0.56 ± 0.06 and 0.24 ± 0.03 SE, respectively, compared with 0.20 ± 0.02 (Cho) and 0.27 ± 0.03 (Cr) in normal occipital brain tissue and 0.26 ± 0.02 (Cho) and 0.24 ± 0.02 (Cr) in corpus nuclei caudati. The detection of Lact in four of the larger lesions coincided with lower Cho (0.36 ± 0.09) and Cr (0.18 ± 0.04) levels and heterogeneous Gd-DTPA enhancement (ring enhancement). There was significant correlation between Gd-DTPA enhancement at T1-weighted MR imaging and the metastatic Cho signal ($r = .70$, $P < .002$; $n = 15$).
Conclusion: In brain metastases of mammary carcinoma, Lact represents a product of ischemia preceding or during tissue decay, resulting in central necrosis, rather than tumor-specific metabolism resulting in increased glycolysis. In all cases where Lact is not detected, Cho levels are higher than in normal brain tissue.
Acknowledgement: Some of the presented data are part of the "Clinical Trial Spectroscopy" organized by Rolf Sauter, PhD, Siemens AG, Erlangen, Germany.

Tuesday Morning • Sapphire Room
Papers 248–249

UPPER ABDOMEN II: Hepatic, Contrast
MODERATORS: PL Choyke, MD
RJ Herfkens, MD

248 • 11:54 AM
Fat-Sat Turbo-Gradient Spin-Echo Imaging of Liver and Pancreatic Lesions
M Mueller-Schimpfle, P Huppert, B Kiefer, HJ Brambs, M Laniado, CD Claussen
Department of Diagnostic Radiology, University of Tübingen, Tübingen, Germany

Purpose: To evaluate the potential of a novel T2-weighted fat-sat turbo-gradient-spin-echo (hybrid) pulse sequence in MR imaging of liver and pancreatic lesions.
Methods: Twenty patients with CT-proved liver and pancreatic lesions were examined. MR imaging was performed at 1.0 T with a body coil and a gradient field strength of 15 mT/m (Magnetom Impact, Siemens). A breath-hold T2-weighted turbo SE (TSE) sequence with single signal averaging (six slices, 17 sec, turbo factor 23) and a non-breath-hold TSE sequence with four averages (16 slices, 7.5 min, turbo factor 5) were acquired. A fat-sat hybrid sequence was employed accordingly, ie, breath-hold (one acquisition, six slices, 17 sec, turbo factor 33) versus non-breath-hold sequences (five acquisitions, 16 slices, 2.5 min, turbo factor 33). The number of lesions, image quality, artifacts, lesion conspicuity, overall diagnostic information, and lesion contrast were evaluated, with random ordering of each of the four sequences.
Results: A total of 64 lesions were evaluated. The image quality of the non-breath-hold TSE sequence was superior to that of the remaining sequences, with the breath-hold hybrid technique yielding the lowest quality. In hemangiomas of the liver ($n = 23$), the breath-hold TSE sequences showed the highest number of lesions. In lesions other than hemangioma, the hybrid sequence with five averages was the best technique.
Conclusion: In the differential diagnosis of hemangioma versus other lesions, the breath-hold TSE sequence is a valuable technique. However, for lesion detection, the non-breath-hold TSE sequence and the hybrid technique are recommended.
B. Kiefer is an employee of Siemens Medical Systems.

249 • 12:04 PM
Pseudofluid on Abdominal MR Images: Unsuppressed Fat in the Right Anterior Diaphragmatic Region Noted on Fat-Suppressed Fast Spin-Echo T2-Weighted Images
K Yoshimitsu, DGK Varma, E Jackson
Department of Diagnostic Radiology, University of Texas, M. D. Anderson Cancer Center, Houston, TX

Purpose: On fat-suppressed fast spin-echo (FSE) T2-weighted (T2W) abdominal MR images, we have noted unsuppressed fat in the right anterior diaphragmatic region mimicking fluid. The purpose of this study was to determine the etiology and incidence of this phenomenon.
Methods: Between April, and August 1993, abdominal MRI, which included FSE T2W images with frequency-select fat presaturation technique (Chem Sat), was performed in 52 cases. All scans were performed on a 1.5-T unit. FSE scan parameters were TR/effective TE = 4,000–6,000/80–150 msec; ET: 12–16; 256 × 192 matrix; 2 NEX; FOV 28–32 cm. Images were retrospectively reviewed with special attention to the right anterior diaphragmatic region. T1W and FSE T2W images from each study were evaluated and compared.
Results: In 42 cases (80%), fat in the right anterior diaphragmatic region (hyperintense on T1W image) was not suppressed on the FSE T2W image with Chem Sat. In 11 (26%) of these 42 cases, subcutaneous fat adjacent to the unsuppressed anterior diaphragmatic fat was well suppressed. This caused the fat in the diaphragmatic region to mimic fluid or peritoneal implants. In 31 other cases, (74%) diffusely distributed unsuppressed fat was noted and therefore was less confusing and more readily attributable to artifact.
Conclusion: Nonsuppression of fat on FSE fat-suppressed T2W images may occur in the anterior diaphragmatic region. This is presumably due to magnetic field inhomogeneity at off-center locations and exaggeration of this phenomenon due to juxtaposition of fat and air at the anterior diaphragmatic region. Radiologists should be aware of this phenomenon to avoid confusion with fluid or metastatic implants at this site. Careful correlation of the FSE T2W images with T1W images is necessary.

Tuesday Morning • Topaz Room
Papers 259–260

VASCULAR IMAGING
MODERATORS: M Bernstein, PhD
DN Firmin, PhD

259 • 12:06 PM
MR Angiography of the Peripheral Arterial System with a Long-Quadrature-Array Extremity Coil
TC Goertzen, RW Jones, RJ Witte, TG Lynch, BT Baxter, TC McCowan, RP Lieberman, RF LeVeen
Department of Radiology, University of Nebraska Medical Center, Omaha, NE

Purpose: MR angiography must image from the aortic bifurcation to the pedal arteries to be a useful noninvasive imaging tool of peripheral vascular disease. A body coil is used to obtain a large field of view but is limited by a suboptimal signal-to-noise ratio when small vessels are imaged. The extremity coil provides a better signal-to-noise ratio but examination time is prolonged due to the small field of view and the need to reposition the coil and patient. The purpose of our study was to image the peripheral vascular system using a specially designed long extremity coil with 2D time-of-flight techniques.
Methods: We used a GE 1.5-T Signa MR imager with standard 2D time-of-flight software and a long quadrature-array extremity coil that imaged from the femoral artery to the pedal arteries. Normal volunteers were studied to optimize scanning parameters. Patients with peripheral vascular disease were studied and images correlated with conventional angiography.

Results: The long quadrature-array extremity coil produces images of diagnostic quality in normal volunteers and patients with peripheral vascular disease. The length of the coil allows scanning of the lower extremities without repositioning the patient, and examination time can be reduced. Good correlation with conventional arteriography is seen.
Conclusion: A long quadrature-array extremity coil with 2D time-of-flight techniques can provide diagnostic images of the peripheral vascular system. With continued technologic advances, MR angiography will be an effective noninvasive tool of the peripheral vascular system.
R.W. Jones is president of Scan Med of Medic, Inc.

260 • 12:16 PM
Dynamic Phase-Contrast Angiography of Normal and Diseased Peripheral Arteries: Experimental and Clinical Studies
B Krug, H Kugel, W Heindel, R Schmidt
Department of Radiology, Universitätskliniken, Cologne, Germany

Purpose: Dynamic phase contrast (PC) angiography is a modified PC sequence that acquires up to 22 phase images per cardiac cycle in a slice orientation parallel to the vessel. It was the purpose of this study to evaluate which functional information can be obtained by the sequence in patients with flow disturbances of the peripheral arteries.
Methods: Dynamic PC angiograms were obtained with a 1.5-T imager in nine healthy volunteers and 10 patients with arterial flow disturbances. A modified ECG-gated FLAG (flow-adjusted gradient) sequence was used, providing flow-sensitive images with suppressed background. Flow patterns and velocities of the investigated vessel segment were visualized as a function of time with a cine mode display. Aortoiliac arteries were investigated in five cases, femoral arteries in 14. The coronal dynamic PC angiograms were correlated with velocity patterns obtained from quantitative flow measurements performed in transverse slice orientation and with vessel morphology confirmed by recent x-ray angiograms.
Results: Image quality was optimized by using flip angles of 8°–15° and flow sensitivities of 0.03–0.8 cycles/(cm/s). The temporal pattern of arterial perfusion corresponded with flow velocity as a function of time as provided by quantitative flow measurements. In healthy persons a triphasic and in vascular patients a monophasic flow pattern was observed. Stenoses > 50% resulted in intraluminal flow accelerations and turbulences. Blood flow eddies were demonstrated in aneurysms.
Conclusion: Accuracy and time resolution of dynamic PC angiography is sufficient to provide functional information on the vascular system.

Tuesday Afternoon • Monet Room
Papers 307–309

PERFUSION AND FUNCTIONAL IMAGING
MODERATORS: TJ Brady, MD
WT Dixon, MD

307 • 4:57 PM
Evaluation of Renal Perfusion with EPISTAR
RR Edelman, M Müller, A Kaiser, P Prasad, S Gladstone
Department of Radiology, Beth Israel Hospital, Boston, MA

Purpose: Evaluation of renal perfusion was performed noninvasively with the EPISTAR technique in an animal model and in humans.
Methods: Breath-hold EPISTAR images of the kidneys were obtained in healthy volunteers in axial and coronal orientations. A 15-mm section thickness was used, with a 37-cm field of view, 128 × 128 acquisition matrix, and an EPISTAR tagging pulse oriented along the axis of the aorta. Breath-hold time was 15–22 seconds for inflow delays of 500–1,600 msec. The method was also validated in a graded renal artery stenosis in a Yorkshire pig model with concomitant flow measurements using an ultrasonic flow probe placed on a segmental renal artery.
Results: With short inflow delays, the renal arteries were depicted. With delays in excess of 900 msec, symmetric renal cortical enhancement occurred. Unilateral occlusion of the left renal artery in the pig model caused complete loss of EPISTAR signal from the left kidney. With release of the occlusion, there was initially a prolonged transit time and decreased EPISTAR signal, with gradual return to normal transit times and signal as the flow returned to baseline values.
Conclusion: Noninvasive depiction of renal perfusion is feasible in a single breath hold with the EPISTAR technique. The method could prove useful in the assessment of renovascular disorders and renal tumors. Further study will be directed toward absolute quantification of renal blood flow.
R.R. Edelman receives research support from Siemens Medical Systems, Inc.

308 • 5:07 PM
MR Perfusion Imaging of the Kidney before and after Stress with Dipyridamole
R Tello, GG Hartnell, TC Hill, C Hoffman
Department of Radiological Sciences, Deaconess Hospital, Boston, MA

Purpose: Animal work demonstrates that renal MR contrast enhancement depends on the timing of image acquisition. Limited human scintigraphic studies have demonstrated the effect of dipyridamole (DP) on renal perfusion. This study assessed the effect of DP on renal perfusion using cardiac gated TurboFLASH MRI in patients undergoing stress scintigraphy.
Methods: Rest MR images are acquired with ECG-gated imaging (TurboFLASH: TE = 12, TR = 6, flip = 10°, TI = 100) 10–45 seconds after a bolus of Gd-DTPA (0.04 mmol/kg) every 3–4 cardiac cycles with a Siemens 1.0-T Magnetom. Stress is induced within the MR scanner with 0.56 mg/kg of DP followed by 25–30 mCi of Tc-99m-MIBI with simultaneous stress MRI after a second bolus of Gd-DTPA in exactly the same position and time intervals. Stress scintigraphic images are acquired 1 hour later. Rest scintigraphic images are obtained 3–4 hours later with 7–10 mCi of Tc-99m-MIBI.
Results: The signal enhancement in the whole left kidney and renal medulla and cortex in five subjects before and after DP demonstrates depression of total renal perfusion, with relative preservation of cortical perfusion at the sacrifice of medullary perfusion.
Conclusion: TurboFLASH can provide adequate time and spatial resolution in renal perfusion MRI, and the depression of renal medullary perfusion after DP may have clinical importance.

309 • 5:09 PM
Modeling Diffusion Effects in MRI of Magnetically Heterogeneous Systems: Application to BOLD Contrast Imaging
H Jara, FW Wehrli
Department of Radiology, University of Pennsylvania Medical Center, Philadelphia, PA

Purpose: Key to understanding functional MRI with blood oxygenation level–dependent (BOLD) contrast is an accurate model for the prediction of the transverse magnetization of protons in the vicinity of capillaries (1). We present magnetization calculations based on the solution of the Bloch-Torrey equation (2) applicable to magnetic fields of arbitrary spatial dependence, such as the field $\Delta B_{zb}(\vec{x})$ induced by an array of cylinders orthogonal to B_0, with susceptibility difference $\Delta\chi$.
Methods: It is shown analytically that given $\Delta B_{zb}(\vec{x})$, the transverse magnetization is

$$m(\vec{x}) = m_0 \cdot \exp[-D \cdot b(\vec{x}, t)] \cdot \exp[-i\phi(\vec{x}, t)] \quad (1)$$

and that for a wide range of diffusion constants D, including the biologic range, the phase ϕ and the b function are

$\phi(\vec{x}, t, t_0)$

$$= \gamma \int_{t_0}^{t} \left\{ \iiint_{\text{Vol.}} W(\Delta\vec{x}, \Delta t, D) \Delta B_{zb}(\vec{x}') d^3x' \right\} dt', \quad (2)$$

$b(\vec{x}, t, t_0)$

$$= \int_{t_0}^{t} \left\{ \iiint_{\text{Vol.}} W(\Delta\vec{x}, \Delta t, D) |\vec{\nabla}\phi(\vec{x}, t')|^2 d^3x' \right\} dt'. \quad (3)$$

$W(\Delta\vec{x}, \Delta t, D)$ is the probability for a proton to displace by $\Delta\vec{x}$ during time Δt for isotropic unrestricted diffusion. Equation (3) was computed numerically assuming a voxel size of 0.2 μm, for 16 cylinders of radius R = 3.5 μm, spaced 20 μm apart, $\Delta\chi = -0.024$ to +0.076 ppm, TE = 5–90 msec, $D = 10^{-8}$ to 10^{-4} cm²/sec.

Results: For gradient and spin echoes the voxel-averaged transverse magnetization, $<m(\text{TE}, D, \Delta\chi) > D\chi)>$ is a monotonically decreasing function of D, TE, and $\Delta\chi$, significantly deviating from single exponential behavior for most values of D and $\Delta\chi$. The results show that for faster diffusion, the refocusing effectiveness of the 180° pulse is increasingly lost.

Conclusion: The Bloch-Torrey equations predict that motional averaging of the fields does not result in magnetization coherence recovery, and consequently these results are at variance with the Monte Carlo simulations and Anderson-Weiss mean field theory, particularly for larger values of D and $\Delta\chi$.

1. Wong, E.C. and Bandettini, 1993 Book of Abstracts, *SMRM*, 10 (1993). 2. Torrey, H.C., *Phys. Rev.* 104(3) (1956).

Tuesday Afternoon • Metropolitan Room Paper 318

CONTRAST AGENTS II

MODERATORS: GD Fullerton, PhD
SW Young, MD

318 • 5:09 PM

Dynamic MR Imaging of Scintigraphically Cold Lesions of the Thyroid

M Mueller-Schimpfle, W Stern, G Brix, A Greschniok, W Mueller-Schauenburg, M Laniado
Department of Diagnostic Radiology, University of Tübingen, Tübingen, Germany

Purpose: To assess the potential of dynamic MRI in the differential diagnosis of scintigraphically cold lesions of the thyroid.

Methods: Twelve patients with one or more scintigraphically cold lesions of the thyroid were examined at 1.5 T. Histopathology or long-term follow-up served as the gold standard. After T1- and T2-weighted axial SE sequences had been acquired (SE 600/15 and 2,300/22,90), dynamic MRI was performed with a rapid SE sequence (SE 100/10). During and after perfusor-controlled infusion of Gd-DTPA (0.1 mmol/kg), 48 consecutive measurements were obtained (13.5 sec/measurement). A computer-based analysis of the pharmacokinetics of Gd-DTPA in normal thyroid, lesions, and muscle provided quantitative data on the degree (amplitude) and velocity (distribution time) of contrast enhancement. These data were retrospectively compared with histopathology. Additionally, the pharmacokinetic data were correlated with anatomy by means of parameter images.

Results: There were six adenomas, four papillary carcinomas, and eight normal thyroid lobes. Except for muscle tissue, the distribution time of tissues was shorter than the time resolution of the method (< 0.05 min). The amplitude of the adenomas was 3.3 ± 1.62 (mean ± standard deviation); the amplitudes of carcinomas and normal thyroid tissue were 1.46 ± 0.59 and 1.28 ± 0.25, respectively. Muscle tissue showed a mean amplitude of 0.47 ± 0.05.

Conclusion: Thyroid tissue as well as thyroid lesions showed a uniformly fast contrast enhancement. However, the amplitude of contrast enhancement seems to provide additional information for the differentiation of adenomas from other thyroid lesions.

Tuesday Afternoon • Miro Room Papers 328–330

MUSCULOSKELETAL I: Joints

MODERATORS: JV Crues, III, MD
EC Unger, MD

328 • 5:09 PM

High-Resolution Imaging of the Wrist: Is It Really Needed?

SMS Totterman, RJ Miller
University of Rochester, Rochester, NY

Purpose: The purpose of this study was to evaluate the resolution required for the visualization and demonstration of extrinsic and intrinsic ligaments of the wrist.

Methods: Five cadaveric wrists were imaged by using 3D data acquisition with GRASS sequences (1-mm, 1.5-mm, 3-mm slice thickness; 8-cm field of view, 256 × 256 matrix; 8-cm field of view, 256 × 128 matrix; 10-cm field of view, 256 × 256 matrix; 10-cm field of view, 256 × 128 matrix; and 12-cm field of view, 256 × 256 matrix and 256 × 128 matrix with one excitation). The visualization of the extrinsic ligaments including the radioscaphocapitate, radioscapholunate, radiolunotriquetrial, and the deltoid and the intrinsic ligaments (scapholunate and lunotriquetrial) were evaluated on a grading scale as "not visualized," "visualized," and "very well visualized."

Results: The extrinsic ligaments of the wrists, including the radioscaphocapitate and radiolunotriquetrial, can be visualized by using 1.5-mm slice thickness. However, their infrastructures were barely visualized in most of the studies using a 3-mm slice thickness. The visualization of the radioscapholunate ligament is obscured with slices thicker than 1 mm. Lunotriquetrial as well as scapholunate ligaments can be seen but not well defined at 1.5 mm. An 8-cm field of view with a 256 × 256 matrix provides the best visualization of the ligaments. When a 256 × 128 matrix is used, the ligaments can still be seen. However, when this is combined with a 10-cm field of view, visualization of intrinsic ligaments deteriorates even with a 1-mm slice thickness.

Conclusion: The optimal visualization of extrinsic and intrinsic ligaments requires very high resolution imaging. The minimum requirement is 1-mm slice thickness combined with 0.3 × 0.3 in-plane resolution. Even higher-resolution imaging would be preferable.

329 • 5:19 PM

High-Resolution MR Imaging of TFCC

SMS Totterman, RJ Miller
University of Rochester, Rochester, NY

Purpose: TFCC tears are classified and treated according to their location and etiology. As MR imaging, even with 3-mm slice thickness, has not been able to visualize different components of the TFCC, its value for treatment planning has been questionable. The purpose of this study was to evaluate whether high-resolution whole-volume MR imaging will be able to overcome this problem.

Methods: Five cadaveric and 20 patient wrists were imaged on a 1.5-T clinical imager (Signa, Milwaukee, WI) with a specially built receive-only surface coil and 3D data acquisition with a GRASS sequence (8-cm field of view, 1-mm slice thickness, 256 × 256 matrix). The MRI appearance of the TFCC and its components, including the triangular fibrocartilage itself, the volar and dorsal radioulnar ligaments, the ulnolunate and ulnotriquetrial ligaments, the meniscus homologue, and the attachment of the TFCC to the styloid, were evaluated on MR images and compared with the findings at surgical dissections.

Results: The striated volar and dorsal radioulnar ligaments were easily visualized in all cadavers and patients. The low-

intermediate-signal-intensity central disk was attached to the tip and to the base of the styloid with striated connections. The primary attachments to the base of the styloid appeared on dissections to be a fold from the dorsal radioulnar ligament. However, some of the MR-visualized striations could not be explained by dissections. The ulnolunate and ulnotriquetrial ligaments were not visualized either on MR images or in dissections as discrete structures. The meniscus homologue was visualized in varying degrees in cadavers and in patients. The prestyloid recess and its opening were always identified in dissections. However, its size varied from a small pouch to a well-developed recess. This correlated well to the MR images.
Conclusion: Whole-volume imaging with 1-mm slice thickness can distinguish components of TFCC and should raise the potential of localizing tears within these components.

330 • 5:29 PM

Real-Time Functional MR Imaging of the Knee and Ankle Joints

RW de Boer, GH van Yperen
Philips Medical Systems, Best, The Netherlands

Purpose: Kinematic MRI has been effectively used for evaluating idiopathic pain syndromes that affect the patellofemoral joint, wrist and ankle. MR acquisition techniques include static MRI (multiple views displayed in a cine loop), motion-triggered cine MRI, and active flexion with ultrafast spoiled gradient-echo sequences. We developed an MR zoom-fluoroscopy real-time imaging technique and studied dynamic joint motion of the knee and ankle joints.
Methods: The experiments were performed on a 1.5-T Philips Gyroscan NT system. Volunteers and patients were imaged with use of flexible surface coils. The joint motion was performed at normal physiologic speeds with active muscle involvement (typically one complete flexion-extension cycle in 1.5 sec). An ultrafast Turbo spin-echo technique was used (typical echo spacings: 4.8–6.0 ms). A rectangular FOV was defined by the intersection of two orthogonal slices. Reduced matrix acquisition in combination with halfscan allowed single-shot acquisition and frame rates of 5–8 images per second. The slice position could be interactively selected from the operator console by using the real-time reconstruction and viewing option.
Results: Knee protocol: FOV = 300 × 75 mm (2.3 × 4.6 mm spatial resolution), acquisition time = 57 ms, TE_{eff} = 16 ms. Sagittal and axial slices of 10 mm were acquired at a rate of five images per second during 13 seconds to study patellar tracking and integrity of the PCL. Ankle protocol: FOV = 350 × 158 mm (2.7 × 4.0-mm spatial resolution), acquisition time = 144 ms, TE_{eff} = 35 ms. Double oblique sagittally oriented slices of 5 mm were acquired at a rate of four images per second during 8 seconds to study tibiotalar rotation and the attachment of the Achilles tendon.
Conclusion: Real-time functional joint imaging (MR zoom-fluoroscopy) with sufficient S/N and spatial resolution can be performed by using ultrashort single-shot TSE with acquisition and viewing rates of up to 10 images per second.
R.W. de Boer is an employee of Philips Medical Systems.

Tuesday Afternoon • Morocco Room
Paper 338

ABDOMEN AND MALE PELVIS

MODERATORS: DG Mitchell, MD
A Yang, MD

338 • 5:09 PM

3D Fat-Suppressed Breath-Hold Imaging of the Kidneys

PD Datoc, D Li, JJ Brown, JA Borrello
Mallinckrodt Institute of Radiology, Washington University School of Medicine, St Louis, MO

Purpose: This study was undertaken to evaluate a 3D fat-suppressed breath-hold sequence (3DFS) for renal imaging.
Methods: Seven patients were imaged with the 3DFS technique before and after IV administration of gadopentetate dimeglumine. Pre- and post-contrast 2D-FLASH images were also obtained. The 3DFS data acquisition structure is a short TR/TE (8/3 ms), low-flip-angle (20°) FLASH sequence with 128 phase-encoding lines and 16 3D partitions, with an imaging time of 18 seconds. A spectrally selective fat-saturation pulse is applied for each 3D acquisition loop. The 2D-FLASH parameters were TR/TE 150/4 ms with a 70° flip angle.
Results: Precontrast SI ratios of renal cortex to medulla were significantly greater with the 3DFS sequence than with 2D-FLASH (P = .30). The S/N of unenhanced renal cortex and medulla and enhanced renal parenchyma were higher for 2D-FLASH images than for 3DFS images (P = .013, .007, and .008, respectively). Twenty-four renal lesions were detected with 3DFS versus 28 lesions detected with 2D-FLASH.
Conclusion: The theoretical advantage of the 3DFS technique is the ability to obtain breath-hold fat-suppressed T1-weighted images with increased through-plane resolution. The lower S/N with 3DFS was expected because of its short TR. Detection of fewer lesions with the 3DFS sequence may have been due to reduced T1 contrast caused by residual transverse magnetization. A modified version of the sequence will incorporate digital RF spoiling to minimize this effect.

Tuesday Afternoon • Sapphire Room
Papers 348–349

HEAD AND NECK

MODERATORS: AN Hasso, MD
KL Nelson, MD

348 • 5:09 PM

MR Imaging of the Cervical Spine during Flexion and Extension: Development and Implementation of a New Technique

FG Shellock, P Sullenberger, JH Mink, AL Deutsch, J Horrigan, A Blozé, R Hashoian
Tower Imaging, Los Angeles, CA

Purpose: To develop and implement a new technique for performing MRI of the cervical spine during flexion and extension.
Methods: Six volunteers and eight patients referred for examination of the cervical spine were studied. A special positioning device (Captain Plastic, Fountain Valley, CA) was constructed and used with a flexible surface coil (8 × 10 cm, GE Medical Systems) to facilitate obtaining MR images of the cervical spine during the extremes of flexion and extension. Flexion and extension views of the cervical spine were obtained in the sagittal plane with a GRE technique (TR/TE 250/15, 45° flip angle). These views were compared with a "routine" MR study of the cervical spine acquired in a neutral position.
Results: Compared with the standard MR examination of the cervical spine, views obtained during flexion and extension provided additional diagnostic information with respect to the presence of disk herniation, spinal stenosis, vertebral subluxation, and instability. These abnormalities were better appreciated during the extremes of extension or flexion in six of the eight patients. Furthermore, the specific technique that was developed greatly enhanced the performance of this examination insofar as the positioning of the cervical spine was standardized and consistent. The flex coil provided a superior signal-to-noise ratio compared with other types of conventional surface coils evaluated for this application.
Conclusion: MR images obtained with the cervical spine positioned at flexion and extension provided supplemental information that may be useful for identifying or characterizing pathology of the cervical spine. Specific indications will be discussed.

349 • 5:19 PM

Flexion/Extension Kinematic Evaluation of the Cervical Spine

CP Ho, RL Moya
Bayside Imaging Center, Redwood City, CA

Purpose: Conventional MRI of the cervical spine done typically in the neutral position may not be ideal for identifying potential instability, cord impingement, or the extent and effects of degenerative disk disease, all of which may be better demonstrated or accentuated by flexion and extension studies.

Methods: Eight male and eight female patients, aged 16–62 years, with neck pain or radiculopathy referred for MRI underwent conventional imaging including sagittal and angled axial sequences in the neutral position on a 0.38-T open-bore MRI system. Each also underwent a kinematic study with sagittal gradient-echo images performed in each of five positions from flexion to extension, initiated entirely by the patient, with a positioning device used to support the patient in each sequential position.

Results: Two patients showed disk protrusions more prominent on extension, with one producing slight anterior cord flattening/impingement on extension, which the patient stated reproduced her pain. One case showed a protrusion with slight cord flattening on extension. Two demonstrated multilevel disk disease with cord impingement on both flexion and extension. Three revealed multilevel disease with narrowing of the subarachnoid spaces but no cord impingement. Three cases of fusion showed decreased/limited kinematic motion, with one revealing a slight posterior impression on the cord in extension. No abnormalities were detected in five patients.

Conclusion: These flexion/extension studies provided valuable additional information with accentuation of disk protrusion and demonstration of cord flattening/impingement not seen with conventional MRI in the neutral position. Although not shown in this limited series, kinematic MRI might also be of value in assessing potential instability.

Tuesday Afternoon • Chantilly West
Papers 361–369

VASCULAR IMAGING: Pulse Sequences

MODERATORS: GH Glover, PhD
MS Silver, PhD

361 • 3:45 PM

MRA Image Appearance: Numerical Simulations of 3D Flow

D Saloner, R Van Tyen, L-D Jou, S Berger
Department of Radiology, Veterans Administration Medical Center, San Francisco, CA

Purpose: Signal intensity on MRA images is often variable, with localized regions of signal loss and others of focal signal enhancement. The origin of the variable signal is poorly understood. We have pursued numerical simulations to aid in understanding signal fluctuations in clinical MRA and as a means of developing improved MRA methods. Previous numerical simulations of MRA studies were extended to include three-dimensional geometries.

Methods: The Navier-Stokes equations were solved to determine particle trajectories through geometries corresponding to the carotid siphon, the carotid bifurcation, and the tip of the basilar artery. The magnetization evolution was calculated incorporating all RF pulses and magnetic field gradients, yielding the k-space data and hence the MR image appearance. Image appearance for high performance gradients with different flow compensation strategies was calculated and compared with that for conventional MRA.

Results: In conventional MRA, imaging of the carotid siphon often shows regions of apparent stenosis in healthy subjects. This appearance has been reproduced in our simulation studies. Geometric distortions accompanying the relative orientation of phase and frequency encoding axes were demonstrated. Simulations of high performance gradients showed reduction of artifactual stenosis and displacement artifacts by using short-duration gradients (TE < 2.5 msec) with first-order flow compensation.

Conclusion: Flow patterns in 3D geometries are fundamentally different from those in 2D models and have significant implications for the prediction of MRA appearance. The simulation package is extremely flexible and permits the prescription of any desired MRA strategy.

362 • 3:55 PM

STAR (Signal Targeting with Alternating Radio-Frequency) Renal Artery Imaging

MK Adamis, J Gaa, RR Edelman
Department of Radiology, Beth Israel Hospital, Boston, MA

Purpose: We have recently described a novel MRA technique for imaging renal arteries called STAR (signal targeting with alternating radio frequency). Renal artery imaging using STAR single-shot echo-planar, cine turboFLASH, and cine segmented turboFLASH was applied and preliminarily compared with our routine 2D-TOF flow-compensated FLASH, segmented turboFLASH, and fat-saturated, postgadolinium FLASH sequences.

Methods: STAR is a breath-hold subtraction technique in which the longitudinal magnitization of the inflowing aortic blood is inverted on alternate acquisitions, with presaturation of background tissue. Readout can be performed with the above-mentioned techniques. The STAR segmented turboFLASH sequence used TR/TE/flip angle = 13 msec/7 msec/20°, 7–21 lines per segment, and 10–35-mm section thickness. Standard FLASH used TR/TE/flip angle = 41 msec/10 msec/40° and 3-mm slice thickness. The techniques were applied to renal arteries in volunteers and patients.

Results: The STAR sequence showed excellent background suppression, with consistent visualization of the entire main renal artery and first-order branches in a single breath hold. Frequently, second-order intrarenal branch vessels were identified. The ability to obtain thick-section slices allowed rapid coverage of the region of interest, with good signal-to-noise ratio. Assessment of flow patterns within a vessel and comparison with the contralateral side could be made with the cine acquisition.

Conclusion: The STAR technique for renal artery imaging shows marked advantages over conventional 2D TOF. They include (*a*) consistent visualization of branch vessels, (*b*) ability to obtain dynamic flow information; (*c*) rapid acquisition time with breath-hold imaging; and (*d*) ability to visualize the entire targeted vascular tree in a single image.

363 • 4:05 PM

Phase-Control MRA: Small Vessel Enhancement by Varying Velocity Encoding with Spatial Frequency

DJ Lomas, RK Butts, RC Grimm, RL Ehman
Mayo Clinic, Rochester, MN

Purpose: To develop a method of enhancing the visibility of small vessels on qualitative phase-contrast MR angiograms (PC MRA) by exploiting the in vivo relationship between flow velocity and vessel diameter.

Methods: The k-space representation of small vessels (diameter ≤ 1 pixel) contains relatively higher spatial frequencies than that for larger vessels (diameter > 1 pixel). By applying a lower encoding velocity to the higher spatial frequencies the signal-to-noise ratio of the smaller vessels is enhanced. The method was simulated mathematically by using a magnitude masked phase-contrast model. Standard 2D and 3D phase-contrast sequences on a Signa 1.5-T imager (Milwaukee, WI) were modified to implement the technique in the phase- and volume-encode axes.

Results: Studies using a simple dual-tube steady-state flow phantom confirmed the simulation prediction that a doubling in peak signal-to-noise ratio for the smaller low-velocity flow vessels could be achieved, compared with the standard

phase-contrast sequence. Preliminary clinical results indicate that the enhancement of smaller-diameter lower-flow blood vessels can be achieved in vivo.
Conclusion: Variation of the velocity-encoding gradient with spatial frequency enhances the visibility of small blood vessels on qualitative phase-contrast angiograms.

364 • 4:15 PM
MR Imaging of Pulmonary Thromboemboli in an Animal Model
JL Friedli, CB Paschal
Department of Biomedical Engineering, Vanderbilt University, Nashville, TN

Purpose: Pulmonary thromboemboli are life threatening. Traditional diagnostic techniques cannot accurately localize or characterize thromboemboli. It is the purpose of this work to demonstrate MRI techniques in an animal model with thromboemboli of known age.
Methods: New Zealand white rabbits were used. One to two baseline MR angiography studies were performed prior to embolization to observe normal pulmonary vasculature. The imaging techniques included three 3D RAGE sequences with various TRs and TEs and a 3D MP-RAGE sequence. These were selected to accentuate differences in T1 and T2* of the clot. Scans were performed with a head coil on a conventional clinical scanner. To embolize, a vessel dilator was inserted into the right femoral vein. Blood was drawn up into a syringe containing thrombin and allowed to clot and then was reinjected into the venous system. A antifibrinolytic agent was given to prevent clot lysis. MRA studies identical to the baseline studies were performed at 0, 2, 5, and 14 days after embolization.
Results: Obstruction of pulmonary blood flow was clearly evident on the day 0 postembolization scan of the first rabbit. Proximal vessels were enlarged while distal vessels were not seen. Over the course of 2 hours, the bulk of the obstruction was cleared. Autopsy revealed infarcted regions of peripheral lung tissue. In subsequent studies, an antifibrinolytic agent was used to prevent clot destruction. The 3D MR images were viewed with multiplanar reconstructions and maximum-intensity projections. Pulmonary vessels are clearly seen. Comparison of pre- and postembolization MR scans reveals the location of thromboemboli.
Conclusion: 3D MR images were obtained of pulmonary thromboemboli of known age in an animal model.

365 • 4:25 PM
Fast Cardiac Phase Contrast: A Multiphase Breath-hold Technique with View Sharing
MA Bernstein, TKF Foo, BD Collick
GE Medical Systems, Milwaukee, WI

Purpose: Retrospectively gated cine phase contrast can provide directional and quantitative flow information. The acquisition time of that method is equal to the time per heartbeat multiplied by the number of phase-encoding views. Thus, one disadvantage of retrospectively gated cine phase contrast is that breath-hold acquisitions are not practical. We developed a prospectively gated, segmented k space, fast cardiac pulse sequence with phase contrast that allows multiphase breath-hold acquisitions. Temporal resolution of phase-contrast acquisitions is also degraded by the need to interleave sequences with varying gradient first moment. To improve the temporal resolution the technique of *view sharing* was employed.
Methods: The fast cardiac phase-contrast pulse sequence supports single-direction two-set or all-direction four-set acquisitions. Both phase difference and complex difference reconstructions are supported. Continuous RF and gradient waveforms allow the magnetization to maintain a steady state throughout the acquisition. The view sharing option improves the temporal resolution by forming images at intermediate cardiac phases.
Results: Given a 14-second breath hold, 60 bpm, a single flow direction, a 256 × 128 matrix with a ¾ field of view, eight views per segment, and view sharing, we were able to obtain seven cardiac phases. Both magnitude and magnitude-masked phase-difference images were obtained during that single breath hold. In general both temporal resolution and scan time increase as the views per segment decrease.
Conclusion: Fast cardiac phase contrast can be used to obtain multiphase phase-contrast images during a single breath hold. Because the method is prospectively gated, a portion of the cardiac cycle is not imaged. This might have an adverse effect on quantitative studies, and this is an area for further study. The breath-hold capability, however, can decrease image blurring.
All the authors are employees of GE Medical Systems.

366 • 4:35 PM
Use of FFT MR Imaging Methods with a Continuously Moving Patient for Very Large Coverage
PM Margosian, SN Mohapatra
Picker International, Inc., Highland Heights, OH

Purpose: To investigate the possibility of acquiring FFT (x-y) MR images while the patient is moved at constant speed through an MR imager. One immediate goal is the ability to cover a meter or more of a patient's body in a single scanning cycle.
Methods: Two 2D field-echo sequences (RF spoiled and SSFP) that were each capable of completing a scan in 1 second or less were used (TE 2, TR 6; TE 3, TR 8). A volunteer was moved through the scanning volume at constant speed while sequential scans were acquired at the center of the magnet (up to 187 slices). Several patient transport speeds were tested.
Results: Images acquired were free from artifacts as long as the distance moved during the acquisition of a single slice was not more than about three-quarters of the slice thickness. More rapid patient transport caused degradation of edges in the images. It was possible to eliminate all effects of patient transport at constant speed by electronically shifting the RF frequency with time so as to cause the excited slice position to move with the patient.
Conclusion: It is possible to emulate the scanning strategy used in spiral CT in an MR unit by using standard FT techniques. Patient coverage of 130 cm was demonstrated in a single scan; full-body coverage is possible.
P.M. Margosian is an employee of Picker International, Inc.

367 • 4:45 PM
Minimization of Dead Time in MR Pulse Sequences for Imaging Oblique Planes
E Atalar, ER McVeigh
Johns Hopkins University, Baltimore, MD

Purpose: When oblique planes are imaged with magnetic resonance (1), minimization of TR and TE is a challenging task because the maximum allowed slew rate and amplitude of the gradients depend on the orientation of the slice and the number of gradients played simultaneously. Efficient waveform design techniques are under investigation (2). We present a method for minimizing dead-time intervals in which certain integrals of the gradients are required but the shape of the gradient waveforms are unimportant. An example of this dead time is the interval between the RF pulse and the readout period in a GRASS pulse sequence.
Methods: In the proposed method, we first transform the requirements of the gradients (the starting and ending levels and the integrals of gradients) to the physical coordinate system and design the waveform that will be applied to the gradient amplifiers directly by using the limitations of each coil and amplifier. In this way, the minimum possible dead periods can easily be calculated and the minimum TR for a given oblique plane can be achieved even with anisotropic gradient sets.
Results: Using this pulse design technique, we have achieved TR values in the range of 6.0–6.5 msec, depending on the orientation of the oblique plane for a 10-mm slice thickness, ±32 kHz receiver bandwidth, 280-mm FOV, matrix size of 256 × 128, partial echo, and partial excitation with standard GE Signa gradients.

Conclusion: We have developed a new MR pulse design method for oblique slices that minimizes dead periods with a noniterative method. Using this method, it is possible to design pulse sequences with ultrashort TEs and TRs for oblique planes with standard gradient amplifiers and coils.
1. M.A. Bernstein, W.H. Perman, M.C. Besozzi, and D.M. Thomasson, *Med. Phys.* 13, 648 (1986), Erratum: Med. Phys. 14(1):145, Jan/Feb 1987. 2. M.A. Bernstein and P.E. Licato. *JMRI* 1994; 4:105–108.

368 • 4:55 PM

Spoiling Transverse Magnetization during the Approach to Steady State

FH Epstein, JP Mugler
Department of Radiology, University of Virginia, Charlottesville, VA

Purpose: To compare artifacts in short-TR, low-flip-angle gradient-echo (GRE) imaging during the approach to steady state using gradient spoiling, radio-frequency (RF) spoiling, ideal spoiling, and gradient refocusing.
Methods: A theoretical model, based on the Bloch equations and resonance offset averaging, was used to simulate the approach to steady state of the MR signal at different spatial positions for T1/T2 = 800 ms/100 ms, a GRE pulse sequence (TR/TE/α = 10 ms/5 ms/15°), and several sequence structures and phase-encoding orders. The sequence structures included (*a*) gradient spoiling, (*b*) gradient refocused and RF spoiling, (*c*) gradient refocused spoiling, and (*d*) ideal spoiling. The phase-encoding orders were sequential and centric. An agarose gel phantom (T1/T2 = 800 ms/100 ms) was imaged by using these configurations (except ideal spoiling) on a 1.5-T whole-body imager (Siemens Magnetom 63SP).
Results: Theoretical: Gradient spoiling closely approximated ideal spoiling for most spatial positions, but the approach to steady state at some positions greatly deviated from the ideally spoiled case. This leads to intensity banding for both sequential and centric phase encoding. Gradient refocusing resulted in an oscillatory approach to steady state, which was independent of position. This can cause imaging blurring and ghosting with centric phase encoding. The approach to steady state using RF spoiling closely approximated ideal spoiling for all positions. Experimental: Images of the phantom displayed the theoretically predicted appearances.
Conclusion: For relaxation times in the range of those considered, RF spoiling may be an effective method for reducing image artifacts in low-flip-angle (<20°) GRE imaging during the approach to steady state.

369 • 5:05 PM

Variable-Angle Uniform Signal Excitation for 3D TOF MR Angiography

A Priatna, CB Paschal
Department of Biomedical Engineering, Vanderbilt University, Nashville, TN

Purpose: To design a new spatially asymmetric RF profile for improving the uniformity of blood signal and vascular contrast. This pulse is the variable-angle uniform signal excitation (VUSE) pulse.
Methods: The VUSE RF profile is generated by using a variable flip angle technique as introduced by Stehling (1), except that the flip angles are incremented as a function of position through the imaging volume instead of as a function of sequence repetition number. The excitation profile provided by the VUSE pulse depends on velocity of through-plane flow, slab thickness, and repetition time. The flip angles are incremented from a very low angle of about 10° up to a maximum of 90° at the region where the flow exits. Computer simulations with different velocities of flow were performed to compare the VUSE pulse with other RF pulses. For implementation, the VUSE pulse has to be truncated and filtered. Phantom and volunteer studies are currently being carried out.
Results: Simulations demonstrate that VUSE gives more uniform blood signal than does tilted optimized nonsaturating excitation (TONE) (2) or a Gaussian truncated by a presaturation pulse (3). After truncation and filtering in the time domain, the general shape of the VUSE pulse is maintained but the maximum flip angle drops to less than 90°, as seen in the simulation and phantom study.
Conclusion: In simulation, VUSE demonstrates more uniform blood signal and better contrast than other RF excitations. However, in practical applications, truncation and filtering of the VUSE pulse gives results similar to those of the TONE pulse.
1. Stehling, M.K., *Magn. Reson. Imag.*, 10, 165–167, 1992. 2. Laub, G. and Purdy, D., *11th Annual Meeting of SMRM*, 882, 1992. 3. Matsuda, T. et al., *Magn. Reson. Med.*, 29, 783–789, 1993.

Wednesday Morning • Monet Room
Papers 408–409

CARDIAC II: Coronary Imaging

MODERATORS: D Li, MS
JD Pearlman, MD, PhD

408 • 11:54 AM

Cardiac Ejection Fraction: Comparison of Ultrafast Echo-planar and Conventional Cine MR Imaging

M Unterweger, JF Debatin, JA Boner, D Wetter, GC McKinnon, GK von Schulthess
Department of Radiology, MRI Center, University Hospital, Zurich, Switzerland

Purpose: The determination of cardiac ejection fraction (EF) and cardiac output (CO) is an integral part of any complete cardiac examination. EF measurements with conventional cine MR are accurate but time consuming. With echo-planar imaging (EPI) data can be acquired much faster. The purpose of this study was to compare EPI with cine MR with regard to EF measurement.
Methods: Ten subjects were examined on a 1.5-T GE Signa imager equipped with an EPI gradient system. With both methods the entire heart was imaged with contiguous axial 10-mm sections. For every section, 16 phase images per heart cycle were reconstructed with cine MR (TR/TE 33/13 ms, flip angle 30°, 2 NEX, 256 × 256 matrix, 24-cm FOV). Twenty-four phase images were obtained over four RR intervals for every slice with nonsequential multiple-shot EPI (TR/TE 32/7 ms, flip angle 45°, 0.5 NEX, 256 × 256 matrix, 40 × 20-cm FOV). For every slice the end-diastolic and end-systolic areas were measured and ventricular volumes determined. EF and CO were calculated in the usual fashion and statistically analyzed.
Results: The EPI sequence had an acquisition time 60 times shorter and a time resolution 50% higher than cine imaging. This facilitated the selection of the end-diastolic and end-systolic images. The delineation of the ventricular lumen from the myocardium was comparable in EPI and cine MR imaging. EPI EF measurements correlated well with cine.
Conclusion: EPI can be used for accurate measurements of EF and CO as part of an integrated MR-based cardiac evaluation.

409 • 12:04 PM

BOLD Contrast of the Heart during Occlusion and Reperfusion

AE Stillman, N Wilke, M Jerosch-Herold, Y Zhang, Y Ishibashi, H Merkle, R Bache, K Ugurbil
Department of Radiology, University of Minnesota, Minneapolis, MN

Purpose: To demonstrate the feasibility of visualizing ischemic and reperfusion changes in the heart by means of functional MR using blood oxygen level–dependent (BOLD) contrast.
Methods: A closed-chest instrumented canine model for myocardial ischemia was studied on a 1.5-T Siemens scanner with an ECG- and respiratory-gated FLASH sequence with TR/TE/α = 24/18/40° and with gradient motion rephasing and a 100 × 128 matrix in a 250-mm FOV. An 18-cm

Helmholtz coil was used to provide a better signal-to-noise ratio.
Results: Significant reductions in the T2*-weighted signal developed in the anterior left ventricular wall, due to increased regional deoxyhemoglobin during occlusion of the left anterior descending coronary artery. Reperfusion was seen as an increase in signal intensity. A diminished response was observed with successive occlusions/reperfusions. This is thought to be due to adaptive perfusion changes in the myocardium.
Conclusion: Functional MR using BOLD contrast of the heart is feasible and provides information regarding ischemic and reperfusion changes in the myocardium. The observed signal intensity changes are a function of changes in deoxyhemoglobin due to changes in both blood volume and myocardial perfusion. The relative contributions from these effects and their clinical value must be determined.

Wednesday Morning • Metropolitan Room
Papers 418–419

MR ANGIOGRAPHY I: Neuro
MODERATORS: C Dumoulin, PhD
KR Marvilla, MD

418 • 11:54 AM
MPRAGE Subtraction Venography: an Alternative to Conventional MR Venography
EA Knopp, JB Stevenson, AW Litt
NYU Medical Center, Brooklyn, NY

Purpose: To obtain a diagnostic-quality MR venogram using a simple postprocessing algorithm in patients undergoing routine pre- and postgadolinium imaging of the brain.
Methods: Preliminary evaluation was carried out in five patients undergoing pre- and postgadolinium MRI of the brain. The patients were imaged with our routine clinical protocol, consisting of a pregadolinium MPRAGE sequence. (TR/TE/flip angle/matrix/FOV: 12/4/15/256/230), as well as axial T2 imaging. This was followed by the intravenous administration of 0.1 mmol/kg of gadopentatate dimeglumine. The MPRAGE sequence was then repeated. Subtraction images were post-processed with an algorithm that calculates the absolute value of signal intensities, on a pixel by pixel basis, of each postgadolinium MPRAGE partition minus the pregadolinium MPRAGE partition. These subtracted partitions were then subjected to our standard maximum-intensity-projection algorithm to obtain the venogram.
Results: In all cases, this method afforded a high-resolution venogram with clear depiction of venous sinus anatomy. In addition, the cortical venous anatomy was also clearly depicted. The venogram was obtained without the need for any additional sequences or saturation pulses.
Conclusion: MPRAGE subtraction venography allows a high-quality MR venogram to be obtained with no scanning time penalty. In addition, since the study is "acquired" in a retrospective manner, it can be obtained after a thorough review of the patient's examination, without the need to recall the patient.

419 • 12:04 PM
Influence of Flow-Sensitive Parameters on 3D Phase-Contrast Angiography of Intracranial Vessels
J Gieseke, E Keller, B Ostertun, M Kouwenhoven, L Solymori, A Steudel
Philips Medical Systems, Bonn, Germany

Purpose: 3D phase-contrast angiograhy (PCA) offers a great potential for differentiating various vascular pathologies in the brain. However, a potential problem is that the blood velocity varies over the vessel lumen, and the flow is pulsatile. Concerning the complex intracranial vascular architecture and flow patterns, the representation of different vessel segments can differ due to the correlation between phase shift and signal intensity. To analyze the influence of physiologic conditions on image quality, the 3D PCA method was evaluated with different velocity-encoding parameters and was additionally correlated with quantitative flow measurements.
Methods: In 10 healthy volunteers, signal-to-noise ratios for different vessel segments (ICA, basilar artery, MCA, vertebral artery, sinus) were compared for various velocity-encoding values (5–200 cm/s) at 0.5 and 1.5 T. All measurements were performed in sagittal, transverse, and coronal orientation with the same geometric parameters (90 slices, 1.5-mm slice thickness, 128 × 256 matrix). In addition, for signal correlation, retrospective and prospective ECG-triggered quantitative flow measurements were performed on slices perpendicular to the basilar and vertebral arteries, the ICA, and both MCAs, with a velocity encoding of 100 cm/s.
Results: In the velocity encoding range of 5–200 cm/s, the signal trends for the ICA, MCA, and basilar artery are similar. There is a strong signal increase from 5 to 30 cm/s and a smaller decrease from 80 to 100 cm/s. For the sinuses, the signal maximum is around 20 cm/s.
Conclusion: The experience with 3D PCA imaging of the intracranial vessels demonstrates that the vessel representation is feasible for a wide velocity-encoding range, although for different segments, optimal image quality can be obtained by properly choosing the encoding velocity.
J. Gieseke is an employee of Philips Medical Systems.

Wednesday Morning • Miro Room
Papers 428–429

MUSCULOSKELETAL II
MODERATORS: JB Kneeland, MD
S Majumdar, PhD

428 • 11:54 AM
MR Imaging Evaluation of Traumatic TMJ Abnormalities: Comparison between T2-weighted and STIR Pulse Sequences
FG Shellock, CJ Schatz, HP Hahn
Tower Imaging, Los Angeles, CA

Purpose: To compare the use of T2-weighted versus STIR pulse sequences for MR imaging of TMJ abnormalities secondary to trauma.
Methods: Thirteen patients (26 TMJs) who sustained trauma to the TMJ were studied with a 1.5-T scanner with dual 3-inch surface coils. Sagittal plane, T2-weighted (TR/TE 2,000/80) and STIR (TR/TE/TI 2,000/25/160) pulse sequences were used to determine the presence of abnormal increased signal intensity indicative of joint effusion and/or muscle injury. Images obtained with T2-weighted and STIR pulse sequences were compared to assess the efficacy of these techniques for showing increased signal intensity of the TMJ and related soft tissues.
Results: Abnormal increased signal intensity findings were present on T2-weighted images in 12 TMJs and on STIR images in 19. STIR images showed seven cases of increased signal intensity not seen on T2-weighted images. The subjective conspicuity of the increased signal intensity findings was greater on the STIR images for nine TMJs and equivocal for three TMJs.
Conclusion: MRI of traumatic TMJ abnormalities with the STIR pulse sequence improves the sensitivity for fluid-related pathology compared with the T2-weighted pulse sequence.

429 • 12:04 PM
MR Imaging Evaluation of Muscle Recruitment Patterns Associated with Different Shoulder Exercises
FG Shellock, J Horrigan, JH Mink, A Deutsch
Tower Imaging, Los Angeles, CA

Purpose: Various exercises are used to treat rotator cuff injuries. With the appropriate MRI technique, exercise-induced enhancement of skeletal muscle can be used to determine the

specific muscle(s) involved in a given movement. The purpose of this study was to use MRI to assess muscle recruitment patterns for different exercises typically utilized for physical rehabilitation of the rotator cuff.
Methods: Five volunteers were imaged before and after performing "Jobes exercise," a lying dumbbell raise, and a seated military press to determine the contribution of the supraspinatus, subscapularis, infraspinatus, teres minor, deltoid, and trapezius muscles during these movements. Resistance was applied by using four sets of 15 repetitions at an amount normalized to the subject's body weight. Coronal images were obtained with an IR-FSE sequence (TR/TE/TE 4,000/35/160). Signal intensity (SI) was measured in ROIs before and after exercise at comparable section locations on MR images that showed each of the muscles.
Results: The deltoid, supraspinatus, and infraspinatus were primarily involved in each of the exercises (% change, $P < .01$), while the subscapularis and trapezius contributed to a lesser degree. None of the exercises worked the teres minor. The supraspinatus appeared to be exercised the best with the lying dumbbell raise.
Conclusion: Each of the shoulder exercises studied involved mainly the deltoid, supraspinatus, and infraspinatus muscles. Of note is that the lying dumbbell raise is considered to be a biomechanically "safer" exercise compared with Jobes exercise or the military press. These data have important implications for rehabilitation techniques used to treat the rotator cuff.

Wednesday Morning • Morocco Room
Papers 438–439

IMAGING TECHNIQUES II
MODERATORS: K Butts, PhD
EM Haacke, PhD

438 • 12:04 PM
A Simple Experiment to Probe the Nature of Fast Spin-Echo Contrast
PJ Keller, BP Drayer, EK Fram, JE Heiserman, JP Karis
MRI Research Department, Barrow Neurological Institute, St Joseph's Hospital and Medical Center, Phoenix, AZ

Purpose: Fast spin-echo images have contrast properties that are substantially different from those of conventional spin-echo images, particularly with respect to fat signal intensity and the response to magnetic susceptibility variations. Many reasons for these differences have been suggested in the literature, including J-modulation of spin echoes, magnetization transfer effects, and stimulated echo effects. The present work tests whether the inclusion of stimulated-echo components alone could explain the observed contrast.
Methods: Three pulse sequences were compared in vitro and in vivo. The first sequence was the vendor (GE)–supplied, standard CPMG spin-echo sequence. The second was derived from the source code from the first sequence and modified to permit stimulated-echo components to contribute to the images. The modifications were minimal: (*a*) all 180° RF pulses had the same phase, (*b*) phase encoding was wound and unwound immediately before and after each readout period, and (*c*) the areas of all pre- and post-180° "crusher" pulses were made equal. The third pulse sequence was the vendor-supplied fast spin-echo sequence with an echo train length of four echoes. Single-slice scans were obtained.
Results: Fourth-echo images from the first two pulse sequences were compared with the fast spin echo, with the fourth echo used to code the middle of k space. The contrast of the fast spin-echo images was found to be essentially identical to that of the modified pulse sequence.
Conclusion: These results exclude J-modulation and magnetization transfer as mechanisms for differentiating fast spin-echo and conventional spin-echo contrast.

439 • 12:04 PM
"High Sort" Assignment of Echoes to Views for Fast Spin-Echo Imaging
PJ Keller, BP Drayer, EK Fram, JE Heiserman
MRI Research Department, Barrow Neurological Institute, St Joseph's Hospital and Medical Center, Phoenix, AZ

Purpose: Fast spin-echo (also called RARE or Turbo spin-echo) images suffer from residual ghosting artifacts due to the echo-to-echo T2 modulation imposed on k space. The usual strategy for minimizing these artifacts is to ensure that adjacent views in k space are sampled with the same echo, or an immediately adjacent echo in the echo train. A second deficit of images obtained with long echo trains is that the edge definition is poor. This results from the assignment of late echoes that yield small signals to the periphery of k space, where the detail information is contained. This work is aimed at alleviating both of these problems.
Methods: An echo-to-view assignment scheme was developed in which views from early echoes and late echoes are immediately adjacent to each other, so that the T2 decay along the echo train is a Nyquist modulation of k space. The single ghost arising from this modulation is easily removed by phase dimension oversampling.
Results: The final assignment scheme for a 16-echo train, beginning at one edge of k space, is the following sequence of echo numbers: 16-1-16-1 . . . 15-2-15-2 . . . 14-3-14-3, etc, until the center is reached, with alternating echoes numbered 8 and 9. The other half of the raw data is symmetrically encoded.
Conclusion: The images resulting from the new assignment system have been shown to have no detectable ghosts and possess much sharper edges than their conventional fast spin-echo counterparts. These superior results have been demonstrated both in phantoms and in patient studies.

Wednesday Morning • Topaz Room
Papers 451–460

FLOW QUANTITATION
MODERATORS: MH Buonocore, MD
J Huston, III, MD

451 • 10:30 AM
Accuracy of Breath-hold MR Flow Measurements in Canine Coronary Arteries
GD Clarke, RW McColl, R Eckels, CR Chaney, JR Dittrich, HF Li, M NessAiver, RW Parkey, RM Peshock
Radiology Department, University of Texas Southwestern Medical Center, Dallas, TX

Purpose: To evaluate the accuracy of coronary artery flow from single breath-hold gated MRI phase-contrast velocimetry measurements in a canine model.
Methods: Four dogs (28–35 kg) were anesthetized and ventilated with room air. A thoracotomy was performed and ultrasonic (US) flow probes placed on the left anterior descending (LAD) and left circumflex (LCX) coronary arteries. Aortic pressure, electrocardiogram, and US flows were monitored continuously. A 1.5-T Picker MRI system was used with phase-encode grouping and respiration suspended during the scan. Prospectively gated velocity-compensated and encoded acquisitions were interleaved. The acquisition parameters were TR 19.1 ms, TE 11 ms, slice-select V_{enc} = 1,384 mm s^{-1}, 7-mm slice, FOV 18–22 cm, aspect ratio 192:256 to 220:256, PEG size 2–3, 4–6 cardiac phases, pixel size 0.7–0.9 mm^2. Thirty-six flow measurements were performed in the LAD and LCX in four animals before, during, and following the infusion of adenosine. Phasic flow volume was derived from the product of vessel area, mean velocity, and the cardiac phase duration.
Results: Coronary flow values ranged from 24 to 160 mL min^{-1}. Correlation of MRI and US data was good (r = .945), with an intercept of 6.94 mL min^{-1}. The mean difference between methods was −2 mL min^{-1}, with 95% of the differ-

ences falling within a range of ±26 mL min^{-1} of the mean difference. The SD of the differences of eight repeated MRI measurements was similar to that of US.
Conclusion: Results suggest that the phase-difference cine MRI flow method may be used to measure coronary arterial flow accurately.

452 • 10:40 AM
Hemodynamically Independent Analysis of Cine Phase-Contrast Measurements of Brain and CSF Pulsations
N Alperin, B Gomez-Anson, DN Levin
Department of Radiology, University of Chicago, Chicago, IL

Purpose: To measure modulation transfer functions, which are hemodynamically independent gauges of the mechanical responses of brain and CSF to cardiovascular pulsations.
Methods: A 1.5-T scanner (GE Signa) was used to study 10 normal volunteers with a velocity-encoded cine phase-contrast pulse sequence. We measured the flows into and out of the cranium through major arteries, veins, and the foramen magnum. The temporal change in the volume of intracranial structures (eg, brain) was deduced by combining the flows measured through these channels and the estimated flow through minor veins. Impulse response functions of these intracranial structures and the spinal canal (at the foramen magnum) were derived by applying a deconvolution technique to these waveforms and to the arterial/venous waveforms. These response functions are independent of the hemodynamics of the vascular "driving force" in each subject.
Results: The derived spinal and cranial response functions showed less variability among subjects than did the net or oscillatory flow volume measurements of spinal flow and intracranial tissue volume changes. The spinal response was delayed and dispersed over time with respect to the vascular "driving force." Intracranial structures responded immediately after a vascular impulse and then "relaxed" back to an equilibrium state.
Conclusion: Transfer function analysis can be used to separate the intrinsic mechanical response of spinal and intracranial structures from the hemodynamic driving forces that are quite variable among individuals. Studies of patients with hydrocephalus and other abnormalities are underway.

453 • 10:50 AM
Time-resolved Velocity Quantification of Pulsatile Flow: Segmented K-Space Bolus Tagging in a Single Breath Hold
D Chien, G Laub, O Simonetti, CM Anderson
University of California, San Francisco, CA

Purpose: To achieve high-speed velocity quantification of pulsatile flow on a conventional system, we have developed and evaluated cardiac-triggered segmented *k*-space bolus tag measurement within a single breath hold.
Methods: Velocity measurements in the descending aorta and the coronary arteries were obtained in normal volunteers with a 1.5-T whole-body imaging system (Magnetom 63SP, Siemens AG, Germany). A breath-hold cardiac-triggered segmented k-space TurboFLASH image was obtained in the plane of the vessel. A flow tagging prepulse was applied prior to every *N* phase-encoding lines. To determine the optimal *N*, images were acquired with $N = 3, 4, 5$, and 6. The scan time was 15, 18, 23, and 31 seconds, respectively (HR = 60 bpm, 256 × 92 matrix). In addition, we compared images obtained with ascending phase-encode order and with centric reordering.
Results: One to 10 images throughout the cardiac cycle could be obtained in one breath hold. $N = 4$ was optimal while the bolus appeared dispersed for $N = 6$. Clear depiction of the flow tag was achieved with centric reordering but not with ascending phase-encode order. The velocities obtained were in good agreement with those obtained with standard bolus tagging (previously validated with a pulsatile flow phantom).
Conclusion: Segmented k-space bolus tagging, which can be implemented on a conventional system without hardware modification, is able to assess pulsatile velocity over the cardiac cycle within a single breath hold.

454 • 11:00 AM
Quantification of Blood Flow: In Vitro and In Vivo Validation of EPI Phase Contrast
JH Boner, JF Debatin, R Botnar, D Wetter, M Unterweger, G McKinnon, GK von Schulthess
Department of Radiology, University Hospital Zürich, Zürich, Switzerland

Purpose: Conventional cine phase-contrast (PC) MR measurements are accurate but time consuming. The purpose of this study was to evaluate an echo-planar PC sequence in a flow phantom, as well as in the ascending and descending aorta of volunteers.
Methods: MR imaging was performed on a 1.5-T system (GE Signa), equipped with additional hardware and software for nonresonant echo-planar MR. With use of the body coil, EPI-PC was evaluated in a laminar flow phantom, containing 16-mm tubes, with flow volumes ranging from 250 to 2,000 mL/min. Twenty consecutive EPI phases (TR/TE 32/8 ms, flip angle 45°, slice thickness 10 mm, velocity-encoding value 60 cm/s, FOV 28 × 28 cm, matrix 128 × 128) were acquired in four nonsequential interleaves over 4 seconds. Subsequently flow in the ascending and descending aorta of 10 normal subjects was determined with EPI-PC at the following parameters: 16 phases, TR/TE 32/8 ms, FOV 32 × 16 cm, 256 × 128 matrix, velocity-encoding value 200 cm/s, and four nonsequential interleaves, whereby the positive and negative velocity encoding is performed during consecutive heart cycles. These measurements were compared with conventional cine PC (TR/TE 24/9, flip angle 45°, section thickness 5 mm, matrix 256 × 256, FOV 24 cm, 2 NEX, velocity-encoding value 200 cm/s). Quantitative blood flow data were measured with flow analysis software.
Results: In vitro flow measured with EPI-PC correlates well with actual flow ($r = .99$, with slope = 1.03). In vivo EPI-PC flow measurements were performed over eight consecutive heartbeats, permitting breath-hold data acquisition. There was good correlation between EPI-PC blood flow measurements and conventional cine PC measurements ($r = .96$).
Conclusion: EPI-PC blood flow measurements are accurate. The short imaging time allows breath-hold examinations. Thus, EPI-PC promises to expand the clinical applications of quantitative MR PC blood flow measurements.

455 • 11:10 AM
Quantitative Assessment of Blood Flow in the Azygos Venous System in Normal Subjects before and after Glucose Administration
DR Wetter, JF Debatin, B Marineck
Department of Radiology, MRI Center, University Hospital Zurich, Zurich, Switzerland

Purpose: Increased blood flow in the azygos venous system is a manifestation of collateral pathways in patients with portal hypertension and is therefore a possible risk indicator for bleeding complications. The goal of this study was to (*a*) demonstrate the reliability of noninvasive MR phase-contrast azygos blood flow measurements and (*b*) determine the effect of glucose on normal azygos blood flow relative to portal blood flow.
Methods: Cine phase contrast flow measurements of the azygos and hemiazygos veins and the portal veins were performed in 10 normal subjects, with the following parameters: TR/TE/flip angle 24/7.8 ms/45°, 5-mm slice thickness, 2 NEX, resolution 0.6 × 0.6 mm for the azygos and 1.2 × 1.2 for the portal vein. Each volunteer was examined at four different times after 6 hours of fasting and following the administration of glucose (200 kcal).
Results: The intersubject variability of azygos blood flow ranged between 8 and 48 mL/min, with a mean of 17 mL/min. The intrasubject variability over the four temporally spaced measurement points was significantly smaller ($P < .05$). After delivery of glucose, blood flow in the portal vein increased significantly (975 mL/min ± 403 to 1,589 mL/

min ± 689), while blood flow in the azygos system did not change.
Conclusion: Blood flow measurements in the azygos system with cine phase contrast are reliable. In normal subjects blood flow in the portal vein increases after delivery of glucose without changing blood flow in the azygos system.

456 • 11:20 AM
MR Angiographic Flow Velocity Measurements in Normal and Atherosclerotic Iliofemoral Arteries
B Krug, H Kugel, U Harnischmacher, W Heindel, R Schmidt
Department of Radiology, Universitätsklinik, Cologne, Germany

Purpose: The purpose of the study was to assess whether quantitative flow measurements in patients have an adequate accuracy and time resolution to provide diagnostic information on the extent of atherosclerotic disease.
Methods: MR flow measurements in the iliofemoral arteries were performed in six healthy volunteers and 30 patients with arteriosclerotic disease with a 1.5-T imager and a sequence for flow quantification based on flow-induced phase shifts. A trigger pulse followed by the acquisition of 30 evenly distributed data sets was applied every second heartbeat, thus eliminating any acquisition gap in a full heart cycle. Slice orientation was perpendicular to flow. For quantitative analysis, flow velocity versus time was registered. "Systolic acceleration," "postsystolic deceleration," and "pulsatility" of flow were calculated and compared with stenosis grades determined from recent arterial angiograms.
Results: An increasing lumen narrowing of the arterial segment proximal to the location of the flow measurements led to a flattening of the flow profiles, confirmed by a decrease in the calculated indexes. The most exact correlations were achieved with indexes based on spatial maximum flow velocity in the vessel cross section (correlation coefficients, .821–.870 on the right and .878–.902 on the left side).
Conclusion: In patients with arteriosclerotic disease, the flattening of the temporal flow profiles over a heart cycle obtained by means of phase-contrast measurements correlated with the local severity of vascular occlusive disease confirmed with DSA. The maximum flow velocity in the arterial cross section showed the most accurate results.

457 • 11:30 AM
Toward Ultrafast Coronary Flow Quantitation
GC McKinnon, JF Debatin, GK von Schulthess
Department of Radiology, University Hospital, Zurich, Switzerland

Purpose: A rapid echo-planar imaging (EPI)–based coronary flow quantitation technique is presented.
Methods: A multiple-shot (or interleaved) EPI sequence has been modified for phase-contrast flow quantitation. One interleaf for all heart phases is acquired during each RR interval. The positive and negative velocity encoding is performed during consecutive heart cycles. With four interleaves and a 32 × 32 cm field of view, a spatial and temporal resolution of 1.25 × 1.25 mm and 35 msec, respectively, are obtained. With a prior RR interval used to create a steady magnetization state, the complete through-plane flow measurement requires only nine heart cycles—well within an easy breath hold.
Results: The measurement time is greatly reduced compared with gradient-echo–based sequences. Further, gated multiple-shot EPI allows both higher spatial and temporal resolution than can be achieved with single-shot EPI. With multiple-shot EPI the left anterior descending and right coronary arteries were clearly visualized in cross section, making flow measurements possible in all subjects.
Conclusion: We have demonstrated, in principle, an ultrafast imaging technique with sufficient spatial and temporal resolution for breath-hold coronary flow quantitation.

458 • 11:40 AM
Vibrations from Gradient Switching Can Affect the Shape of Velocity Profiles Measured with MR Phase Velocity Mapping
JN Oshinski, DN Ku, JM Siegel, RI Pettigrew
Department of Radiology, Emory University, Atlanta, GA

Purpose: To evaluate whether the flow field and corresponding MR velocity measurements distal to a stenosis can be altered by acoustic vibrations from MR gradient switching.
Methods: Steady flow at a Reynolds number of 1,000 was pumped through a smoothly shaped 90% stenosis. Velocity profiles were measured 75 mm downstream of the throat of the stenosis (location of maximum turbulence intensity) by using (*a*) a laser Doppler anemometer (LDA) under quiescent laboratory conditions, (*b*) an interleaved MR phase velocity mapping sequence on a Philips Medical Systems 1.5-T scanner, and (c) LDA with a loudspeaker simulating the MR gradient switching.
Results: The velocity profile obtained with LDA under quiescent conditions showed that a significant recirculation region remained. The velocity profiles obtained with MR and with LDA when the loudspeaker was used matched closely, both showing no recirculation region. The peak velocity measured with LDA under quiescent conditions was twice that measured with MR or LDA when the loudspeaker was used. The velocity profile changes induced by gradient switching and loudspeaker excitation are likely due to an upstream movement of the turbulent transition point caused by vibrational energy input to the flow field.
Conclusion: Acoustic vibrations from gradient switching can have the required frequency and the adequate power to change the flow field and hence the shape of the velocity profiles in turbulent flows. Care should be taken when comparing MR velocity profiles with those obtained in quiescent laboratory settings or from computer simulations, since the scanner may alter the flow field.

459 • 11:50 AM
MR Flow Quantitation: In Situ Validation with Laser Doppler Velocimetry
D Saloner, K Selby
Department of Radiology, Veterans Administration Medical Center, San Francisco, CA

Purpose: Techniques for MRI velocity measurement are typically verified by using constant-velocity phantoms. Those studies do not assess the temporal response of MR methods to velocity changes and cannot investigate effects of dynamic variations in spatial velocity profiles. The accuracy of MRI in measuring velocities in a pulsatile flow phantom was assessed by using an independent gold standard. The performance of MRI methods for different spatial velocity profiles was also evaluated.
Methods: We evaluated bolus tagging and phase mapping with laser Doppler velocimetry (LDV). Our LDV system is MRI compatible, permitting simultaneous LDV and MRI measurements at the same location in the center of the magnet bore. A wide variety of pulsatile waveforms were evaluated, ranging from waveforms comparable to those in the popliteal arteries, to waveforms comparable to those in the carotids.
Results: Both MRI methods were in excellent agreement with LDV. Discrepancies between MRI and LDV velocities were less than 10%. Bolus tagging was suboptimal for velocities lower than 10 cm/s, requiring particular care when evaluating reverse flow. With appropriate calibration, phase mapping gave accurate velocity measurements, including the low velocities in reversal. For flow reversal, flow can be in opposite directions in different regions of the vessel lumen, and flow measurements are sensitive to placement of the ROI. Correct placement is readily accomplished with bolus tagging, since flow distributions across the lumen are visually portrayed. ROI determination for phase mapping is more difficult.
Conclusion: MRI methods can accurately measure velocities for pulsatile flow typical of that in vivo.

460 • 12:00 PM

In Vivo Monitoring of Atherosclerotic Disease Progression with MR Imaging

LM Mitsumori, C Yuan, MP Skinner, JA Nelson, R Ross, EW Raines

Department of Bioengineering, University of Washington, Seattle, WA

Purpose: In the study of the pathogenesis and progression of atherosclerosis—the principal cause of cardiovascular mortality in the United States—a noninvasive method is needed to examine the temporal changes that occur in the vessel wall. The ability to image plaque with MRI has been demonstrated, suggesting a potential application in in vivo animal models. In this study, we present initial results in the use of MRI to monitor changes over time in the morphology and composition of atherosclerotic lesions in a rabbit model of the disease.

Methods: Six rabbits with catheter-induced atherosclerotic lesions and one control have been imaged with use of a novel, phased-array coil and a 1.5-T Signa (GE) scanner. 2D/3D fast spin-echo pulse sequences with flow suppression and spatial saturation were used to obtain axial images of the abdominal aorta in each animal. To assess lesion composition, images were generated with and without fat suppression and with T1, proton density, and T2 weightings.

Results: There were qualitative and quantitative differences between the vessel images. Increased wall thickness and vessel tortuousity were apparent in the diseased animals, and variations in plaque contrast were observed over time and with different image weightings. Serial measurements of aortic dimensions showed a decrease in lumen cross-sectional area and a compensatory increase in total vessel area with disease. Histologic validation of the structural and biochemical information obtained from the images will soon be completed.

Conclusion: These results illustrate the promise of using MRI to assess plaque development in vivo, facilitating future studies of the disease process and potential therapeutic interventions.

Wednesday Afternoon • Monet Room
Papers 508–509

MAMMOGRAPHY II: Contrast

MODERATORS: SE Harms, MD
CL Partain, MD, PhD

508 • 4:09 PM

Dynamic MR Mammography: How Apparent Is the Diagnosis?

M Mueller-Schimpfle, W Stern, A Rieber, HA Hirsch, P Huppert, CD Claussen

Department of Diagnostic Radiology, University of Tübingen, Tübingen, Germany

Purpose: The purpose of the study was to evaluate the diagnostic confidence of Gd-enhanced FLASH 3D MR mammography (MRM).

Methods: The examinations were done on a 1.0-T MR imager with a double breast coil and a gradient field strength of 15 mT/m (Magnetom Impact, Siemens). Precontrast axial fat-sat T2-weighted Turbo SE images were acquired. Dynamic MRM (0.16 mmol/kg Gd-DTPA) was performed over 10 minutes with an axial FLASH 3D sequence (TR = 9; TE = 3; flip angle = 50°; FOV = 350 mm; matrix = 200 × 256; 32 slices/slab; 4-mm slice thickness; acquisition time 60 sec/slab). Sagittal FLASH-3D images (TR/TE/fa 22/6/50°; FOV 250 mm; slice thickness 3 mm) concluded the examination, with a total examination time of less than 20 minutes. Reading of films, calculation of subtraction images, as well as signal-to-time curve calculations in operator-dependent ROIs were performed for data evaluation. The findings in 182 breasts of 91 consecutive patients were retrospectively analyzed according to the following scale: 0 indicated no pathology; 1, most likely benign; 2, probably benign; 3, probably malignant, and 4, most likely malignant.

Results: Sixty-seven (37%) MR mammograms were unremarkable and 22 (12%) and 53 (29%) were compatible with most likely and probably benign disease, respectively. Eleven cases (6%) were probably malignant, and 29 (16%) MR mammograms were indicative of most likely malignant disease. Of the 35 cases with histopathologic correlation, one false-negative MR mammogram (carcinoma in sclerosing adenosis) and one false-positive case (mastitis) were found.

Conclusion: Based on the 35 cases with histopathologic correlation, MR mammography showed high diagnostic accuracy. However, in approximately one-third of all MR mammograms, the diagnostic confidence was low. Consequently, x-ray mammography and US must be included into the diagnostic workup of the breast.

Wednesday Afternoon • Metropolitan Room
Papers 517–519

BRAIN III: CSF Flow, Other

MODERATORS: WG Bradley, Jr, MD, PhD
VM Runge, MD

517 • 3:57 PM

Quantitative T1 Measurement in Functional MR Imaging

KK Kwong, DA Chesler, BR Rosen

NMR Center, Massachusetts General Hospital, Charlestown, MA

Purpose: To measure quantitative T1 changes accompanying perfusion changes in human photic stimulation and in animal models of hypercapnia and to compare the character of this T1 change with that of simple inflow refreshment.

Methods: An echo-planar T1-weighted inversion-recovery spin-echo (IRSE) sequence was used to collect 15 different TI points at the human visual cortex with starting TI = 100 ms, TI interval = 100 ms, and TE = 30 ms. We used standard photic stimulation protocols of expanding and contracting random dots projected onto a screen inside the bore of a 1.5-T GE Signa scanner. Fitted T1 maps were generated from the data collected during nonstimulating (darkness) and stimulating periods. In animal (a pig and two rabbits) hypercapnia experiments, similar T1 data points were acquired before and during the application of 7% CO_2.

Results: From three volunteers, T1 values at the visual cortex regions were smaller during photic stimulation than during darkness. T1 changes were on the order of 1%. T1 changes were on the order of 3%–5% in animal hypercapnia experiments.

Conclusion: The experimental results of T1 changes do not suggest simple inflow refreshment, which would shift the whole data curve upward by a constant. Instead, our data are in reasonable agreement with the T1 perfusion model (1,2), which suggests that higher blood flow leads to shorter T1. The perfusion model may help separate tissue perfusion from large-vessel flow.

1. Detre et al (1992) *Magn. Reson. Med.* 22, 159.
2. Kwong et al (1992) *P.N.A.S.* 89, 5675.

518 • 4:17 PM

Time Course of Regional Cerebral Blood Volume and Transit Time in Cocaine-treated Rats with Dynamic MR Imaging

KL Li, JN Suojanen

Department of Radiology, Deaconess Hospital, Boston, MA

Purpose: Administration of cocaine to animals previously exposed to cocaine produces variable extracellular dopamine concentrations in central brain structures. We are using functional MR imaging techniques to help determine the relationship of cocaine-mediated changes in regional cerebral blood

volume (rCBV) and transit time in these same structures to the observed changes in extracellular dopamine.
Methods: Male Wistar-Furth rats were pretreated with two doses of cocaine and then divided into four groups. Groups 1, 2, and 3 had intervals of 8, 11, and 16 days between their last pretreatment dose with cocaine and acute injection of cocaine. Animals in group 4 had saline administered acutely. Dynamic FISP images were obtained on a 4.7 T magnet before and after IV injection. Gd-DTPA boluses with changes in intensity used to calculate the rCBV and transit time.
Results: Animals in groups 1 and 2 had increased rCBV and transit time while group 3 animals showed decreases. Animals receiving saline showed no changes.
Conclusion: Cocaine administration produces changes in rCBV and transit time in pretreated animals that depend on the length of time between the last pretreatment injection and the acute injection. These changes seem to parallel cocaine-mediated changes in extracellular dopamine concentrations.

519 • 4:27 PM
FMRI, ERP, CIT, and Dipoles: Utilizing Multimodality Techniques to Obtain Simultaneous Spatial and Temporal Information on Cortical Activity

DJ Vincent, MS Worden, W Schneider, J Shedden
Department of Radiology, Medical University of South Carolina, Charleston, SC

Purpose: Through combination of functional MR imaging (FMRI), high-density evoked response potentials (ERP) recordings, and mathematical analysis, the neural generators of cortical activity may be mapped in space and time. FMRI can provide millimeter spatial resolution of activation but has poor temporal resolution. Contrarily, ERP recordings have millisecond temporal resolution but poor spatial resolution. To merge these data, different mathematical techniques are being integrated.
Methods: In the initial single-subject study, uni- and bilateral stimuli were presented to either the upper or lower visual field in a rapid (~ 2 Hz) presentation attentional search paradigm. The subject was scanned in a 1.5-T GE Signa whole-body scanner with a single 5-inch surface coil over the occipital cortex. ERPs were recorded with 64 electrodes. ERPs yield the time points of interest and FMRI shows the locations, but not separated in time. The cortical imaging technique (CIT), a mathematical algorithm, is used to identify which areas are active at each time point, and then dipoles are placed at these locations and forward solutions computed.
Results: FMRI produced multiple discrete areas of activation. FMRI, ERP recordings, and CIT mappings all showed lateralization. Further mathematical analysis continues to be investigated.
Conclusion: Any single noninvasive technique (eg, PET, MEG, SPECT, BEAM) provides only partial information about the neural generators of cortical activity, but the merging of FMRI and ERP with sound mathematical formulations may elucidate these generators better than any method alone.

Wednesday Afternoon • Miro Room
Papers 528–529

MR ANGIOGRAPHY II

MODERATORS: JE Siebert, MD
S Wann, MD

528 • 4:09 PM
Evaluation of Aortic Disease by Noninvasive MR Measurement of Vessel Wall Distensibility

MS Relvas, BD Bolster, Jr, CJ Hardy, EA Zerhouni
The Johns Hopkins University School of Medicine, Baltimore, MD

Purpose: In vivo measurements of aortic distensibility may be useful in the evaluation of aortic pathology. A recently developed MR method allows noninvasive estimation of aortic distensibility from measurements of wavefront velocity during systole (1,2). Such measurements in patients with known aortic disease may provide a correlation between aortic distensibility and patient prognosis.
Methods: We studied the ascending and descending aortas of seven patients, using a previously described MR method (1,2). By observing the propagation of the blood velocity wavefront within a cylinder of excitation positioned within the aorta, we determined the distensibility of the vessel. We studied four patients with Marfan syndrome, one with normal aortic dimensions, one with a small aneurysm, and two with composite grafts of the ascending aorta. Another two patients with aortic aneurysms and one with an aortic dissection were studied. We compared these patients to an age-indexed control group that had normal aortic distensibility measures, ($10.3 \leq D \leq 81.8\ \mu m \cdot s^2/kg$), with a significant inverse correlation with age.
Results: All patients with aneurysms showed aortic distensibility measures well below the normal group, ($2.95 \leq D \leq 10.3\ \mu m \cdot s^2/kg$), when indexed with age. Although the grafts in the two patients with Marfan syndrome were of the same type, the older graft had a lower distensibility value. One patient with Marfan syndrome with a slightly dilated ascending aorta demonstrated a very low distensibility value.
Conclusion: This preliminary study suggests that MR distensibility measurements may help assess the functional status of normal and diseased aortic wall, thereby predicting the progression and outcome of aortic disease and guiding the management of such patients.
1. Hardy CJ, Bolster BD, McVeigh ER, et al., *Magnetic Resonance in Medicine*, In Press, 1994. 2. Hardy CJ, Bolster BD, McVeigh ER, et al., *SMRM Twelfth Annual Meeting*, p 148, 1993.

529 • 4:19 PM
Phase-Contrast and 2D Time-of-Flight MR Angiography in Near-Complete Carotid Occlusion

AW Litt, A Setton
Department of Radiology, New York University Medical Center, New York, NY

Purpose: To evaluate phase-contrast (PC) and time-of-flight (TOF) MR angiography (MRA) in patients with near-complete carotid occlusion indicated by conventional angiography.
Methods: Five patients with a near-complete carotid occlusion at the bifurcation seen with selective catheter angiography were examined with MRA of the neck and skull base. Routine 3D TOF sagittal and coronal MRA was performed, followed by a series of 2D PC MRA acquisitions in the skull base for only three velocity encodings (10, 30, and 60 cm/sec). In each, there was one flow-compensation acquisition and three flow-encoding acquisitions for the three orthogonal planes. Magnitude and phase images were reconstructed. Based on 2D PC MRA, 3D PC MRA with the best velocity was then performed along with axial 2D TOF angiography with a "traveling" superior saturation band.
Results: In all cases, routine coronal and sagittal MRA demonstrated either complete occlusion of the internal carotid artery at the bifurcation or an attenuated vessel that could be either internal carotid or ascending pharyngeal. The intracranial vessel signal was poor. 2D PC MRA demonstrated petrous and supraclinoid carotid flow on at least one velocity encoding. The direction of flow was ascertained from the phase images. The velocity correlated with the flow rate observed on the conventional angiogram. 2D TOF MRA always demonstrated the distal internal carotid with caudocranial flow.
Conclusion: Patients with suspected carotid occlusion based on conventional MRA studies should undergo either PC MRA or 2D TOF MRA of the skull base to detect a near-complete occlusion.

Wednesday Afternoon • Morocco Room
Papers 538–539

SPECTROSCOPY III

MODERATORS: DN Levin, MD
MD Osbakken, PhD

538 • 4:09 PM

In Vivo Multiple Quantum Surface Coil MR Study of Sodium in Rat Liver

V Seshan, MJ Germann, CR Malloy, AD Sherry, N Bansal
Department of Radiology, University of Texas Southwestern Medical Center, Dallas, TX

Purpose: It has been theorized that sodium binding to macromolecules only in the intracellular compartment may give rise to multiexponential decay characteristics, providing a means of distinguishing intra- and extracellular sodium by detecting multiple quantum coherences. In this study, we test this theory in the in vivo rat liver with a surface coil.
Methods: 80mM Tm-DOTP^{5-}, a sodium shift reagent (SR), was infused into an anesthetized rat, while interleaved single quantum (SQ) and triple quantum (TQ) spectra were collected from the exposed liver with a 4.7-T system and a surface coil.
Results: Two TQ resonances were observed in vivo from the *live* rat—intracellular and extracellular. The extracellular TQ signal disappeared when the rat died. Respiratory gating produced no change in this observation. In the TQ spectrum, it was observed that the extracellular signal did not have the same shift as the corresponding SQ signal. In alternate experiments using a two-cell phantom (with a saline-SR mixture circulating through the outer cell and NaCl bound in agarose gel in the inner cell), there was no TQ signal from the saline, indicating that the TQ filters were functioning properly.
Conclusion: This study indicates that the extracellular signal passes through the TQ filter when the animal is alive but is not detectable when the animal dies. This signal could be due either to blood flow or to biexponentially decaying sodium in the extracellular compartment.

539 • 4:19 PM

Effects of Hemorrhagic Shock on Hepatic Cellular Function: A Multinuclear MR Study

N Bansal, MJ Germann, V Seshan, GT Shires
Department of Radiology, University of Texas, Southwestern Medical Center at Dallas, Dallas, TX

Purpose: This study was planned to assess the effects of hemorrhagic shock and resuscitation on hepatic cellular energy level, pH, and intracellular Na^+ in an intact animal model by interleaved multinuclear MR techniques.
Methods: 80 mM TmDOTP^{5-}, an Na^+ shift reagent (1), was infused into anesthetized rats (n = 5), while interleaved ^{23}Na/^{31}P data were collected on a 4.7-T/40-cm Omega system. Baseline data were collected for 60 min, then the animals were bled to 30 mm Hg MAP for 60 min and resuscitated by reinfusion of withdrawn blood.
Results: TmDOTP^{5-} produced well-resolved intra- and extracellular ^{23}Na resonances without affecting ^{31}P spectra during the 60-min baseline period. Hemorrhagic shock decreased the hepatic ATP level to below 10% within 10 minutes, with cellular acidosis. Intracellular Na^+ signal remained unchanged for 30 min and then slowly increased to 130% by the end of the shock period. On resuscitation, the ATP level and intracellular pH did not return to the baseline value. Intracellular Na^+ returned to the baseline value 20 min after resuscitation.
Conclusion: The observed lag in Na^+ increase relative to the decrease in ATP during hemorrhagic shock agrees with a previously reported study of perfused mouse liver during nitrogen hypoxia (2). This lag may be due to a reduced influx of Na^+ into the cells after shock or to partial visibility of ATP and intracellular Na^+ with MR.

1. Bansal N, Germann MJ, Seshan V, et al., *Biochemistry*, 22, 5838. 2. Bowers JL, Lanir A, Metz KR, et al., *Am J Physiol*, 282, G638.

Wednesday Afternoon • Sapphire Room
Papers 548–550

DIFFUSION

MODERATORS: JA Helpern, PhD
RR Price, PhD

548 • 4:09 PM

Early Detection of Renal Ischemia with Diffusion-weighted Echo-Planar Imaging

VS Vexler, TPL Roberts
Department of Radiology, University of California, San Francisco, CA

Purpose: This study tested the hypothesis that diffusion-weighted echo-planar imaging (DW-EPI) can be used for early detection of renal ischemia in a rat model.
Methods: High-resolution DW-EPI coronal rat kidney images (64 × 64) were obtained with a GE 2.0-T CSI system. A diffusion-sensitized EPI sequence with orthogonal 90° and 180° selective pulses for field of view restriction was implemented (TE 40 ms, FOV 35 mm, slice thickness 2 mm). ADC (apparent diffusion coefficient) maps were obtained from a set of 11 differently sensitized (b factors from 10 to 1,210 s/mm^2; total acquisition time, 3 min) single-shot respiratory-gated coronal images acquired at 4-second intervals. A set of DW-EPI images was acquired before, immediately after (0 min), and at various time points after induction of focal renal ischemia with IM glycerol injection according to a well-studied model. Glycerol causes a vasoconstrictive decrease in renal perfusion (microsphere data). In our study, renal perfusion was noninvasively characterized in the same rat by using blood oxygenation–dependent (BOLD) imaging (Vexler et al, JMRI 1993; 3:483).
Results: The ADC values for normal kidneys were about 65%–70% of ADC values for the pure water at room temperature. Glycerol immediately induced a decrease in ADC values, most pronounced in the outer medulla (about 35% from control value) at 5–30 minutes after glycerol injection. BOLD images did not show any significant changes at these time points.
Conclusion: The results suggest that DW-EPI can be used for sensitive early detection of tissue abnormalities in a rat model of renal ischemia.

549 • 4:19 PM

MR Imaging of Brain Injury by Focal Ischemia: Effect of Inhibition of the Synthesis of Nitric Oxide

E Kozniewska, TPL Roberts, M Tsuura, J Mintorovitch, ME Moseley, J Kucharczyk
Department of Radiology, University of California, San Francisco, CA

Purpose: The present study was designed to determine, using high-speed MRI, the effect of nitro-L-arginine, the inhibitor of nitric oxide synthesis, on the evolution of cytotoxic brain edema during focal cerebral ischemia.
Methods: Diffusion-weighted and contrast-enhanced, perfusion-sensitive MR imaging was performed in anesthetized mechanically ventilated rats at 30 minutes and 1, 2, and 3 hours following occlusion of the middle cerebral artery combined with coagulation of the basilar artery. At the onset of ischemia, the animals were infused intravenously with 0.5 mL of either 0.9% NaCl or nitro-L-arginine (30 mg/kg). The severity of cytotoxic edema was evaluated based on changes in the water apparent diffusion coefficient (ADC) derived from diffusion-weighted images. Infarct size after 3 hours of ischemia was evaluated with 2,3,5-triphenyltetrazolium chloride staining.
Results: The percentage of decrease in ADC in the striatum of rats pretreated with nitro-L-arginine was significantly

smaller ($P < .05$) than in the control group at 30 minutes and 1 and 2 hours of ischemia. The ADC in the injured cortex of nitro-L-arginine–treated rats did not differ significantly from the ADC value measured in the contralateral cortex until 3 hours following occlusion. However, at 3 hours of ischemia the percentages of decrease in ADC in both the striatum and the cortex of either group of rats were similar. This transient attenuation of ADC drop during ischemia following nitro-L-arginine pretreatment occurred concurrently with a transient improvement in blood supply to the ischemic regions. The final infarct volume after 3 hours of ischemia did not differ between control and nitro-L-arginine–treated rats.
Conclusion: Nitro-L-arginine delays the development of ischemic injury by retarding cytotoxic brain edema. This effect is, at least partially, mediated by an improvement in blood supply to the ischemic tissues.

550 • 4:29 PM

ADC Changes during Physiologic Adaptation of the Brain to Chronic Hyponatremia

E Kozniewska, TPL Roberts, AI Arieff, J Kucharczyk
Department of Radiology, University of California, San Francisco, CA

Purpose: Hyponatremia results in a volume-regulatory response of brain cells. The immediate reaction (up to 2 hours) is to gain water (cytotoxic edema) followed by the regulatory volume decrease. This study examined the relationship between the apparent diffusion coefficient (ADC) for water protons (sensitive to cytotoxic edema) and the course of adaptation of the brain to hyponatremia.
Methods: Hyponatremia was induced in adult SD rats either for 90 minutes (acute) or for 3.5 days (chronic) with vasopressin and 140mM glucose. Diffusion-weighted and contrast enhanced (Sprodiamide, Sterling Winthrop, Collegeville, PA) perfusion-sensitive echo-planar imaging was performed in a 2-T animal imaging system in two groups of animals. In six rats after control imaging during normonatremia, acute hyponatremia was induced and imaging repeated 45 and 90 minutes thereafter. In another six rats imaging was performed after 3.5 days of hyponatremia. On completion of the MRI protocol, brain water and electrolyte content were evaluated.
Results: During acute hyponatremia (plasma Na^+ = 116mM ± 1) a 14% drop ($P < .01$) in ADC along with a 53% decrease ($P < .001$) in cerebral perfusion were observed at 45 minutes of hyponatremia. The ADC remained at the same lower level at 90 minutes of hyponatremia, whereas perfusion returned to the prehyponatremic value. Neither ADC nor cerebral perfusion differed from control values after 3.5 days of hyponatremia (plasma Na^+ = 102mM ± 4). Brain water content was elevated ($P < .01$) by 6.7% and 5.6% of the control value at 45 and 90 minutes of acute hyponatremia, respectively. After 3.5 days of hyponatremia, brain water was elevated by only 4% ($P < .01$) of the normonatremic value, which represented a significant decrease ($P < .05$) compared with acute hyponatremia.
Conclusion: ADC is sensitive to acute cytotoxic edema resulting from hyponatremia and may be used to monitor brain fluid electrolyte adaptation to this metabolic brain disorder.

Wednesday Afternoon • Topaz Room
Paper 559

OTHER: Instrumentation, Safety, Relaxometry

MODERATORS: E Kanal, MD
SR Thomas, PhD

559 • 4:21 PM

Ex Vivo Evaluation of Ferromagnetism, Heating, and Artifacts for 13 Different Heart Valve Prostheses Exposed to a 1.5-T MR System

FG Shellock, SM Morisoli
Tower Imaging, Los Angeles, CA

Purpose: To determine the ferromagnetic qualities, presence of heating, and artifacts for 13 different heart valve prostheses during MR imaging at 1.5 T.
Methods: Thirteen different heart valve prostheses (seven aortic, six mitral; pyrolytic carbon and titanium; CarboMedics, Austin, TX) were evaluated for safety compatibility with a 1.5-T MR system. A previously described, standardized protocol was used to measure deflection forces indicative of ferromagnetism. Artifacts were determined by attaching the heart valve prostheses to a fluid-filled QA phantom and imaging with a fast spoiled GRASS pulse sequence. The following scale was used to classify imaging artifacts: +, artifact smaller than implant metal; ++, equal in size to implant metal; +++, at least two times larger than implant metal. Heating was assessed by measuring surface temperature with a noncontact infrared thermometer immediately before and after a 30-minute, 3D GRASS, MTC pulse sequence (peak SAR > 3.0 W/kg).
Results: There was no measurable attraction to the 1.5-T static magnetic field exhibited by any of the 13 heart valve prostheses, and only minimal artifacts were observed (ie, +). The highest temperature change was +0.2°C.
Conclusion: MR procedures performed with a 1.5-T MR system may be performed safely in patients with any of the 13 different heart valve prostheses evaluated in this study.

Scientific Posters

The Scientific Poster Exhibits offer SMR attendees an opportunity to examine and discuss scientific material in a more intimate atmosphere.

Discussion periods, moderated by individual Scientific Poster presenters, are scheduled daily throughout the Meeting. A schedule of the discussion times follow:

Section:	**Diffusion/Perfusion/Functional/ Contrast Agents/Spectroscopy**
Poster #:	**P020-P030**
Day, Date:	**Sunday, March 6**
Time:	**12:00 PM - 1:30 PM**
Section:	**Clinical MRI: Head, Spine and Body**
Poster #:	**P145-P160**
Day, Date:	**Monday, March 7**
Time:	**12:30 PM - 1:30 PM**
Section:	**Vascular Imaging & Flow Quantification/Cardiac**
Poster #:	**P221-P228**
Day, Date:	**Tuesday, March 8**
Time:	**12:15 PM - 1:30 PM**
Section:	**Artifacts/Instrumentation/ Safety/Pulse Sequences**
Poster #:	**P319-P332**
Day, Date:	**Wednesday, March 9**
Time:	**12:15 PM - 1:00 PM**

SCIENTIFIC POSTER EXHIBIT AREA

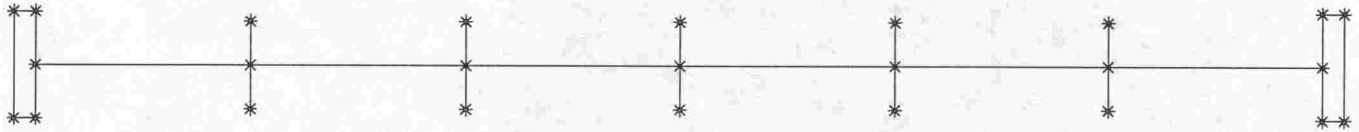

AISLE 000 –Diffusion/Perfusion/Functional/Contrast Agents/Spectroscopy

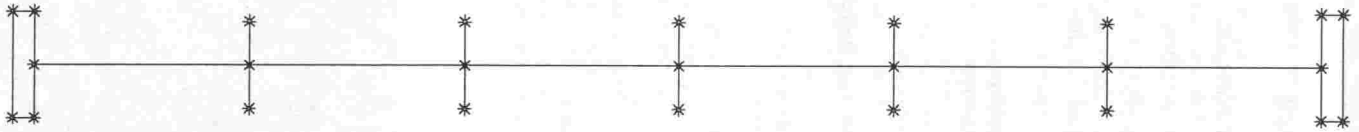

AISLE 100 – Clinical MRI: Head, Spine, and Body

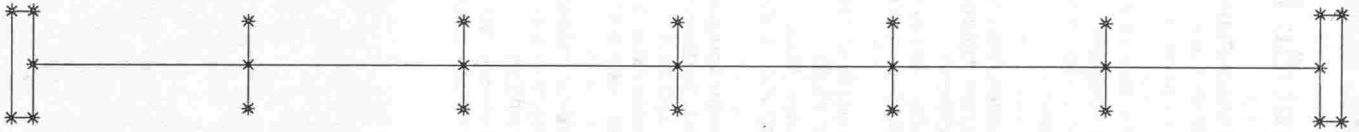

AISLE 200 – Vascular Imaging & Flow Quantification/Cardiac

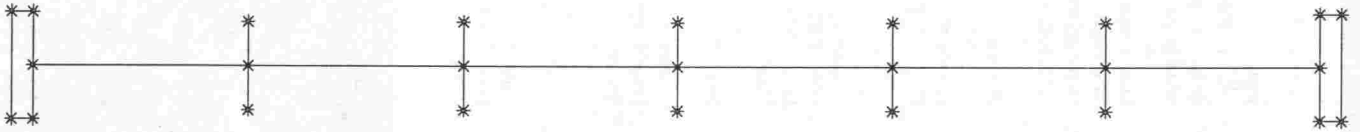

AISLE 300 – Artifacts/Instrumentation/Safety/Pulse Sequences

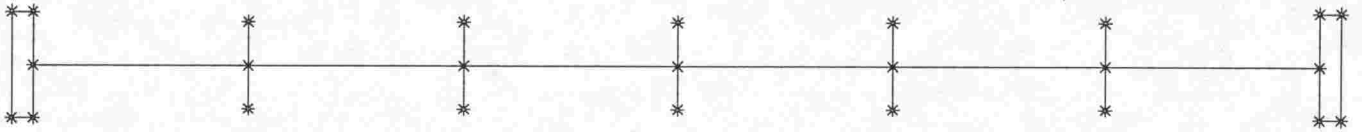

SMR '94 Works in Progress
Poster Abstracts

Sunday, March 6, 12:00 PM–1:30 PM
DIFFUSION/PERFUSION/FUNCTIONAL/ CONTRAST AGENTS/SPECTROSCOPY
Posters P020–P030

P020
Diffusion, Restricted Diffusion, and Susceptibility-induced Gradients in Celery and Spinal Cords at 200 mHz

JD Trudeau, WT Dixon, RC Long, Jr, JM Hawkins
Department of Radiology, Emory University Hospital, Atlanta, GA

Purpose: Diffusion measurements show large differences between white and gray matter and are sensitive to white-matter fiber orientation. Because magnetic susceptibility of internal structures should produce orientation-dependent changes in diffusion measurements, we examined the effects of both susceptibility and restricted diffusion on apparent diffusion coefficients (ADCs).
Methods: Diffusion measurements along the x, y, and z axes were performed on fresh celery stalks and freshly excised pig spinal cords. A Stejskal-Tanner pulse sequence was used with symmetric unipolar sensitizing gradients (PGSE) and antisymmetric bipolar gradients (BGP). The PGSE sequence underestimates diffusion in the presence of susceptibility-induced gradients along the measurement axis while the BGP sequence does not. Measurements were made with samples parallel and perpendicular to the static magnetic field.
Results: The apparent diffusion coefficient in celery obtained with the BGP sequence is isotropic and independent of sample orientation. The PGSE sequence also indicates an isotropic ADC when the celery stalk is oriented parallel to the magnetic field but shows an anisotropic ADC when perpendicular. When perpendicular, the diffusion coefficient along the celery axis exceeds the other two components by 40%. Both the BGP and PGSE sequences indicate an anisotropic ADC in the pig spinal cord with the diffusion coefficient along the axons being three to four times that of the other two components.
Conclusion: The PGSE sequence gives an anisotropic apparent diffusion coefficient in celery while the BGP sequence does not. This is evidently due to susceptibility differences within the sample. Similar susceptibility effects were not seen in spinal cord.

P021
Determination and Reduction of Statistical Error in Measurement of the Anisotropic Diffusion Tensor

JS Shimeny, VG Gulani, S Chandra
Biomedical Magnetic Resonance Laboratory, University of Illinois Urbana-Champaign, Urbana, IL

Purpose: Recently, interest in measuring the full anisotropic diffusion tensor (ADT) has been increasing (1). The techniques of multiple linear regression have great advantages in extracting the ADT from multiple images with varied gradient factors. In addition to their computational efficiency these methods enable rapid calculation of the statistical errors. These error estimates can be used to plan experiments that minimize statistical error.
Methods: Following the analysis of (2), also presented in (1), the damping b factors can be expressed as a function of the diffusion gradients G, with i,j taking on the values of x,y,z:

$$b_{ij} = \gamma^2 \int (\int G_i dt')(\int G_j dt')\, dt$$

The diffusion image intensity I at each pixel can be expressed as a function of the original image intensity and the ADT D, weighted by the damping b factors:

$$I = I_0 \exp[-\Sigma\, b_{ij} D_{ij}]$$

Taking the natural logarithm of the above expression brings it into a form amenable to analysis by multiple linear regression, but the errors must also be transformed to weight them properly (3). Combining expressions from images with different diffusion gradients gives a curvature matrix that can be inverted to solve for the ADT and also give the error matrix. The simulated statistical errors in the ADT can be minimized by careful selection of the diffusion gradients.
Results: Early results for the case of an isotropic diffusion coefficient indicate that linear stepping of the b factor gives better results than a polynomial (linear stepping of the gradients) or exponential distributions. The best results are obtained with the points evenly distributed between $b = 0$ and b selected such that the damping factor in the exponent is approximately -2. This result depends only weakly on the signal-to-noise ratio. Work is underway to study optimum gradient selection for the ADT case.
Conclusion: Multiple regression analysis can be used as a powerful tool to help plan diffusion experiments in order to minimize statistical error.
1. P.J. Basser, J. Mattiello, D. LeBihan, Diagonal and off-diagonal components of the self-diffusion tensor, SMRM book of abstracts, p. 1222, 1992.
2. E.O. Stejskal, *J. Chem. Phys. Vol.* 43, p. 3597, 1965.
3. P.R. Bevington, Data Reduction and Error Analysis for the Physical Sciences, McGraw-Hill, 1969.

P022
First-Pass Multislice Myocardial Perfusion Imaging in Patients at 1.5 T

EG Walsh, M Doyle, M Lawson, GG Blackwell, GM Pohost
Department of Medicine, Division of Cardiovascular Disease, University of Alabama at Birmingham, Birmingham, AL

Purpose: First-pass imaging with freely diffusing gadolinium contrast agents shows promise for clinical use in myocardial perfusion imaging. However, studies to date with adequate temporal resolution have been limited to single-slice acquisitions. The technique described permits acquisition of three image slices during the passage of a contrast agent through the myocardium, permitting assessment of perfusion in clinical studies.
Methods: The technique is an extension of the "keyhole" imaging method. In our technique, following acquisition (fast gradient echo, TR = 7 ms, TE = 3 ms) of a full resolution baseline matrix (128 × 128), the keyhole samples are further divided into two halves that are acquired on alternate heartbeats. These halves are then Fourier interpolated and assembled to form the complete keyhole sample, each sample consisting of an acquired half and an interpolated half to preserve the correct temporal relationship of the time varying information. By this means, 16 k-space lines per slice are acquired (in 112 ms) on each heartbeat (instead of 32 in 224

ms). T1 weighting is produced by inversion recovery. Imaging was performed in patients ($n = 11$) at rest and under stress (dipyridamole) concurrently with T1-201 and Tc 99m MIBI scans. Gadoteridol was injected as a bolus in doses of 0.05–0.1 mmol/kg.
Results: Comparison with nuclear scans indicates the ability to distinguish moderately reduced perfusion as well as severe perfusion deficiencies.
Conclusion: Dynamic MR imaging of the first pass of available gadolinium contrast agents can provide information currently provided by nuclear scans for the clinical assessment of myocardial perfusion.

P023
Vectorial Analysis of Blood Movement in the Aortic Arch
GA Rolland, A Verri
Institute of Radiology, University of Genoa, Genoa, Italy
Purpose: Along the aortic arch the blood reverses its flow direction. Due to the radius of curvature and high speed, the blood flow is unlikely to be laminar and the arterial wall is subject to pressure of variable intensity. Excessive pressure over small areas of the aortic arch has often been indicated as an important cause for arteriosclerotic and aneurysmatic pathologies. In order to evaluate the stress of the aortic wall, we propose a pointwise analysis of the complex movement of the blood in the aortic arch of normal and pathologic volunteers.
Methods: Six patients (three young normal patients, two with dissecting aneurysms, and one with a spindle-shaped aneurysm) were submitted to MR examination with a 0.5-T field strength magnet (Vectra GE). In order to obtain multiple sequential images (16–32) over a single cardiac cycle, a cine loop technique was used (gradient echo TE 15, FA 35°, ECG gated, sagittal-oblique single plane). The vectorial movement of the blood was computed by means of an optical flow technique in which a group of pixels is tracked frame by frame.
Results: The proposed technique appears to be adequate for a detailed analysis of the blood movement, especially in pathologic subjects, and for estimating the pointwise stress of the aortic wall. High stress was demonstrated at the proximal dissecting flaps in the examined chronic dissecting aneurysms and at the level of thinner wall in the spindle-shaped aneurysm. In contrast, a relatively lower level of stress was noted with parietal thrombosis.
Conclusion: The preliminary results are very promising. Clinical validation of the proposed method is ongoing.

P024
Theory of MR Signal Dephasing in the Presence of a Blood Vessel Network
DA Yablonskiy, EM Haacke
Mallinckrodt Institute of Radiology, St. Louis, MO
Purpose: The subject of this presentation is a theory of MR signal dephasing in the presence of static magnetic field inhomogeneities created by the network of blood vessels.
Methods: Blood vessels in the human brain form an interconnecting network of tubes that range in radius from 2–5 μm for small capillaries to 10–50 μm and larger for arterioles, metarterioles, venules, etc. This suggests that the blood vessel network may be divided into at least two subnetworks: a capillary network and a mid- to large-vessel network (MLN). The signal change resulting from these two networks may be separated out due to the motional narrowing effect. To calculate the MR signal decay caused by the MLN, we have applied a statistical approach similar to that described by Abragam for point dipoles (1). The MLN was modeled as a set of randomly distributed cylinders with different radiuses and random directions of their axes.
Results: The characteristic frequency shift describing this system is $\delta\omega = 4 \cdot \pi \cdot \gamma \cdot \Delta\chi \cdot B_0/3$. For the short time scale $\delta\omega \cdot t < 1.5$ the signal decay obeys the following law: $S(t) = (1 - \varsigma) \cdot \exp[-0.3 \cdot \varsigma \cdot (\delta\omega \cdot t)^2]$. For the long time scale $\delta\omega \cdot t > 2$ the signal obeys the monoexponential decay $S(t) = (1 - \varsigma) \cdot \exp[-R2^* \cdot |t - t_c|]$ with the relaxation decay rate $R2^* = \zeta \cdot \delta\omega$. In the above formulas $\Delta\chi$ is the susceptibility difference between blood and tissue, B_0 is magnetic inductance, ς is the volume fraction occupied by the MLN, and $t_C = 1/\delta\omega$.
Conclusion: The statistical approach allows an analytical calculation of the MR signal dephasing resulting from the blood vessel network. It gives direct insight into the precise signal shape and its dependence on blood volume fraction, magnetic inductance, and blood susceptibility.
1. A. Abragam. Principles of nuclear magnetism. Oxford University Press (1961).

P025
MR Imaging Contrast Effect of Gd-DTPA-BMA in Experimental Models
Y Tateno, K Yamada, H Kato, M Koga, F Shishido, H Ikehira, H Sugihara
National Institute of Radiological Sciences, Tokyo, Japan
Purpose: Gd-DTPA-BMA (Omniscan, Nycomed Imaging AS) is a new paramagnetic and nonionic contrast agent for MR imaging. The purpose of this study was to confirm the diagnostic potential of Gd-DTPA-BMA in various experimental models.
Methods: Male Sprague-Dawley rats (350–500 g), male SHR-SP ($\approx$250 g), and New Zealand White rabbits of each sex (1.7–3.4 kg) were used for the investigations. Gd-DTPA-BMA was administered intravenously at 0.1 mmol/kg (0.05 mmol/kg only for hydronephrosis), an anticipated clinical dose. Experimental models were as follows: brain tumor, SHR-SP, middle cerebral artery occlusion, lung tumor, liver tumor, hepatocellular carcinoma, hydronephrosis, ovarian tumor, bone tumor, and muscle tumor. All lesions were identified by means of histopathologic examinations. MR images were obtained with either a 1.5-T Gyroscan S15 (Philips Medical Systems, The Netherlands), or a 2.0-T RS-200 (Siemens-Asahi Medical Technology, Japan).
Results: Gd-DTPA-BMA showed varying degrees of contrast effect and persistence in different models. The signal intensity of the postcontrast imaging was superior to that of the precontrast imaging. The findings obtained with enhanced MR imaging were consistent with morphologic changes in respective models.
Conclusions: These differences among the models may be related to differences in the permeability of microvasculature and in the blood flow. The models employed were adequate for predicting the clinical usefulness of the contrast agent. The above result suggests that Gd-DTPA-BMA should be useful for the diagnosis of tumors under these experimental conditions.
K. Yamada has conducted cooperative studies at Daichi Pharmaceuticals, Ltd.

P026
Gadolite: A Novel Contrast Agent for MR Imaging of the Gastrointestinal Tract
KJ Balkus, Jr, I Bresinska
Department of Chemistry, University of Texas at Dallas, Richardson, TX
Purpose: The harsh environment of the gastrointestinal (GI) tract presents a particularly difficult challenge for the development of suitable MR contrast media. Zeolites, a special class of microporous metal oxides, have been modified with gadolinium and found to be effective MR contrast agents for the GI tract. The pharmaceutical formulation known as Gadolite is currently in clinical trials. This paper will address the physicochemical properties of Gd(III)-exchanged zeolites, including relaxivity.
Methods: Zeolite modification with gadolinium was accomplished with conventional ion exchange methods and assayed by means of titration with EDTA. Relaxivities were measured by using the T_{null} method.
Results: The ion exchange of Gd(III) into zeolite NaY can be accomplished reproducibly (±0.1% Gd by wt). Acid stability tests reveal indicate that a <1% suspension is stable to a pH of 2.5. Significant amounts of Gd(III) are not released until the pH is much lower. The GdNaY zeolites are stable to Na^+ and K^+ but partially exchange with Ca^{2+} and Mg^{2+}. Animal studies have shown no toxicity or side effects. The relaxivity

was found to vary with gadolinium loading as well as the thermal history of the molecular sieves. The relaxivities increase as the zeolites become more magnetically dilute. Additionally, the relaxivities depend on the intrazeolite location of the paramagnetic ion. Preliminary imaging results will be discussed.
Conclusion: Gadolinium-exchanged NaY zeolites were found to be stable under simulated physiologic conditions. Suspensions of GdNaY exhibit image brightening at low concentrations and provide excellent contrast in the GI tract of animals.
K.J. Balkus, Jr, is a consultant for Pharmacyclics, Inc.

P027

New Chelate Gd Complexes as MR Contrast Agents

SP Vasilievich, SN Lvovich, PK Ivanovich, BE Nikolaevna, PV Olegovich, ES Vladimizovna, AT Abdullaevich, MD Alexandrovich
MRI Laboratory, Institute of Chemical Physics, Moscow, Russia

Purpose: To study application of new original modified chelate Gd complexes (Gd-TGEID – 0.33 mmol/kg, Gd-EDF – 0.016 mmol/kg, Gd-TPED – 0.267 mmol/kg, and Gd-DTPA – 0.5 mmol/kg; synthesized at the Institute of Chemical Pure Reactives of the Russian Academy of Sciences, Moscow, Russia) as the base of MR contrast agents with intravenous and with oral administration. Their performance is compared with Magnevist (Schering, Berlin Germany).
Methods: All T1 measurements were obtained on the IVR-3-NMR relaxometer with magnetic field pulsed gradient and with a resonance frequency of 22 MHz and an inversion-recovery pulse sequence (T = 293K). We studied the relaxation efficiency of different concentrations of Gd complexes in phosphate buffer solutions (pH = 7.4) and in organs and tissues after paramagnetics administration in brain, liver, kidneys, blood and heart of normal white rats (160–180 g) at 10, 20, 30, 40, and 60 minutes after tail vein injection and at 1, 2, 3, and 4 hours after oral administration of Gd-TGEID. The toxicity of substances was tested with standard methods. To compare relaxation activity we used ΔW_1: $\Delta W_1 = (1/T1_{\text{after contrast administration}} - 1/T1_{\text{before contrast administration}})/(1/T1_{\text{before contrast administration}})$.
Results: All substances appeared to have very low toxicity. All of the investigated Gd complexes had more influence on the T1 than Magnevist, both in phosphate buffer solutions and in rat organs and tissues. Similar kinetics of the biodistribution were observed in blood; maximum enhancement of ΔW_1 of ^1H in blood was measured in vitro 10 minutes after administration of the Gd-TPED, and then a decrease occurred. Gd-DTPA showed maximum activity 20 minutes after injection. The maximum change in the liver and kidneys occurred at 4 hours and in the heart at 3 hours. Data showed that the maximum relaxation activity of Gd-TPED did not differ from the efficiency of Gd-DTPA, and Gd-TGEID from Magnevist. The relaxation efficiency of Gd-DTPA and Magnevist was the same in the liver. In most cases Magnevist had lower efficiency at maximum effect than Gd-TPED and Gd-DTPA.
Conclusion: From these data we conclude that all studied agents provided a strong and persistent decrease in T1 in solutions and in tissues of rats and had low toxicity. They may become the base of new MRI contrast agents after further investigation.
Disclosure unavailable at time of publication.

P028

Pharmacokinetics of the Hepatobiliary MR Contrast Agent Gd-EOB-DTPA in Humans: Results of Phase I Clinical Trials

A Muhler, T Frenzel, H Vogler, T Staks, HJ Weinmann
Contrast Media Research, Schering AG, Berlin, Germany

Purpose: In animal experiments, the hepatobiliary contrast agent Gd-EOB-DTPA has shown promise for improved detection of liver tumors with conventional MR imaging and was found to be nontoxic. Thus, the agent was advanced into first clinical trials. The current report describes the elimination and pharmocokinetics of Gd-EOB-DTPA in human volunteers.
Methods: Four doses of Gd-EOB-DTPA (lot SHL 569 B) have been used in phase I clinical trials: 10, 25, 50, and 100 μmol/kg. Eight volunteers per dose group were evaluated for pharmacokinetics. Blood serum, feces, and urine were collected in fractions over a 4-day observation period. The biologic samples were digested and homogenized by means of microwave irradiation under strongly acidic conditions. Gadolinium concentrations were determined by means of ICP-AES (inductively coupled plasma atomic emission spectrometry) at a wavelength of 342.247 nm. A two-compartment model was chosen as the best fit for the evaluation of the obtained data.
Results: The MR contrast agent was eliminated from the body through two excretion pathways to about the same extent. Between 43% and 53% of the injected dose was excreted via the urine, and 41%–51% appeared in the feces. Only a minor dependence on the injected dose has been observed regarding the relationship between renal and extrarenal elimination. However, the elimination half-life from blood serum increased from 1.1 hours at a dose of 10 μmol/kg to 1.7 hours at 100 μmol/kg. The terminal distribution volume was found to be 0.26–0.29 L/kg, a sign of the accumulation of Gd-EOB-DTPA outside the extracellular space (most likely the liver compartment). The renal clearance (114–126 mL/min) corresponded well with the known glomerular filtration rate in humans. Whole-body clearance decreased from about 300 to 237 mL/min, with increasing doses confirming the nonlinear kinetics of the extrarenal elimination pathway via a saturable transport system in the liver.
Conclusion: In humans, about half of the injected dose of Gd-EOB-DTPA is rapidly taken up by liver cells and is subsequently excreted via bile and feces. These properties are unique among current hepatobiliary agents in clinical trials, making Gd-EOB-DTPA well suited for hepatobiliary MR imaging. The data in humans fully support the results in preclinical development of Gd-EOB-DTPA, and those obtained preclinical results may likely reflect the situation in patients.

P029

Etiology of Liver Abscesses: Identification with Proton MR Spectroscopy

HK Singh, KN Prasad, SS Baijal, S Roy, SK Jain, RB Gujral
Department of Radiology, S.G.P.G.I.M.S., Lucknow, India

Purpose: Effective medical treatment of liver abscesses requires precise identification of etiologic agent(s). Diagnostic techniques such as US, CT, microbiology, and serology, often fail to be specific and/or require several days of work-up. The present study aimed to identify the etiologic agent(s) (pyogenic or amebic) with proton MR spectroscopy (H-1 MRS).
Methods: Water-suppressed H-1 MRS, performed with a 400-MHz WM400 MR machine, was done on supernatants of eight drained liver abscesses from seven patients. The supernatants were obtained by freezing and thawing, ultrasonication, and centrifugation at 2,000 *g*. The pus samples were also processed by means of microbiologic techniques to ascertain the etiology (amebic or pyogenic).
Results: All four amebic diagnosed samples show the intensities of 1, 4.17 ± SD 0.19, and 10.3 ± SD 1.41 at 8.65, 7.46, and 6.06 ppm, respectively, at H-1 MRS study. The four pyogenic diagnosed abscesses exhibited corresponding intensities of 1, 2.78 ± SD 0.38, and 5.47 ± SD 0.82. Several additional peaks have also been noticed in pyogenic abscess in the same range of chemical shift.

Conclusion: Amebic and pyogenic liver abscesses can be differentiated with H-1 MRS by comparing the ratio of the intensities. This approach may be helpful in the diagnosis of etiologic agent(s) of other abscesses also.

P030

Application of the Accurate Assessment of Intracellular Magnesium and pH to Neonatal Hypoxia-Ischemia

GD Williams, MB Smith
Department of Radiology, NMR Division, Hershey Medical Center, Pennsylvania State University College of Medicine, Hershey, PA

Purpose: To apply, for the first time, our technique for the accurate noninvasive assessment of intracellular magnesium ion and pH from the P-31 chemical shifts of ATP. This work tests the sensitivity of the method by application to a perinatal asphyxia model in brain tissue.
Methods: Model calibration solutions were prepared as a function of total Mg/ATP and pH, and the three P-31 MR chemical shift differences of ATP were numerically modeled for these two parameters (GD Williams et al., Anal. Biochem. 214, 458–467, 1993). The effect of 3 h of hypoxic-ischemic insult on intracellular brain (Mg) was evaluated at 9.4 T in a well-established 7-day-old-rat model of cerebral hypoxia-ischemia (GD Williams et al., Neurosci Lett 144, 103–106, 1992).
Results: Since the accuracy of the chemical shift differences limits the technique's in vivo application, we first performed numerous averaging of these individual shifts to reduce the uncertainty. During the final hour of hypoxia-ischemia there was a significant increase ($P < .0001$) in free magnesium. The normal, late hypoxia-ischemia, and early (1.0–2.0 h) recovery values of free Mg were 0.336 ± 0.015, 0.501 ± 0.104, and 0.326 ± 0.08 respectively. The pH of the ATP compartment was also calculated from the shifts.
Conclusion: The changes in free magnesium during neonatal hypoxia-ischemia are consistent with the temporal decrease in ATP during hypoxia and its return toward the normal neonatal value of 2.8 mM during recovery. This evaluation of ATP shifts is general for most in vivo applications and will favor lower Mg_f values than most prior estimates.

Monday, March 7, 12:30 PM–1:30 PM
CLINICAL MRI: Head, Spine and Body

Posters P145–P160

P145

MR Imaging Observation of a High Frequency of Cerebral Ventricular Enlargement in a Strain of Beagles

T Vullo, RP Manzo, A Tankhiwale, DG Gomez, MDF Deck, PT Cahill
Department of Radiology, Methodist Hospital, Brooklyn, NY

Purpose: Clinically asymptomatic hydrocephalus in certain breeds of dogs is relatively common, particularly in miniature breeds having dome-shaped heads. It also occurs in the beagle as a developmental anomaly or is prevalent in particular strains but not in the general beagle population. In the current study, MR imaging was performed in asymptomatic adult purebred beagles acquired from the same breeding colony. The size of the lateral ventricles were graded visually and determined quantitatively.
Methods: Seventeen clinically asymptomatic adult purebred beagles were acquired from a single supplier that bred its own specific strain. T1-weighted MR images were acquired at 2.0 T. The beagles' lateral ventricular sizes were graded visually by eight observers on a scale from 0 to 3, and quantitative measurements were performed by computer. In beagles having large ventricles, Gd-DTPA was introduced into the cisternal magna, and the presence of communicating versus noncommunicating hydrocephalus was determined.
Results: Overall, four beagles were graded as normal, and four with slight, three with moderate, and six with significant ventricular distension. Quantitated ventricular volumes ranged from 77 to 11,726 mm^3. Communicating hydrocephalus was seen in all dogs tested with Gd-DTPA.
Conclusion: In all, 76% of the beagles were graded as having some degree of ventricular enlargement. Since these canines were acquired as adults, the origin and progression of their communicating hydrocephalus could not be determined.

P146

Diagnosis of TIA and Minor Stroke with Diffusion and Metabolic Imaging

JW Hugg, SR Levine, GG Brown, JR Ewing, TJ Dombi, KMA Welch
Neurology Department, Henry Ford Health Sciences Center, Detroit, MI

Purpose: Meta-analysis of PET, SPECT, and gamma camera studies showed persistent focal metabolic or blood flow deficits in 61 ± 5% of patients with transient ischemic attack (TIA) or minor stroke. This ongoing clinical research program uses noninvasive MR measures to sharpen and improve clinical diagnosis and vascular risk prediction for patients with TIA or minor stroke.
Methods: We perform diffusion-weighted imaging (DWI) and both H-1 and P-31 MR spectroscopic imaging (MRSI) with our 3-T Magnex clinical system with SMIS console. Patients also undergo T2-weighted MRI, CT, neuropsychological testing, and often SPECT. We study patients acutely within 48 hours of ictus, subacutely at 5–10 days, and chronically at 2–3 months. We follow patients clinically to determine if MR findings can help predict vascular risk for subsequent stroke or heart attack. We are developing MR perfusion-weighted imaging to measure blood flow and rapid MR protocols to shorten the examination time.
Results: In the first few patients in this new program, we have observed minor stroke with DWI. P-31 MRSI has shown persistent focal metabolic deficits in the vascular region of transient neurologic deficits. H-1 MRSI has shown neuron loss in infarcts.
Conclusion: DWI and MRSI can help detect minor stroke, neuron loss, and metabolic deficits to improve clinical diagnosis and, perhaps, risk prediction in TIA or minor stroke.

P147

Dextran-covered Superparamagnetic Iron Oxide: Efficacy for Detection of Metastatic Nodes in Head and Neck Cancer

Y Anzai, RB Lufkin, K Blackwell, S Hirshowitz, J Rogers, Y Sato, WTC Yuh, V Runge
UCLA Medical Center, Los Angeles, CA

Purpose: The efficacy of dextran-coated superparamagnetic iron oxide (BMS 180549) as a new intravenous MR contrast agent for differentiation of metastatic from benign nodes was investigated in 13 patients with head and neck cancer.
Methods: BMS 180549 at a dose of 1.7 mg Fe/kg was injected intravenously. Pre- and postcontrast (10–48 hours) MR examinations were performed. The final pathology of each node was correlated with MR findings. Ninety-two pathology-proved nodes were visually analyzed. The minimum axial diameter of each node was measured. The criteria for the iron contrast study were compared with the size criteria in terms of detection of metastases. In addition, quantitative image analysis was performed with visually selected regions of interest, and signal intensities were measured for 66 lymph nodes as well as the adjacent muscles.
Results: Forty-one of the 43 histologically proved metastatic nodes showed high signal, and 41 of 49 benign nodes showed homogeneous low signal intensity following contrast administration, providing a sensitivity of 95.3% and a specificity of 83.7%. The signal intensity ratio of benign nodes was significantly lower than that of metastatic nodes. Furthermore, 13 of 14 normal-sized metastatic nodes were detected with this iron agent.
Conclusion: MR imaging with BMS 180549 yielded tissue-specific differentiation of metastatic from benign nodes in patients with head and neck cancers. This agent may have

potential to enhance the detection of metastatic lymph nodes in cancer patients and deserves further investigation.

P148

Clinical Experience in FDG PET Imaging with PET-MR Coregistration in Head and Neck Cancer

Y Anzai, C Hoh, U Sinha, S El-Saden, R Hawkins, J Bailet, M Mendekarm, R Lufkin
UCLA Medical Center, Los Angeles, CA

Purpose: The efficacy of FDG PET is investigated for detection of (*a*) the primary lesion in clinically "primary unknown cancer" patients, (*b*) early recurrent cancer in previously treated patients, and (*c*) lymph node metastases. We summarize 39 cases of our experience with FDG PET and MRI correlation for head and neck cancers and discuss clinical indications of FDG PET in the head and neck.
Methods: MRI was performed on a 1.5-T unit with T1- and T2-weighted spin-echo sequences. PET imaging was performed with CTI931/08-12 and 931-53. FDG (10 mCi) was injected intravenously after 4 hours of fasting. PET and MRI coregistration was developed by modification of the surface-matching algorithm. Thirty-nine patients with head and neck cancer were evaluated in this study.
Results: In two of five cases of clinically primary unknown cancer patients, FDG PET could demonstrate the area of abnormality suggesting primary tumor. These lesions were confirmed by biopsy. Thirteen patients underwent FDG PET for detection of recurrent tumor following radiation therapy. FDG PET could detect the presence of recurrent tumor, whereas MRI was inconclusive. Twenty-two of 25 metastatic nodes and 17 of 115 nonmetastatic nodes also showed increased activity, resulting in 88% sensitivity and 85.2% specificity.
Conclusion: Although clinical use of PET imaging has been criticized for its high cost, FDG PET imaging is helpful for determining the localization of tumor, where MRI and clinical examination are nondiagnostic or inconclusive.

P149

High-Resolution Fast SE MR Imaging of the Internal Auditory Canal: Is Contrast-enhanced Imaging Still Necessary?

KB Remley, AE Stillman, DJ Loes
Department of Radiology, Neuroradiology Division, University of Minnesota Hospital and Clinics, Minneapolis, MN

Purpose: Contrast-enhanced T1-weighted MR imaging is the current technique of choice for evaluating the internal auditory canal (IAC) and cerebellopontine angle (CPA) in patients with asymmetric or unilateral sensorineural hearing loss. This study compared high-resolution fast SE (FSE) imaging with standard contrast-enhanced T1-weighted imaging in patients with suspected acoustic schwannoma.
Methods: Two hundred twenty-seven patients with suspected acoustic schwannoma were evaluated with 1.0- or 1.5-T imaging systems. Acquisitions included pre- and postcontrast axial T1-weighted sequences (600/20, 3-mm sections, 16–20 field of view [FOV], 256 × 192 matrix) and a T2-weighted FSE coronal sequence (4,000–5,000/100–120, echo train length of 16, 3-mm sections, 18–22 FOV, 512 × 384 matrix). The FSE and T1 precontrast pair were blindly reviewed together by three independent readers, followed by blinded review of the T1 pre- and postcontrast pair by the same readers.
Results: Twenty-one lesions in 20 patients were identified in the CPA/IAC with the contrast-enhanced T1-weighted sequence. The FSE/precontrast T1 pair detected 19 lesions (two readers) and 20 lesions (one reader), for an average sensitivity of 92% and specificity of 99%. Sensitivity dropped to 72% for the detection of intracanalicular tumors ($n = 5$).
Conclusion: The combination of the coronal FSE and axial nonenhanced T1 sequences provides excellent sensitivity and specificity for screening the CPA/IAC, when compared with contrast-enhanced imaging, although very small intracanicular tumors can be missed. This alternative unenhanced screening examination may have important future economic implications as health care spending is restricted.

P150

High-Resolution MRI of the Aquatic Turtle

A Tankhiwale, T Vullo, PT Cahill
Department of Radiology, Methodist Hospital, Brooklyn, NY

Purpose: The aquatic turtle is unique in that it can withstand long periods of apnea without respiratory or cardiac deficit. The resistance of the turtle's heart when exposed to anoxia and acidosis has warranted it as a research model of these conditions. To date, only a few MRI and MRS analyses of limited scope have been reported for the turtle. Here, a complete high-resolution MRI study of the gross anatomy of the turtle is presented.
Methods: Aquatic turtles were anesthetized with an intramuscular injection of ketamine/xylazine. Multiplanar, multislice T1- (TR/TE = 750/25), T2- (TR/TE = 2,000/75) and proton- (TR/TE = 2,000/25) weighted MR images were acquired at 2.0 T, with a slice thickness of 1.0 mm, interslice gap of 1.0 mm, and intraplanar resolution of 0.35 mm. In addition, separate high-resolution MR images (intraplanar resolution, 0.20 mm) of the brain and spine were also obtained.
Results: The complete gross anatomy of the turtle was clearly defined by high-resolution MR imaging. The brain and spinal cord could be clearly visualized, in addition to the individual vertebral bodies. On the whole, the turtle has a very small percentage of fat, which serves to reduce contrast on T1-weighted images. On the other hand, the aquatic turtle has a high water content (as evidenced by T2-weighted MR images) with respect to the total body mass.
Conclusion: To our knowledge, this is the first complete high-resolution MRI study of the turtle. Additional studies will investigate the use of MRI in evaluating the physiology of the turtle and other aquatic organisms in medical research.

P151

MR Imaging of the Endometrium Prior to Embryo Transfer

LW Turnbull, SR Killick, CF Rice, A Horsman
Centre for Magnetic Resonance Investigations, Hull Royal Infirmary, Hull, England

Purpose: Unsuccessful embryo transfer (ET) remains the commonest cause of failed in vitro fertilization (IVF) treatment. Controversy exists as to whether transvaginal ultrasound (TVS) assessment of endometrial thickness and echogenicity can be used to determine the likelihood of successful ET. Although from ex vivo histologic studies there is a discrepancy between the zonal anatomy measured by MR imaging and TVS, MR imaging does provide accurate quantitative data and the relative signal intensity can be calculated to provide information concerning tissue characterization. This pilot study aims to investigate the possible role of MR imaging in the investigation of uterine receptivity.
Methods: Sixteen women were recruited who were undergoing stimulated IVF and had three or more fertilized oocytes. MR imaging was carried out 18 hours prior to ET. A 1.5-T system (IGE Signa Advantage) with a pelvic phased-array coil was used. T2-weighted fast spin-echo images were acquired parallel and perpendicular to the long axis of the uterus, with use of a 256 × 256 matrix, and a 4-mm slice thickness. Images were analyzed for endometrial thickness, cross-sectional area, and total volume on an ISG Allegro Workstation. TVS (ALT Ultramark 4, 5-MHz probe) was performed on the day of ET to assess endometrial thickness.
Results: There was no significant difference in the maximum AP endometrial thickness between the pregnant and nonpregnant groups with either MR or TVS, nor was there a significant difference between the volumes of the junctional zone or myometrium. The mean (±SD) total endometrial volume was similar for the six conceptual treatments (56.8 cm^3 ± 29.7) and the 10 nonconceptual treatments (40.9 cm^3 ± 18.5), but the mean cross-sectional area of endometrium was significantly greater in the conceptual group (7.6 cm^2 ± 2.0 vs 5.0 cm^2 ± 2.0; $P < .02$). The SI of the junctional zone was simi-

lar in both groups, that of the endometrium was less but not significantly so in the pregnant group, while that of the myometrium was significantly less in the pregnant group (81.3 ± 28.8 vs 117.8 ± 28.3; $.05 > P > .02$).
Conclusion: Despite the small numbers in this pilot study an interdependence has been demonstrated between endometrial cross-sectional area, myometrial signal intensity, and successful implantation, and it is hoped that in the future MR will provide additional useful information on uterine receptivity, which will aid in the understanding of implantation.

P152
High-Resolution Wrist MR Imaging at 1.5 T
WCE Kwok, S Totterman, R Miller
University of Rochester, Rochester, NY
Purpose: To develop a high-resolution SE pulse sequence for wrist MR imaging on a 1.5-T clinical imager and test it on cadaveric wrists.
Methods: To achieve that goal we modified the existing 2D SE sequence on a GE Signa (version 4.8) 1.5-T system. Due to the limit of gradient strength of 1 G/cm, the width of gradient pulses were lengthened to increase the resolution. The slice selection and the RF pulse widths were doubled to reduce the slice thickness. To double the resolution in the frequency encoding direction, the readout bandwidth was reduced by half to ±8KHz. This doubled the readout time, and the readout gradient was lengthened accordingly. The phase-encoding pulse had the shape modified from half-sine to trapezoid to reduce the increase in pulse width. These modifications resulted in an in-plane resolution of 156 μm (4-cm FOV with 256 × 256 matrix), a slice thickness of 1.5 mm, and a minimum TE of 32 msec for nonobliqued full-echo acquisition. To increase the S/N, specially designed perpendicular wrist coil arrays were used. Five cadaveric wrist specimens were imaged with this pulse sequence at a TR of 2,200 msec, a TE of 32 msec, and 1 NEX.
Results: Anatomic details observed in the tendons, ligaments, and trabecular structures of the wrists were very well visualized. Chemical shift artifacts were observed due to the lower receiver bandwidth, but they were not significant.
Conclusion: The modified 2D SE pulse sequence provides high-resolution MR images of the wrist within normal imaging time. It should be very helpful in clinical evaluation of painful wrist.

P153
Assessment of Primary Bone Tumors with Chemical Shift MR Imaging
F Schick, S Duda, M Müller-Schimpfle, M Laniado, O Lutz, CD Claussen
Institute of Diagnostic Radiology, Tübingen, Germany
Purpose: The frequently used spin-echo and gradient-echo MR imaging sequences provide signal contrast based on the total proton density and relaxation times. Therefore, small concentrations of water within yellow bone marrow as in subtle edema or due to tumor cell infiltration are not visible in the surroundings of the bone tumors. On the other hand, small fractions of fat within tumors are often not well demonstrated. The selectivity of gradient-echo sequences with fat saturation (STIR) is sometimes reduced due to inhomogeneities of the RF field, and the provided signal intensity might be reduced due to microscopic B_0 inhomogeneities with gradient-echo refocusing. Therefore the value of single-slice spin-echo fat or water images with frequency-selective excitation was studied in the course of 35 examinations in 22 primary bone tumors.
Methods: Chemical shift selective spin-echo imaging (SENEX [1,2]) of the fat and water protons was compared with proton density–, T1-, and T2-weighted standard spin-echo imaging on a 1.5-T whole-body unit (Siemens). A representative slice of the tumor and the adjacent bone marrow was recorded in the examinations of 22 patients (five osteosarcomas, two chondrosarcomas, two Ewing sarcomas, 13 benign tumors). The visibility of the peritumorous edema and the fat signals within the tumors were evaluated. The MR findings were compared with parallel histologic typing.
Results: Peritumorous edema was indicated in five cases with T2-weighted SE imaging. Water-selective SENEX imaging showed edema (or slight tumor infiltration) in 13 cases. The extension was clearly better demonstrated on the SENEX water images than on T2-weighted standard SE images. All malignant tumors showed perifocal edema in water-selective SENEX images. Only four of the benign tumors showed clear peritumorous water signals on the SENEX images. The tumor masses of the malignant tumors were free of fat signals, whereas in three osteochondromas fat signals could be seen with using fat-selective imaging.
Conclusion: Application of MR imaging methods with high sensitivity and specificity to small fractions of water in yellow bone marrow and small amounts of fat in tumor masses can provide additional information in diagnosis and delimiting of primary bone tumors.
1. Braun M., Jung W.-I., Lutz O., Oeschej R. *Z. Naturforsch.* 42a, 1391 (1987). 2. Schick F., Bongers H., Jung W.-I., Skalej M., Lutz O. *Magn. Reson. Imaging* 9, 509 (1991).
Disclosure unavailable at time of publication.

P154
Role of MR Imaging in the Evaluation of Metastasic and Recurrent Epithelioid Sarcoma
JA Romero, EE Kim, IS Moral, R Benjamin
University of Texas M. D. Anderson Cancer Center, Houston, TX
Purpose: Since its first description in 1970, epithelioid sarcoma has been known to be a soft-tissue sarcoma that presents numerous recurrences and metastases. Intratumoral hemorrhage has been seen in 20% of cases. We evaluated MRI findings of metastasic and recurrent epithelioid sarcomas with or without hemorrhage.
Methods: Thirty-one MRI studies were restrospectively analyzed in 11 patients with histologicaly proved epithelioid sarcoma. These were correlated with clinical follow-up findings, including serial MRI scans for an average period of 34.18 months for all the patients and 25.3 months for patients with hemorrhagic tumors.
Results: Metastasis was observed in 54.5% of total patients. However, it was seen in all patients with hemorrhagic epithelioid sarcoma but only 33% of those with nonhemorrhagic sarcomas. The average time of metastasic appearance was 5.0 months for hemorrhagic lesions (SD 2.8) and 27.6 months for nonhemorragic lesions (SD 8.5). Recurrent sarcoma was seen in 33% for both hemorrhagic and nonhemorragic groups, appearing after 18 and 22–25 months, respectively.
Conclusion: Patients with hemorrhagic epithelioid sarcoma appear more common and have earlier appearing metastasic lesions than those with nonhemorrhagic lesions. This suggests that the presence of hemorrhage might be useful as a prognostic factor in epithelioid sarcomas. There is no significant difference in recurrence time between hemorrhagic and nonhemorrhagic sarcomas.

P155
MR Imaging Evaluation of Biologic Differences in Desmoid Tumors
JA Romero, EE Kim
University of Texas M. D. Anderson Cancer Center, Houston, TX
Purpose: Previous pathologic studies have suggested the existence of biologic differences in desmoid tumors in patients in different age groups. Tumors in the juvenile group (aged < 15 years) may be related to congenital anomalies of the connective tissue, and those in the fertile group (aged 15–50 years) are probably related to traumatic and hormonal factors. We evaluated MRI findings in desmoid patients to identify such biologic differences.
Methods: We retrospectively reviewed 105 MRI studies in 32 patients with histologically proved desmoid tumors. MRI analysis was attempted to detect the presence of fibrosis, configuration of tumor (infiltrative versus nodular), and the frequency and timing of the tumor recurrence. The average follow-up period was 60.4 months.

Results: The frequency of the presence of fibrosis in juvenile and fertile groups was 40% and 57.2%, respectively. The juvenile group showed infiltrative patterns at a greater proportion (60%), while the nodular pattern was present in 86% of the fertile group. All patients from the juvenile group showed a recurrence in an average period of 23 months, whereas only 40% of the patients from the adult group showed a recurrence in an average period of 63.4 months.
Conclusion: MRI findings of the morphologic pattern and tumor recurrence confirm previous pathologic reports about biologic differences in desmoid tumors in patients of different ages. It is suggested that younger patients require more aggressive therapy and follow-up due to more infiltrative and recurrent tumors in a relatively shorter period.

P156
Double-Echo Steady State: A Novel Imaging Technique of the Knee Joint
K Toyoda, M Ida, Y Hata, H Tanaka, K Fukuda, T Irie, S Tada, S Katano
Department of Radiology, Jikei University School of Medicine, Tokyo, Japan

Purpose: Double-echo steady state (DESS) is a technique that generates two signals (FISP and PSIF) within one repetition time interval without increasing scan time. The purpose of this study was to evaluate clinical utility of DESS in the knee joint compared with FISP and PSIF sequences.
Methods: DESS was implemented on a 1.0-T clinical imager (Siemens) (3D DESS; TR = 28 msec, TE = 9 msec, 256 × 256 matrix, FOV = 110 cm, 1.0–2.5-mm thickness, 64 partitions, measurment time = 7′42″). 3D DESS was compared with standard FISP, PSIF, and fat-suppression T1-weighted imaging. Ten healthy volunteers, 15 patients with injury, and 10 with degenerative disease were included.
Results: The optimal flip angle in the DESS sequence was 30°–40° for anatomic detail and tissue contrast. DESS was equal or superior to FLASH in depicting ligaments, menisci, and cartilage. DESS images agree with PSIF in diagnosing fluid in joint space or bursae. Although fat-suppression T1-weighted imaging was superior to DESS, FISP, or PSIF in diagnosing cartilage, contrast between fluid or tear and adjacent cartilage or ligament was greater on the DESS images. DESS provides a higher signal-to-noise ratio than other sequences. In the clinical study, DESS enabled identification of injury of the ACL or meniscus, fluid collection, hemorrhage, and degenerative changes of cartilages in the knee joint.
Conclusion: The DESS technique provides high-quality images of the knee joint with both T1- and T2*-weighted contrast behavior. It saves time in MR studies of the knee joint.

P157
MR Imaging of Thermally Coagulated Blood: Applications in Image-monitored Thermal Ablations
RB Lufkin, RE Saxton, K Kirlew, S Sinha, Y Anzai, AAF De Salles, KL Black
Department of Radiological Sciences, UCLA School of Medicine, Los Angeles, CA

Purpose: Focal regions of tissue T1 shortening are present on MRI-monitored procedures involving thermal ablation. We performed experiments to determine the signal-enhancing effect of thermally coagulated hemoglobin as a possible control mechanism.
Methods: Fresh samples of whole blood, separated plasma, intact red blood cells, lysed red blood cells, and free hemoglobin suspension were uniformly heated in a water bath for 5 minutes at constant treatment temperatures (T_{max} = 23°C–80°C), including the 60°C coagulation threshold of proteins. Following heating, T1- and T2-weighted (T1W and T2W) spin-echo images (20/500 and 80/2,000) were acquired of all specimens.
Results: In comparison with noncoagulated specimens (T_{max} < 60°C), all thermally coagulated samples that contained hemoglobin appeared hyperintense on T1W and hypointense on T2W images, except for coagulated free hemoglobin–containing solution, which appeared hyperintense on both T1W and T2W images. The signal enhancement on T1W images of hemoglobin-containing coagulated samples was about 200%.
Conclusion: Thermal denaturation of hemoglobin facilitates oxidation of the heme group, leading to methemoglobin formation, which is primarily responsible for the T1-shortening effect. In consideration of the temperature dependence of protein coagulation and T1W signal enhancement of blood, hemoglobin may provide a useful basis for development of heat-activated contrast agents. Heat-induced methemoglobin formation is discussed in relation to MRI-monitored thermal ablation of brain tumors.
Disclosure unavailable at time of publication.

P158
Is MR Mammography Diagnostically Reliable at 0.5 T? Comparative Study of Diagnostic Accuracy at 0.5 and 1.5 T
CK Kuhl, A Eleveld, BP Kreft, H Kooijman, J Gieseke, A Steudel, M Reiser
Department of Radiology, University of Bonn, Bonn, Germany

Purpose: Controversy exists as to whether or not the diagnostic value of dynamic contrast-enhanced MR mammography (MRM) depends on the system's field strength. It has been assumed that MRM is not diagnostically reliable with systems of 0.5 T or less. To clarify this we examined 37 patients on both a high- and a midfield system and compared the diagnostic accuracy of both.
Methods: Thirty-seven patients with contrast-enhancing lesions were examined at 1.5 and 0.5 T (Philips ACS II and T5 II). A T1-weighted 2D (3D) FFE sequence was used, with TR/TE/FA of 190/3.4/80° (25/3.3/40°), 19 (25) slices, 5-mm thickness, and temporal resolution of 40 (70) sec. Subtraction images were calculated by both systems. Image quality, number of enhancing lesions, and lesion conspicuity (as assessed by lesion enhancement velocity) were compared by two independent readers.
Results: No differences were found as to image quality or the number and morphology of lesions detected by both systems. However, both enhancement velocity and grade of enhancement were higher (up to 2.5-fold) on 0.5-T 3D FFE than on 1.5-T 2D images. In 10 cases where the 1.5-T study was equivocal or negative, the 0.5-T examination allowed a definite true-positive diagnosis. No false-negative findings were seen at 0.5 T.
Conclusion: With an adequate pulse sequence, MRM is possible on mid-field-strength systems, and specificity may be greater. Obviously, pulse sequence is more important than field strength.

P159
Differential Diagnosis of the Intrapancreatic Mass from the Extrapancreatic Mass with T2-weighted Imaging
Y Imanishi, F Nakayama, Y Kondou, VY Hou, H Suzuki, EA Zerhouni, M Fujikawa
St Marianna University, Touyoko Hospital, Kawasaki, Japan

Purpose: To determine how intrapancreatic masses may be differentiated from extrapancreatic masses on conventional T2-weighted images.
Methods: In 25 patients with a mass in or near the pancreatic head and/or uncinate process or with enlargement of them, T2-weighted images (TR/TE = 2,500 or 2,700 msec/80 msec) of the upper abdomen were obtained on a 1.5-T system. Abdominal operation was performed in 23 of the 25 patients, and lymph node biopsy was performed in the other two. The masses included 19 intrapancreatic tumors (15 pancreatic carcinomas and four cholangiocarcinomas of the pancreatic portion) and six extrapancreatic masses (one retropancreatic fat necrosis, one duodenal carcinoma, two malignant lymphomas, etc). T2-weighted images of the upper abdomen in 89 patients without any clinical findings or history of pancreatic disease were used as controls.

Results: All six patients with an extrapancreatic mass had no abnormality of the pancreas comparing intensity (excluding tumor portion), pancreas margin, or pancreatic duct on T2-weighted images. In contrast, 17 of 19 patients with a intrapancreatic tumor had such abnormalities, which depended pathologically on attendant pancreatitis.
Conclusion: In many cases intrapancreatic tumors in the pancreas head can be differentially diagnosed from nearby extrapancreatic masses by noting the presence of attendant pancreatitis on T2-weighted images.

P160
Use of Dynamic Contrast-enhanced Breath-hold MR Imaging to Identify and Characterize Abdominal Masses

AH Sonin, SW Fitzgerald, ME Bresler, FL Hoff
Department of Radiology, Northwestern University, Chicago, IL

Purpose: To study the efficacy and accuracy of dynamic MR contrast techniques in evaluating abdominal masses.
Methods: Twenty patients with suspected or known abdominal masses were imaged by means of a breath-hold FLASH technique and rapid serial acquisitions before, during, and after contrast enhancement. Results were compared with those of other imaging modalities if available, and MR studies were retrospectively reviewed after pathologic diagnosis was made available in order to analyze potentially useful enhancement patterns.
Results: All patients were able to cooperate with the breath holding protocol. The sensitivity of MR imaging for detecting masses was 100% with the dynamic enhancement technique. In all cases, conspicuity of the mass with dynamic MR contrast was thought to be as good as or superior to that with conventional imaging techniques. In one case, a renal cell carcinoma that could not be identified on CT or precontrast MR images was clearly seen with dynamic MR contrast administration; in two other cases, a pattern of progressive centripetal MR enhancement correctly suggested hemangiomatous tumors after CT, and unenhanced MR imaging failed to allow a specific diagnosis.
Conclusion: Preliminary results suggest that breath-hold imaging of the abdomen with dynamic contrast enhancement can serve as a valuable tool in identifying and characterizing abdominal masses that present a diagnostic challenge on CT and nonenhanced MR images.

Tuesday, March 8, 12:15 PM–1:30 PM
VASCULAR IMAGING AND FLOW/QUANTIFICATION/CARDIAC

Posters P221–P228

P221
Nonlinear Excitation Profiles for 3D Inflow MR Angiography

T Nägele, U Ixlose, W Grodd, I Nüsslin, K Voigt
Department of Neuroradiology, University of Tübingen, Tübingen, Germany

Purpose: Signal loss due to spin saturation in 3D time-of-flight (TOF) MR angiography can be reduced by the use of RF pulses with flip angle distributions that spatially vary across the excitation volume (slab). For this purpose, linearly increasing excitation profiles (TONE pulses) have been successfully introduced. However, the highest possible vessel signal uniformly distributed across the slab can be reached only with excitation profiles increasing nonlinearly in the main direction of flow.
Methods: We developed a computer simulation program that allows signal calculation of the protons flowing through the slab for an arbitrarily given flip angle distribution, depending on the relaxation times of blood (T1, T2) and the sequence parameters TR and TE. Inversely the program could be used to determine the flip angle distribution necessary to achieve a homogeneously high vessel signal. The time domain representation of the RF pulse with the so-obtained optimal excitation profile (optform pulse) was generated by Fourier transformation. Integration in a standard flow-compensated 3D FISP sequence allowed comparison of the optform pulse with conventional (constant flip angle) and RF TONE pulses.
Results: Three-dimensional MR angiogram data sets of the lower-leg arteries (relatively slow but unidirectional flow) were acquired on a 1.5-T whole body system (Siemens Magnetom GBS II) with the three different RF pulse shapes. It could be shown that, with use of the optform pulse, signal strength and homogeneity could essentially be increased, resulting in improved angiogram quality.
Conclusion: The gain in MR angiogram quality with linearly increasing excitation profiles (TONE pulses) can be increased considerably by application of numerically optimized nonlinear excitation profiles.

P222
Application of Self-Refocusing Slice-Selective Radio-Frequency Pulses for Pulmonary MR Imaging and Angiography

WW Wlodarczyk, T Schäffter, JC Böck, B Sander, K Petermann, R Felix
Universitätsklinikum Rudolf Virchow, Berlin, Germany

Purpose: The most important imaging strategy for minimizing the signal loss from T2 and T2* decay in the pulmonary region, for increasing the inflow effect, and for reducing respiratory and flow artifacts is to shorten the echo time (TE). The purpose of this contribution is to demonstrate the application of self-refocusing slice-selective radio frequency (RF) pulses to shorten TE in 2D gradient-recalled echo (GRE) sequences for the evaluation of pulmonary vessels. Unlike the conventional sinc pulses with a linear phase dependence of frequency offset, they do not require a slice-refocusing gradient after the RF excitation, thus reducing TE.
Methods: Using a maximum gradient strength of 10 mT/m and slew rate of 10 mT/m/ms, available on our 1.5-T whole-body MR imager (Magnetom SP, Siemens), phase-encoding and frequency-prephasing gradients were calculated in order to minimize TE for each given set of sequence parameters, such as receiver bandwith (BW), field of view (FOV), and acquisition matrix. An additional reduction of TE was possible by acquiring offset gradient echoes (eg, TE/BW/FOV/matrix = 2.6 msec/130 Hz/250/128 × 256). Because of poor signal from vessels surrounding lung tissue, magnetization recovery does not substantially reduce the contrast, allowing general surveys of the thorax with a long TR ($\approx$ 1,000 msec) and multiple slices ($\leq$55). However, the long TR requires a large flip angle excitation to increase vascular signal. A computer optimization technique of simulated annealing was used to design self-refocusing slice selective $\pi/2$ pulses of 5.12-msec duration exciting 2-mm-thick slices.
Results: Both base images and time-of-flight angiograms obtained with self-refocusing slice-selective RF pulses demonstrated good visualization of pulmonary vascular patterns. The same sequences used with conventional pulses produced a marked reduction in image quality.
Conclusion: The merits of self-refocusing slice-selective RF pulses are ascertained for the minimization of TE in 2D GRE sequences applied in pulmonary MR imaging and angiography.

P223
Intravascular MR Imaging in a Pig Model

AJ Martin, RM Henkelman
University of Toronto, Sunnybrook Health Science Centre, Toronto, Ontario, Canada

Purpose: Intravascular MR imaging has been proposed as a means of attaining sufficient SNR to image arterial structures at high resolution. Placement of an RF coil within the vasculature of a living system, however, is likely to result in severe motion artifacts. The goal of this research was to assess the feasibility of performing intravascular MR imaging in an animal model.
Methods: All imaging was performed on a standard 1.5-T clinical scanner. The intravascular coil had a 3.5-mm diam-

eter and was based on an opposed solenoid design. The coil was introduced into the aorta of a 25-kg New Hampshire swine, just distal to the renal artery. Intravascular images were then generated, with FOVs ranging from 4 to 12 cm and with a variety of motion artifact reduction schemes.
Results: A total of five animals have been imaged with this protocol to date. By far the most significant source of motion artifact was found to arise from the motion of the intravascular coil within the artery. Restricting the coil to the center of the artery and saturating the blood signal superior to the imaging planes proved to be an effective means of minimizing this artifact. Relatively artifact-free, high-resolution images could then be generated with sufficient resolution to clearly delineate the media and adventitia of the aorta.
Conclusion: Artifacts arising from intravascular coil motion can be overwhelming if steps are not taken to minimize this source of ghosting. However, if appropriate measures are taken, intravascular MR imaging can provide high-resolution images of vascular structure in living systems.

P224
MR Angiography of the Popliteal Artery: Vascular Compression in Normal Subjects
MR Baker, EC Unger, L Erdoes
University of Arizona, Tucson, AZ

Purpose: The initial description of popliteal artery entrapment was reported by Stuart in 1879. Since that time, there have been numerous reports of anatomic variants resulting in the popliteal artery entrapment syndrome, including the functional popliteal artery entrapment syndrome. The purpose of this study was to evaluate the popliteal artery of normal subjects during rest and isometric flexion for extrinsic compression.
Methods: MR imaging with MR angiography of the popliteal artery was performed in 13 healthy individuals (26 lower-extremity studies). The MR studies were all performed on the same unit (Signa 0.5-T GE) and with the same imaging protocol sequences (2D time of flight), both with subjects at rest and during isometric flexion of the quadriceps and plantar flexion of the foot. The axial plane images prior to reformatting and reformatted 2D time of flight images were then interpreted with regard to the presence of anatomic variations and the presence and location of popliteal artery compression.
Results: A total of 13 individuals (26 legs) were evaluated. All patients demonstrated normal anatomy of the popliteal fossa. Five individuals (eight legs) were capable of occlusion of the popliteal artery. The location of the occlusion was at a similar level in all patients capable of occlusion. The location of the occlusion occurred in the distal popliteal artery between the head of the lateral gastrocnemius and popliteus muscles.
Conclusion: The study demonstrates that normal individuals are capable of occlusion of the popliteal artery. Thus, the presence of popliteal artery occlusion during exercise does not necessarily indicate a pathologic state.

P225
Bilateral Internal Carotid Thrombosis: Three Cases
VM Sanjuan, D Geffner, SR Penderia, AB Ferrandis, SF Mengual, CS Sayas, JG Nieto
Hospital General Universitario, Valencia, Spain

Purpose: We report three cases in which MR angiograms revealed bilateral thrombosis of the internal carotid arteries.
Methods: Patients were referred to this MRI Center from another hospital (Castellon Hospital, Valencia, Spain) with clinically and echo-Doppler–suspected calcifications of the internal carotids and significant stenosis. The following protocols were evaluated: coronal 2DPC (VENC = 40 cm/sec), sagittal 2DPC (VENC = 30 cm/sec), axial 2DPC (VENC = 40 cm, 7 seg, flow direction A/P and R/L), axial 3DTOF (supra-aortic trunks), coronal 3DPC (neck coil), and axial 2DTOF (neck coil). These images were postprocessed with the IVI.
Results: Patients were male and aged between 48 and 70 years. The coronal and sagittal 2DPC sequences showed absence of flow in both internal carotid arteries. The 3DTOF sequence revealed a weak flow in the midcerebral arteries. The images with flow direction were seen to fill from the posterior communicating arteries. The vertebral and basilar arteries exhibited significant flow. The 2DTOF sequence likewise confirmed the finding.
Conclusion: MR angiography has helped us to detect a highly infrequent finding. We considerer that the thrombosis is chronic and based on an arteriosclerotic stenosis, for had it been acute the patients would possibly not have reached our unit.

P226
Peripheral Arterial Modifications during Joint Movements: Evaluation with MR Angiography
C Marcus, C Avisse, V Ladam-Marcus, F Gausserand, B Flament, B Menanteau
Department of Radiology, University Hospital, Reims, France

Purpose: To study dynamic arterial aspects during movements such as pronation-supination of the forearm and flexion-extension of the knee.
Methods: Radiographs obtained after vascular injection (radiographs in front and lateral views, dissections) were correlated with MR angiograms in seven volunteers. Time-of-flight MRA images were obtained on a 2-T unit with 2D acquisitions (multiple axial sequential slices of 2-mm thickness with tracking presaturation) and postprocessing of the images by maximum-intensity projection (MIP).
Results: We have found several mechanisms of arterial adaptation, such as rotation and torsion of the radial artery during forearm pronation-supination or curvature inversion and twisting of the popliteal artery during knee flexion-extension. Loss of signal intensity according to hemodynamic changes in regions of vessels curvature or bifurcation and complex pulsatile flow at lower limb levels did not affect the image quality.
Conclusion: MRA appears to be a tool for studying functional vascular anatomy. In addition, better understanding of dynamic arterial changes should help explain complications after surgical flow restoration, such as vascular graft plication or false aneurysm development.

P227
MR Imaging of Cardiac Amyloidosis
J Loichat, U Helber, V Schuelen, P Huppert, F Schick, HU Hoffmeister, CD Claussen
Department of Diagnostic Radiology, University of Tübingen, Tübingen, Germany

Purpose: MRI was performed in patients with suspicion of cardiac amyloidosis. The results were compared with MRI findings in hypertrophic cardiomyopathy. The aim of this study was to evaluate MRI signs of cardiac amyloidosis.
Methods: MRI (1.0 T) was performed in two patients with suspicion of cardiac amyloidosis, two with confirmed cardiac amyloidosis (cardiac biopsy), and five with hypertrophic cardiomyopathy. The thickness of the myocardium and the volume of the left ventricle were measured with FISP 2D sequences. Three planes of the heart in the short axis, a septum orthogonal, and a septum with a parallel-oriented axis were obtained. Gd-DTPA (TURBO-FLASH sequence) was used in three patients to evaluate the dynamic perfusion pattern of the myocardium.
Results: In all cases the left ventricle was normal sized but showed concentric hypertrophy. Biventricular hypertrophy was seen only in patients with cardiac amyloidosis. The thickness of the myocardium was 1.4–2.4 cm in amyloidosis and 1.2–1.7 cm in hypertrophic cardiomyopathy. Systolic wall thickening was less than 30% in all patients and did not permit differentiation of amyloidosis from cardiomyopathy. The ejection fraction was normal in all cases. Administration of Gd-DTPA did not result in a specific MRI pattern of the myocardium, in contrast to echocardiography (sparkling appearance of the myocardium).
Conclusion: Cardiac amyloidosis has no specific patterns in MRI. However, severe concentric hypertrophy of both normal-sized ventricles in the absence of valvulopathy and positive extramyocardial biopsy are highly suggestive of cardiac amyloidosis.

P228

MR Imaging in the Diagnosis of Aortic Dissection Compared with Multiplanar Echocardiography and Spiral CT

T Sommer, N Holzknecht, AV Smekal, W Fehske, K Seelos, F Poppenborg, Y Gieseke, GP Kirchhoff, A Steudel
Department of Radiology, University of Bonn, Bonn, Germany

Purpose: MRI has been shown to be accurate in the detection of aortic dissection, providing higher sensitivity and specificity than CT and transesophageal echocardiography. However, new improved imaging modalities such as spiral CT (SP-CT) and multiplane transesophageal echocardiography (MP-TEE) have not been systematically compared with MRI. The aim of this prospective study was to compare MRI, SP-CT and MP-TEE in the evaluation of (*a*) the presence and extent of aortic dissection membrane (type A or B?), (*b*) periaortic pathology, (*c*) thrombus formation, and (*d*) involvement of aortic arch vessels.
Methods: MRI: 0.5-T Gyroscan T5II, body wraparound surface coil, ECG-triggered spin-echo and multislice-multiphase gradient-echo sequences, 5-mm slice thickness. SP-CT: Somatom Plus S, 3-mm slice thickness, 120 mL of contrast media IV, 2D reconstructions in various planes. MP-TEE: multiplane color-flow TEE and transthoracic echocardiography. Thirty-six patients were investigated: 25 with clinically suspected acute aortic dissection (nine type A, eight type B), 11 with aortic repair (7 of 11 with persisting distal dissection).
Results: The sensitivity in the detection of aortic dissection was 100% (18 of 18) for MRI, 100% (24 of 24) for SP-CT, and 100% (22 of 22) for MP-TEE. The specificity was 90% (9 of 10), 100% (12 of 12), and 92% (11 of 12). There was a 100% correlation in the assessment of periaortal/periprothetic pathology and thrombus formation between MRI, SP-CT and MP-TEE. In 11 patients, there was an involvement of aortic arch vessels; 63% (5 of 8) were detected with MRI, 100% (11 of 11) with SP-CT, and 73% (8 of 11) with MP-TEE.
Conclusion: Concerning sensitivity, specificity, and assessment of periaortic pathology and thrombus formation, SP-CT and MP-TEE have been shown to be equal to MRI in the evaluation of thoracic aortic dissection. In the assessment of aortic arch vessels, SP-CT is superior to MRI and MP-TEE and may become the method of choice.

Wednesday, March 9, 12:15 PM–1:00 PM
ARTIFACTS/INSTRUMENTATION/SAFETY/ PULSE SEQUENCES

Posters P319–P331

P319

Effects of Eddy Currents on 1D and 2D Selective Excitations

Y Li, B Rajagopalan
Radiology Department, Mount Sinai Medical Center, New York, NY

Purpose: Rapid switching of magnetic gradient induces eddy currents in the nearby conducting materials. The authors studied the effects of eddy currents on 1D (step G_z) and 2D (spiral G_x, G_y) selective excitations.
Methods: We numerically solved the Bloch equations for 1D and 2D selective excitations with and without the eddy-current effects. In the L-R model, the eddy current–induced gradient is a multiexponentially decaying field for step gradients and a dominantly oscillating field for spiral gradients.
Results: Computer simulations demonstrate that the selected slice in 1D and the selected area in 2D may be significantly increased relative to those that would be produced by the applied current alone. However, although the eddy current–induced fields due to switching on may be large, as long as the pulse duration T is small in comparison with the time constant of the major decay component W_k at time $t > T$, they are largely canceled by those due to switching off. By a simple analysis, it is shown that in a conventional refocusing pulse sequence, the eddy current–induced gradient at $t > T$ is of the order of $(T/W_k) \exp[-(t - T)/W_k]$. In an inherently refocused gradient sequence, it is reduced further to $(T/W_k)^3 \exp[-(t - T)/W_k]$. In 2D excitations, the oscillating parts are exactly cancelled and the residual exponential contributions are negligible.
Conclusion: The major effect of the eddy current on a 1D or 2D selective excitation is that it may consume a significant amount of additional power in order to select a slice (1D) or area (2D) with the desired value. The dephasing due to eddy current–induced gradient (long W_k) at $t > T$ can be neglected for a symmetric gradient sequence, such as the inherently refocused pulse sequence.

P320

Theoretical and Experimental Analysis of Geometric Distortions in MR Imaging

JA Bertolina, TA Spraggins, JC Goble, NF Kossell
Department of Neurosurgery, University of Virginia, Charlottesville, VA

Purpose: MR images are commonly used for stereotaxic surgical planning. MRI is desirable for stereotaxy because of its 3D capabilities as well as its superb soft-tissue differentiation. On the downside, MRI has been shown to have geometric distortions. Contributors to these distortions include static field inhomogeneities (patient and machine dependent), gradient nonlinearities, linear scale errors of the gradients, eddy currents, and chemical shifts. Where spatial accuracy is a concern, it is important to understand and minimize these errors. These distortions have been addressed individually in MR literature, but we have yet to find a cohesive analysis of all of these. We have also found some of the theory to be incomplete.
Methods and Results: We begin from basic principles and derive a theoretical framework from which these geometric errors can be explained. We use this model to show how each of the above-mentioned phenomena will affect an image. We also discuss how distortions from each source can be minimized. We then use phantoms or computer models to verify these results. Finally, we construct a table that outlines the sources of error as well as methods to minimize or eliminate them.
Conclusion: For MR imaging applications where spatial accuracy is important (eg, stereotaxic surgical planning), it is important to understand, measure, and minimize geometric distortions. We have developed a theoretical and experimental analysis to assist in understanding and minimizing geometric distortions.

P321

Receiver Design Constraints for Prepolarized MR Imaging

GC Scott, SM Conolly, A Macovski
Department of Electrical Engineering, Stanford University, Stanford, CA

Purpose: Prepolarized MRI (PMRI) [1] is a new approach that combines a strong, inhomogeneous, and localized field to generate magnetization and a very weak but relatively homogeneous bias field to collect the echo. To achieve low cost while maintaining performance comparable to that of a high-field system, the weak bias field must allow sample noise to dominate. Here we analyze the receiver constraints on minimum bias field strength and imaging bandwidth.
Methods: We compute inductance-resistance ratios for head-size solenoids tuned below 500 kHz. The minimum turns and winding area are set so sample noise dominates. The noise properties of FET, BJT and SQUID preamps are compared to determine the limiting (voltage, current, or equivalent flux) noise. The minimum impedance transformation is then estimated to ensure sample noise dominance over the imaging bandwidth.
Results: Our analysis suggests that litz wire [2] solenoids (possibly cryogenic) provide sufficient sensitivity for head-size sample volumes. Superconductors are needed for much smaller volumes. Since PMRI employs relatively broad percentage bandwidths below 500 KHz, the noise-matching net-

work and preamp are also critical. The high inductive reactance of the receiver coil imposes a gain-bandwidth limitation on the noise-matching network. This requires transformer or inductive coupling for which a FET or SQUID preamp is compatible.

Conclusion: The ultralow bias field of PMRI introduces new engineering problems for receiver design. Aside from the obvious need for a high-sensitivity receiver coil and preamplifier, the fundamental limitations of broadband matching will constrain the minimum field and imaging bandwidth.

1. Macovski and S. Conolly, *Magn. Reson. Med.*, 30, 221–230 (1993). 2. A. Ferreira, *IEEE Proceedings B*, 139, 21–25 (1992).

P322

Constraints on an Oscillating Bias Field for Prepolarized MR Imaging

PN Morgan, SM Conolly, GC Scott, A Macovski
Department of Electrical Engineering, Stanford University, Stanford, CA

Purpose: Prepolarized MRI (PMRI) employs two separate fields for polarization and readout. The strong polarizing field creates sample magnetization. After the polarizing field is extinguished, the weak bias field determines the readout frequency. An oscillating bias field allows the use of inexpensive magnets for PMRI [1,2]. Here we present constraints on the oscillating bias field due to DC magnetic shielding requirements and SAR.

Methods: Shielding or bucking of transverse stray fields, such as the Earth's field, is required to prevent dephasing during signal readout. We employ a rotating frame analysis to determine a relation for the bias field parameters that minimizes the effects of the stray field. This relaxes the shielding requirements. We verify these results with numerical simulations of the Bloch equation. We also analyze SAR due to the oscillating bias field to obey FDA limits [3].

Results: We employ a sinusoidal bias field, $B_0 \cos \omega t$. We set the ratio $\gamma B_0/\omega = 2.4$ to minimize the effects of the stray field. For an oscillation frequency of 100 kHz and a readout for $T_2 \approx 100$ ms, one must suppress the Earth's field by a factor of 10. The SAR limit is reached for samples 20 cm in diameter.

Conclusion: The oscillating bias field allows PMRI to use inexpensive magnets. We may set the bias field parameters to reduce the shielding requirements for PMRI. The maximum oscillation frequency of the bias field is limited by SAR.

1. Macovski and S. Conolly, *Magn. Reson. Med.*, 30, p. 221 (1993). 2. Morgan et al., Proc. Twelfth SMRM, p. 1366 (1993). 3. Schaefer, Proc. AAPM Summer School, p. 607 (1992).

P323

Considerations for Prepolarized MR Imaging with RARE

SM Conolly, GC Scott, PN Morgan, A Macovski
Department of Electrical Engineering, Stanford University, Stanford, CA

Purpose: To specify the system requirements for an inexpensive prepolarized MRI system using the RARE imaging sequence.

Methods: The basic idea of prepolarized MRI [1,2,3] is to polarize spins with a strong field and to switch quickly to a weak "bias" field during signal reception. The polarizing coil can be very inhomogeneous because it is absent during signal reception; indeed, the field in our hand-sized prototype solenoid varies by 37%. Making the polarizing coil small reduces the stored energy (1 kJ at 0.5 T) and allows reasonable switching times (100 ms) with conventional linear power supplies (two Techron 8604s). Using a weak bias field (< 100 G) allows relatively inhomogeneous bias coils and renders susceptibility-induced dephasing negligible. In [3] we considered oscillating the bias field to refocus any dephasing due to spatial variations. This technique allows one to use very inhomogeneous bias coils, but the SAR is high. Here we specify constraints on a more conventional prepolarized system using a constant bias field during a RARE imaging sequence.

Results and Conclusion: Spin-echo sequences are immune to known bias field variations provided the readout gradient exceeds the inhomogeneity gradient [4]. At a bias frequency of 250 kHz, when using 2 G/cm gradients, a RARE imaging sequence will tolerate 1% inhomogeneity in the bias field. Because both the bias and polarizing coils can be inhomogeneous, such MRI systems should be inexpensive. This system also requires an ultra-low-noise receiver and broad-band matching network.

1. Packard and R. Varian, *Phys. Rev.* A93, p. 941, 1954. 2. Carlson et al., *Radiology* 184, p. 635, 1992. 3. A. Macovski and S. Conolly, *MRM* 30, p. 221, 1993. 4. K. Sekihara et al., *Phys. Med. Biol.* 29, p. 15, 1984.

P324

A Simple Exercise Device for Quantification of Work Done While in the MR Imager

RJ Kurland, S Mensch, M Yeager, ED Newman
Geisinger Medical Center, Danville, PA

Purpose: To develop a simple exercise device for quantification of work performed by subjects while they are within the bore of the MR scanner. A previously reported study (1) had shown a rough correlation between exercise and metabolite levels measured with P-31 MRS of the quadriceps and shown that there were differences between normal controls and patients with polymyositis and dermatomyositis, but effort put forth during the exercise could not be measured precisely.

Methods: Nonmagnetic weights (sandbags) are attached, via a cord and pulley arrangement, to the ankle of the subject, who is supine with legs bent at the knee; the weight is pulled up by leg lifts in a regular cadence. The work done during the lifting can be calculated from the distance traveled by the weight. This distance is measured as follows: an infrared beam passing through holes in the periphery of the rotating pulley wheel is converted to pulses by an optocoupled interrupter and counted. An exercise test is carried out by each subject on a Biodex Isokinetic Dynamometer before the MRS study to determine a maximum work level. The exercise program for the MRS study consists of three stages, each lasting approximately 6 minutes, with weights attached to give, respectively, 10%, 30%, and 50% of maximum effort, as measured by the Biodex. P-31 MRS spectra are taken as a baseline, before the exercise begins, continuously during the exercise, and for 10 minutes after the third stage of exercise ends, during recovery. A GE Signa (1.5-T) scanner is used, with a GE transmitter/receiver coil, double tuned for proton and P-31, placed over the quadriceps area of the subject's thigh. A pulse repetition time of 10 s was used; spectra were analyzed at various averages to ensure that a steady state of metabolite level had been reached.

Results: Four normal controls and four patients have been studied to date with this system. Only the results for the normal controls (matched in age and sex to the patients) will be reported here. The maximum effort of the normal controls corresponded to weights in the 50% stage ranging from 15 to 22 lb. The maximum increase (at the 50% stage) in integrated intensity of inorganic phosphorus (Pi) ranged from 2.4 to 3.1; the maximum decrease in integrated intensity of the PCr peak ranged from 19% to 32%. The relative increase of integrated Pi intensity and relative decrease of integrated PCr intensity showed a linear relation to power (total work/time during an exercise stage): coefficients for Pi and PCr, respectively, were 9 ± 2 watts^{-1} and -1.6 ± 0.18 watts^{-1}.

Conclusion: A simple, inexpensive exercise device and method has been developed that allows quantification of work performed while the subject is within the magnet bore. The utility of this exercise system is demonstrated by the fact that the relative (to initial baseline) Pi increase and PCr decrease show a good linear dependence on work per time for the control studies. We also note that this device may have broader potential use, for example for work quantification during cardiac MRI.

1. Newman ED & Kurland RJ, 1992: P-31 Magnetic resonance spectroscopy in polymyositis and dermatomyositis—Altered energy utilization during exercise. *Arthritis & Rheumatism*, 35:199–203.

P325

Fast T2-weighted Imaging of Upper Abdomen: Advantages and Limitations of Turbo SE and Turbo Gradient SE with Breath-hold, Breath-gating, and Fat-Suppression Techniques

Y Hata, K Toyoda, H Tanaka, S Matsumoto, K Mizunuma, S Tada, S Katano

Department of Radiology, Jikei University School of Medicine, Tokyo, Japan

Purpose: To compare images of the upper abdomen with turbo SE (TSE) and turbo gradient SE (TGSE) and to assess the efficacy of breath-hold, breath-gating, and fat-suppression techniques.

Methods: TSE and TGSE sequences were implemented on a 1.0-T clinical imager (Siemens). Routine TSE: 11 echoes per TR, TR = 4,200 msec, TE = 90 msec, six acquisitions, 7'39". Routine TGSE: 33 echoes (GE, 67%), TR = 3,300 msec, TE = 140 msec, 10 acquisitions, 3'18". Breath-hold (BH) TSE: 23 echoes, TE = 128 msec, one acquisition. BH-TGSE: 33 echoes (GE, 67%), one acquisition. Breath-gating (BG) TSE: 23 echoes, TE = 90 msec, one or two acquisitions. BG TGSE: 33 echoes (GE, 67%). IR-TSE (fat-suppression): 11 echoes, TI = 100–140 msec, TE = 60 msec. CHESS-TSE (fat-suppression) preceded by a 1-3-3-1 fat-selective prepulse: five echoes, TE = 90 msec.

Results: TSE was superior to TGSE in signal-to-noise ratio (TGSE had ringing artifacts or blurring in some cases), but TGSE showed less respiratory artifact because subcutaneous fat signal in the ventral wall was suppressed. Breath-gating TSE with one or two acquisitions provided the qualitatively best image of the upper abdomen of all sequences. Fine anatomic detail, less motion artifact, and excellent signal-to-noise ratio were obtained with breath-gating. The real measurement time with BG-TSE is about 2–4 minutes per acquisition. BH-TSE or TGSE had a low signal-to-noise ratio because of one acquisition, but the BH imaging was superior to BG-TSE when the respiratory phase is irregular. Both IR-TSE and CHESS-TSE are useful for detecting focal hepatic lesions, especially hepatocellular carcinoma in cirrhosis, but the contour of the pancreas or GI tract was not well assessed with the fat-suppression TSE.

Conclusion: Breath-gating TSE is the best sequence for fast imaging of upper abdominal organs. Breath-hold TSE or TGSE is complementary to BG-TSE, when the respiratory cycle is irregular. Fat-suppression TSE provides better contrast to detect focal hepatic lesions.

P326

Rapid High-Resolution, Three-dimensional Spin-Echo Imaging of Large Volumes with Single- or Multiple-Echo Trains

JP Mugler III, JR Brookeman

Department of Radiology, University of Virginia, Charlottesville, VA

Purpose: To develop 3D spin-echo (SE)–based pulse sequence that (*a*) use single (eg, interleaved EPI) or multiple (eg, GRASE) gradient-echo trains to acquire several phase encodings for each TR; (*b*) provide single-slab imaging of large volumes, such as the whole head, in clinically reasonable times; and (*c*) yield image quality and contrast comparable to that of 2D-SE imaging.

Methods: Our initial studies have concentrated on T1-weighted 3D echo-train techniques for whole-head imaging. Images of phantoms and healthy volunteers were acquired at 1.5 T (Siemens Magnetom 63SP) with two sequence implementations: a single RF-refocusing pulse and one seven-echo train (matrix 112 × 128 × 128, 8.5 min) or two RF-refocusing pulses and two five-echo trains (matrix 120 × 128 × 128, 6.4 min). Both sequences used TR/TE 250/25–27, FOV 250 mm, and slab thickness 160 mm. Phase-encoding steps and FOV were restricted by imager software and gradient limitations, respectively. The durations of the echo trains were chosen to limit off-resonance effects.

Results: Phantom and head images demonstrated generally good image quality and the expected T1-weighted image contrast. However, subtle ghosting was apparent on many images, probably secondary to eddy currents in our unshielded gradient system.

Conclusion: T1-weighted 3D echo-train pulse sequences produced promising results on our current-generation imager. These results indicate that, with the availability of stronger gradients on next-generation imagers, much smaller voxel sizes could be achieved with adequate S/N in the same imaging times. We anticipate that the ghosting artifacts would be eliminated with a shielded, high-performance gradient system. Future work includes development of T2-weighted implementations.

P327

Measurement of Absorbed Dose Distributions in Radiation Therapy Applications with MR Imaging

S Johansson, P Magnusson, A Fransson, LE Olsson, JO Christoffersson, A Montelius, S Mattsson

Department of Radiation Physics, Lund University, Malmö, Sweden

Purpose: A dosimetry system for relative absorbed dose measurement in radiation therapy has been developed. The dose distributions are obtained by a dosimeter gel evaluated in an MR scanner (0.5 T). The purpose of this work was to study this dosimetry system in practical radiation therapy situations.

Methods: Body-shaped phantoms were prepared with dosimeter gel. The phantoms were given radiation therapy treatments, including dose planning prior to the irradiation. The MR evaluation was carried out with one pre- and one postirradiation scan followed by 1/T1 calculations to get the absorbed dose matrix. Various MR acquisition methods were studied in order to improve the precision of the calculated absorbed dose.

Results: Dosimeter gel data show good agreement with data from a dose planning system. From MR images, three-dimensional dose distributions were also produced and visualized on an image processing system. Optimizing the MR acquisition parameters allowed a higher precision in the dose determination.

Conclusion: These results indicate that the dosimeter gel can be used to study various complex irradiation geometries. The results may be used to verify the calculation algorithms of a dose-planning system. The dosimeter gel can be prepared in arbitrary shapes, and the MR scanner can produce slices in any direction. This dosimetry technique seems to be a useful tool in radiation therapy applications.

P328

MR Imaging Relaxation Characteristics of Oil and Fat

H Li, LH Riina, MA Salvitti, TM Button

Department of Radiology, State University of New York, Stony Brook, NY

Purpose: To find materials that simulate breast adipose tissue. The materials will be used in an MRI breast phantom insert to simulate the detection of an aqueous lesion within a fatty matrix.

Methods: Evaluation of fat-simulating materials included measurement of T1 and T2 and the temperature effect on T1 and T2. The T2s were determined with a spin-echo sequence, and the data were fitted by means of a standard least-square regression procedure. The T1s were determined by using an inversion-recovery sequence, and the data were fitted by means of a nonlinear least-square regression. All of the data were measured on a clinical 1.5-T imager (GE Signa). The temperature effect on T1 and T2 was examined by using a constant temperature circulating water bath system.

Results: We measured 11 liquid oils, three solid fats, and some other industrial materials in three temperatures (room temperature, 30°C, and 40°C). At room temperature, the range of T1 is between 129 and 280 ms and the range of T2 is between 53 and 82 ms. With three exceptions, the T1s of all other materials are increased when temperature increases. The T2s of all materials decreased at 30°C and slightly increased at 40°C compared with 30°C.

Conclusion: Of the materials tested, we found that none of them is suitable at room temperature to simulate breast adipose tissue. However, two of them (flax oil and soybean oil) at 40°C have very close relaxation characteristics compared with breast adipose tissue. A temperature-controlled breast phantom is under investigation.
Disclosure unavailable at time of publication.

P329
On the Fractal Nature of MR Images of Trabecular Bone

H Chung, C Chu, M Underweiser, FW Wehrli
Department of Radiology, University of Pennsylvania Medical Center, Philadelphia, PA

Purpose: Fractal analysis has been used as a means of characterizing the structure on high-resolution MR images of cancellous bone (1,2). This work reexamines the possible fractal nature of such structures.
Methods: MR microscopic images of trabecular bone in vitro were acquired at 9.4 T and at various resolutions and SNRs. In addition, in vivo images of the human finger were obtained at 1.5 T. Boundary tracking, box counting, and linear regression were implemented to measure slopes of the log-log plot (perimeter vs box size) as a means of determining the fractal dimension.
Results: On MR microscopic images at high resolution and SNR, the log-log plot was found to be nonlinear, with the slope approaching unity at small box size. This behavior coincides with the case of a smooth surface (eg, a circle [3]) and thus implies the nonfractal nature of the trabecular surface. Specifically, the region of linearity in the log-log plot associated with fractal structure increases as SNR and resolution decrease.
Conclusion: The results demonstrate that, under currently achievable resolution, the box-counting algorithm is not suitable for fractal analysis on MR images of trabecular bone and that the fractal nature of the trabecular network reported previously was due to noise and insufficient resolution.
1. S Majumdar, A Gies, M Jergas, S Grampp, H Genant, *SMRM*, 455 (1993). 2. S Majumdar, RS Weinstein, RR Prasad, *Med Phys*, 20, 1611–1619 (1993). 3. BB Mandelbrot, The fractal geometry of nature, p. 33 (Freeman, New York, 1983).

P330
3D Surface Rendering of Phase Difference Renal MR Angiography

WCE Kwok, R Kraft, SP Meyers, L Shapiro, S Totterman
University of Rochester, Rochester, NY

Purpose: To improve the visualization of renal arteries with MRA by editing phase difference images and applying 3D surface rendering.
Methods: The renal arteries of five normal volunteers were imaged on a GE Signa 1.5-T system with a 3D phase contrast sequence, TR/TE of 25 ms/8 ms, 20° flip angle, VENC of 60 cm/sec, 256 × 192 matrix, 24-cm field of view, 1.5-mm slice thickness, 28 slices, 1 NEX, and first-order gradient moment nulling. Phase difference images were reconstructed for each flow direction in addition to the regular-speed image reconstruction. These images were postprocessed on a SUN Sparc10 workstation with use of SunVision and some additional programs written by R.K. and L.S. To enable separate postprocessing of left and right renal vessels, the image set was divided in two halves, and with use of flow directional information the veins were removed. Then the three orthogonal flow components were combined vectorially to give a speed image. After background noise and extraneous artifacts were eliminated, the image data set was surface rendered into 128 angular views.
Results: The surface-rendered images in all volunteers yielded better depiction of the arterial origins and overlapping vessels than the MIP images. With the veins removed, the branches of the renal arteries were better visualized. In addition, surface rendering gave a better overall 3D perspective compared with the MIP images.
Conclusion: 3D surface rendering of flow-edited renal MR angiography was superior to the regular MIP display in the visualization of renal arteries.

P331
Application of a PC-based Expert System for Quantitative Analysis of Dynamic MR Mammography Reduces Costs and Improves Diagnostic Accuracy

HB Bieling, CK Kuhl, A Steudel
Department of Radiology, University of Bonn, Bonn, Germany

Purpose: Diagnosis with dynamic MR mammography (MRM) is based on the detection of lesions showing a signal intensity increase of 90% or more within the first minute after Gd-DTPA administration. Reading of dynamic MRM studies is time consuming, since numerous images have to be carefully searched for enhancing areas and time/signal intensity curves (TIC) of lesions have to be determined. We present a computerized method for dynamic MRM data analysis.
Methods: MRM images (25 slices × 8 dynamic scans) are automatically transferred to a standard PC (80486 CPU) via network. The program generates subtraction and quotient images (showing absolute and relative enhancement). In parameter images, areas surpassing a selectable enhancement threshold are superimposed on the anatomic images. Diagnostic accuracy and time needed for quantitative analysis of MRM images with the standard software of the system's console (ROI-based TIC) or the PC (parameter images) were evaluated.
Results: Especially in high-risk patients with disseminated, multifocal enhancement due to proliferative mastopathy, the PC program enables immediate and accurate detection of even the smallest conspiciously enhancing lesion. The average time needed for thorough analysis is reduced by a factor of 8. Moreover, patient throughput is increased because quantitative analysis is shifted from the system console to a separate unit.
Conclusion: The PC-based expert system cuts down costs because it reduces the time needed for MRM analysis and increases patient throughput. Moreover, it improves diagnostic accuracy.

P332
Reducing Magnetic Susceptibility Differences with Liquid Perfluorocarbon Pouches: Results with Spectral Presaturation of Fat

SS Eilenberg, VM Tartar
Tri City Medical Center, Oceanside, CA

Purpose: Excellent magnetic field homogeneity is important for achieving spectral presaturation of fat (fat saturation). Field inhomogeneity develops at skin-air interfaces, degrading image quality. Perfluorochemicals have similar magnetic susceptibility as soft tissue, but contain no protons. Perfluorochemical-filled pouches placed on the skin to eliminate the air–soft tissue interface should improve the quality of fat saturation.
Methods: The neck, foot, and ankle were studied in 23 individuals with fat saturation technique. Imaging was performed both with and without the pouches placed around the area of interest. The completeness and homogeneity of the fat saturation, motion suppression, and overall image quality were rated by two blinded reviewers.
Results: Completeness and homogeneity of fat saturation with the pouches was rated as good to excellent in 95% and 90% of cases, respectively, versus 62% and 19% without the pouches. Motion suppression and overall image quality with the pouches was rated as good to excellent in 100% of cases, versus 66% and 28%, respectively, without the pouches.
Conclusion: The placement of perfluorochemical-filled pouches around the neck, foot, and ankle eliminates the skin-air interface and reduces the magnetic susceptibility artifact. This improvement in the local field homogeneity improves the performance of fat saturation. The weight of the pad also acts as an immobilizer and motion damper, further improving image quality.
S.S. Eilenberg is an investor in Alliance Pharmaceutical.

Notes

Indices and Information

- **Author Index**
- **Meeting Comments**
- **1994 Corporate Contributions and Acknowledgments**
- **Call for Papers**

PLAN YOUR INDIVIDUAL ITINERARY

To help you plan your week at SMR, the Works in Progress index lists all Works in Progress proffered papers and poster presentations. All papers are categorized by author with the abstract number of each paper found following the author name. The first eight co-authors per paper are listed individually.

The type of work is indicated by one of two abbreviations preceding the abstract number. An abbreviation key appears opposite the Author Index. All numbers listed in the Index reference the paper number and not the page number on which the abstract may be found.

Key to Abbreviations in Author Index

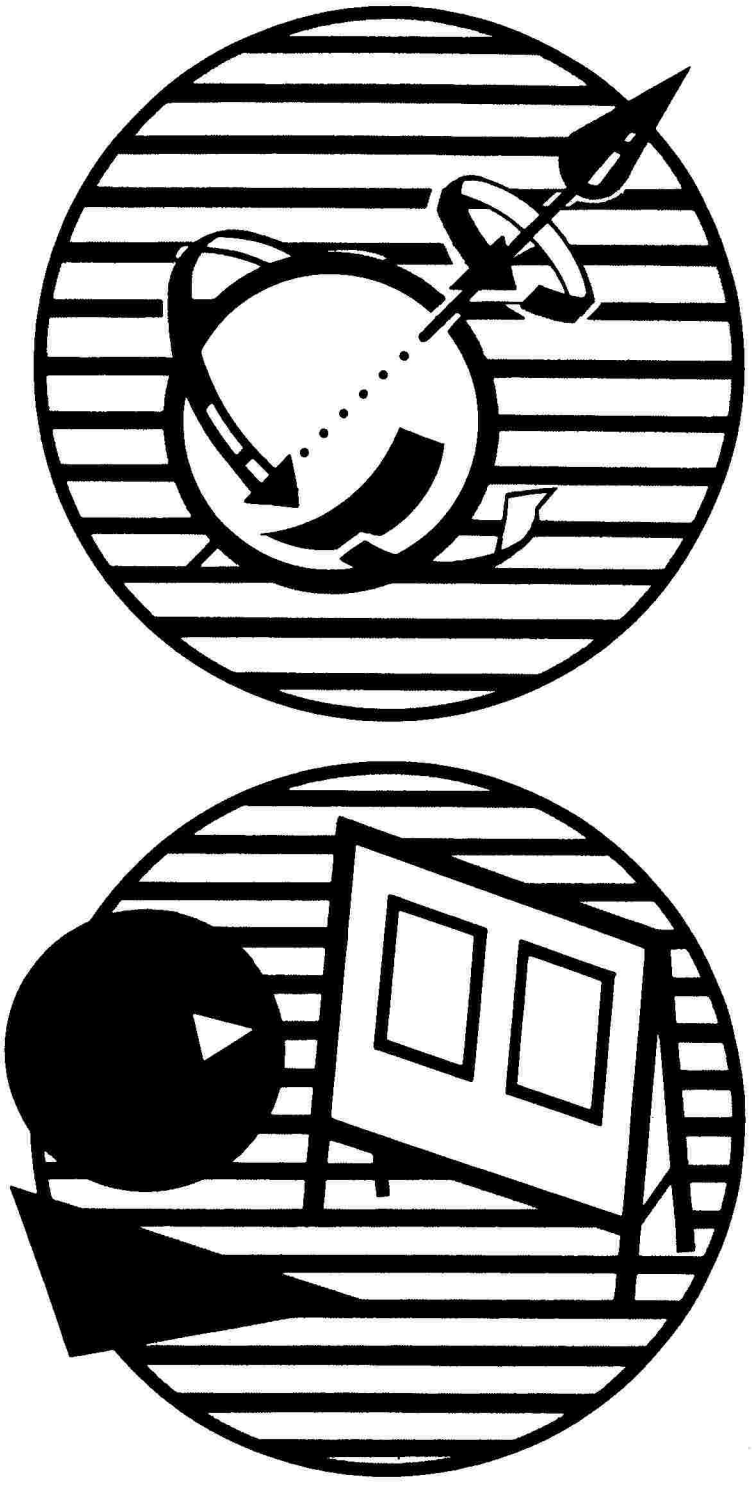

Key to Abbreviations:
 # - proffered papers
P - scientific poster presentations

1994 Author Index

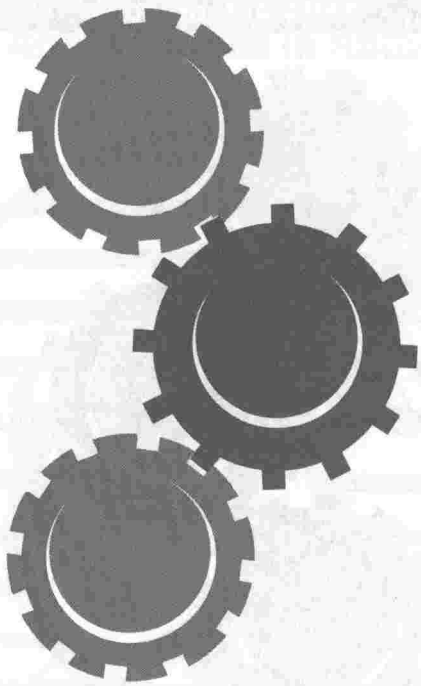

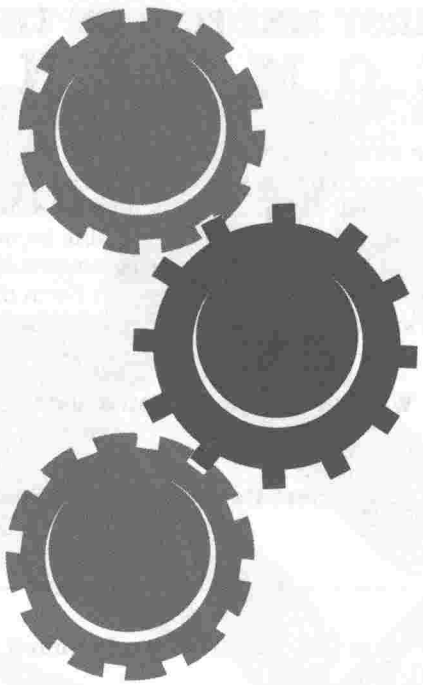

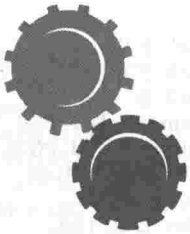

Program Objectives

Scientific Program

At the conclusion of this Program, participants should be able to:

- **identify** appropriate applications of MRI in a quality and cost sensitive environment;
- **evaluate** strategies for assessing MRI technology;
- **recognize** the potential impact of future MR system architectures on clinical practice;
- **comprehend** issues related to magnetic field strength in MRI;
- **recognize** current trends in the application of MRI for neurological, functional, musculoskeletal, cardiovascular, and breast imaging;

Scientific Program: Morning Tutorial

At the conclusion of this program, participants should be able to:

- **improve** their accuracy in clinical MRI interpretation;
- **develop** greater understanding of the basic physics and clinical interpretation of MRI.

Educational Program

At the conclusion of this program, participants should be able to:

- **understand** clinical MRI techniques and applications in multiple body parts, including brain, spine, abdomen/pelvis, musculoskeletal and breast imaging;
- **formulate** scanning strategies, for multiple anatomic locations, at multiple field strengths;
- **improve** their basic understanding of the technical basis of MRI, and how basic sequence parameters impact on image signal-to-noise, resolution and contrast;
- **appreciate** the uses of currently available contrast body agents in body and neurologic applications of MRI;
- **incorporate** new information on areas of most rapid development within MRI.

Educational Program: Economic Symposium

At the conclusion of this program, participants should be able to:

- evaluate and apply new developments in the acquisition, siting and operation of MRI and other imaging technologies.

FIRST MEETING OF THE SMR
C O M M E N T S

The meeting programming committees would appreciate receiving your comments regarding the First Meeting of the SMR in Dallas. Those comments will be collated and forwarded to the Annual Meeting and Education Coordination Council for possible incorporation in upcoming educational programming. While your comments may also be provided on the Evaluation/CME Accreditation Form distributed at each session, please let us know your thoughts regarding the following:

1. **Which Program did you attend?**_____

2. **Did it meet its stated objectives? Yes____No____Why?**_____

   _____

3. **What should have been included in the Program that was not?**

   _____

   _____

4. **What should have been excluded from the Program?**

   _____

   _____

5. **What Program revisions would you like to see implemented next year?**

   _____

   _____

6. **General Comments:**

   _____

   _____

Please return this form to the SMR Registration Area, Chantilly Foyer, Lobby Level of the Loews Anatole Hotel by Wednesday, March 9, or mail it to the SMR Central Office (Chicago location) at the following address:

Society of Magnetic Resonance, Chicago Office
213 West Institute Place, Suite 501
Chicago, Illinois 60610 USA

Future Meeting Dates

1995: August 19-25, Nice, France
1996: Spring, New York, NY
1997: April 10-19, Vancouver, BC

Society of Magnetic Resonance
Chicago Office
213 West Institute Place
Suite 501
Chicago, IL 60610

Phone: (312) 751-2590 Fax: (312) 951-6474

1994 Corporate Acknowledgments

The Society gratefully acknowledges the generous grants received in support of Society goals and specific educational/scientific programs at the First Meeting of the SMR from the following corporate sponsors:

Society Corporate Contributions

Three-Year Gold Corporate Members

Siemens Medical Systems, Inc.
Squibb Diagnostics

Three-Year Silver Corporate Members

Picker International, Inc.
Sanofi Pharmaceuticals and Eastman Kodak Company, Health Sciences Division

Three-Year Bronze Corporate Members

Bruker Instruments, Inc.
Hitachi Medical Systems America, Inc.
Mallinckrodt Medical, Inc.

Educational Grants

Bracco s.p.a.
General Electric Medical Systems, Inc.
Sanofi Winthrop Pharmaceuticals
Siemens Medical Systems, Inc.
Squibb Diagnostics, Inc.
Toshiba America Medical Systems, Inc.

Meeting Totes

Squibb Diagnostics, Inc.

Meeting Luncheons

Berlex Laboratories, Division of Berlex Laboratories, Inc.

Published based on information available December 17, 1993.

MResource Guide Order Form

SMRI

the critical link between science and the clinical application of medicine, provides yet another important and helpful tool...
the MResource Guide

Photo by Al Francekevich

The second edition of the MResource Guide will be published inside the JMRI November/December 1993 issue. Additional copies of the Guide will be available and may be ordered by faxing this Order Form to the **SMRI** Central Office at 312/951-6474. If questions, call 312/751-2590.

Take control of a critical variable in magnetic resonance...order your MResource Guide today.

Name _____

Address _____

_____

City/State/Zip Code _____

Country _____

Phone _____ **FAX** _____

Number of MResource Guides:

☐ **1992 Edition** **@ $15.00 each**

☐ **1994 Edition** **@ $15.00 each**

$ _____ ***Total***

Payment enclosed (U.S. Funds only) ☐

MasterCard/Visa ☐

Name _____

Account #/Exp. date _____

Society for Magnetic Resonance Imaging

213 West Institute Place, Suite 501, Chicago, Illinois, 60610, Phone: 312/751-2590 FAX: 312/951-6474

CALL FOR PAPERS

SECOND MEETING OF THE SOCIETY OF MAGNETIC RESONANCE

San Francisco, California, USA
August 6-12, 1994.

DEADLINE FOR SUBMISSION:

APRIL 12, 1994

For information and abstract forms, contact

Society of Magnetic Resonance
Berkeley Office
1918 University Avenue, Suite 3C
Berkeley, CA 94704 USA
Tel: (510) 841-1899
Fax: (510) 841-2340